Doctoral Thesis

Time scale evaluation for formation processes of humic-like substances simulated by the Maillard reaction

February 2019

Department of Earth and Space Science,

Graduate School of Science, Osaka University

Yuki Nakaya

博士論文

メイラード反応により模擬した
腐植様物質生成過程の時間スケールの評価

2019 年 2 月

大阪大学理学研究科宇宙地球科学専攻

中屋　佑紀

Abstract

In this thesis, for evaluating time scales of formation processes of humic-like substances simulated by the Maillard reaction, hydrothermal changes in glycine + ribose mixture solutions and their interactions with an iron hydroxide (goethite) were examined.

First, in situ hydrothermal spectroscopic measurement systems for the simulated Maillard reactions were developed. An original heatable liquid cell and spacers of 0.05 mm thick provided a stable hydrothermal system without solution escape. In situ infrared (IR) and ultraviolet–visible (UV–Vis) spectroscopic measurements for the Maillard reaction of 0.5 mol l^{-1} glycine + ribose mixture solution at 60–80 °C were conducted using the in situ hydrothermal spectroscopic measurement systems. Kinetic analyses for decreases in the starting material (represented by decreases in band areas around 1100 and 1330 cm^{-1}: $IR_{1100\ and}\ IR_{1330}$) and browning process (represented by increases in absorbance at 420 nm: Vis_{420}) gave activation energies of 90–100 kJ mol^{-1} and frequency factors of 1.2×10^{9}–4.8×10^{9} s^{-1} at 60–80 °C.

Second, for tracing UV spectral changes in detail, in situ UV–Vis spectroscopy for 0.1 mol l^{-1} glycine + ribose solutions at 60–80 °C was performed. Increases in the products during the heating of glycine + ribose solution (0.1 mol l^{-1}) at 80 °C were quantitatively traced by UV–Vis, 3D excitation emission spectroscopy and size exclusion liquid chromatography. And 2D correlation spectroscopic analyses suggested that a band area around 280 nm (UV_{280}) and 254 nm absorbance (UV_{254}) can be used as measures of the formation of furfural-like intermediates and humic-like products, respectively. They were monitored by in situ UV–Vis spectroscopy with the original heatable liquid cell at 60–80 °C. Kinetic analyses for changes in UV_{280} and UV_{254} at the first order reaction progress stage after an induction stage gave activation energies of 87 and 88 kJ mol^{-1} and frequency factors of 8.1×10^{6} and 1.0×10^{6} s^{-1} at 60–80 °C, respectively.

Third, changes in Vis_{420} were analyzed for batch experiments of glycine + ribose solutions at 60–80 °C in the presence and absence of an iron hydroxide (goethite). Their kinetic analyses gave activation energies of 110 and 137 kJ mol^{-1} and frequency factors of 2.0×10^{10} and 9.1×10^{13} s^{-1} at 60–80 °C for 0.1 mol l^{-1} reactant solution with and without goethite, respectively. Enhancement of reaction rates in the presence of goethite was recognized. Effects of initial concentrations (0.5 or 0.1 mol l^{-1}) were also noticed.

Fourth, adsorption on goethite of reactants and products of the Maillard reaction at room temperature was measured by attenuated total reflection infrared (ATR-IR) spectroscopy. This adsorption process was within a few hours at room temperature and was faster than the formation enhancement of humic-like and brown products in several days at 60–80 °C. Later processes on the goethite surface after the fast adsorption are considered to be rate-limiting for the reaction

enhancement. An in situ hydrothermal ATR-IR cell under development can be used for further detailed kinetic studies including surface processes on goethite layers at different temperatures (20–80 °C).

Finally, time scales of the studied processes were compared by the half-lives of Vis_{420} changes, and were estimated to be around 5 years at a minimum and 2000 years at a maximum by extrapolation of experimental results to 15 °C. This was in agreement with a few decades of time scale for increase of fluorescence intensities in the bottom sediments of Ago bay, possibly due to the formation of humic-like substances. The present method can be applied to the Maillard reactions under other experimental conditions with various initial concentrations of reactants in future studies. These further researches will give constraints on the better understanding of the time scales of formation processes of humic-like substances.

要旨

本論文は，メイラード反応により模擬した腐植様物質の生成時間スケールを推定するため，グリシン・リボース混合水溶液の加熱変化を追跡し，また，水酸化鉄（ゲーサイト）との相互作用についても検討した．

まず，メイラード反応の水熱その場分光測定システムの開発を行い，独自に設計した水熱その場分光セル及びスペーサーにより試料溶液の漏出のない安定した測定を実現した．開発したセルを用いて 0.5 mol l^{-1} グリシン・リボース混合水溶液の 60–80 ℃におけるその場赤外・紫外可視分光測定を行ったところ，反応物（グリシンとリボース）の減少（1100 および 1330 cm^{-1} 吸収帯面積の減少）と試料溶液の褐色化（420 nm 吸光度の増加）について 90–100 kJ mol^{-1} の活性化エネルギーおよび 1.2×10^{9}–4.8×10^{9} s^{-1} の頻度因子が得られた．

次に，紫外領域におけるスペクトル変化を詳細に追跡するため，0.1 mol l^{-1} グリシン・リボース混合水溶液の 60–80 ℃におけるその場紫外可視分光測定を行った．80℃で 0–168 時間加熱したバッチ試料を紫外可視・3 次元蛍光スペクトルとサイズ排除クロマトグラフィーにより測定し 2 次元相関分光法により分析したところ，280 nm 吸収帯面積（UV_{280}）がフルフラール様中間生成物の指標，254 nm 吸光度（UV_{254}）が腐植様生成物の指標として使えることが示唆された．60–80 ℃における水熱その場紫外可視分光測定を行ったところ，両指標はある導入時間ののちに見かけの 1 次反応により増加した．また，その速度論的解析によりフルフラール様中間生成物・腐植様生成物の増加についてそれぞれ 87・88 kJ mol^{-1} の活性化エネルギーおよび 1.2×10^{9}・4.8×10^{9} s^{-1} の頻度因子が得られた．

ゲーサイト添加有・無の 0.1 mol l^{-1} グリシン・リボース混合水溶液を 60–80 ℃で加熱したバッチ試料の 420 nm 吸光度変化を速度論的に解析したところ，110・137 kJ mol^{-1} の活性化エネルギーおよび 2.0×10^{10}・9.1×10^{13} s^{-1} の頻度因子が得られた．また，ゲーサイト添加による反応の促進が見られ，0.5 mol l^{-1} グリシン・リボース混合水溶液の 60–80 ℃におけるその場紫外可視分光測定の解析結果と比較して，初期濃度が高いほど反応が早く進むことが示唆された．

さらに，メイラード反応の反応物（グリシンとリボース）と生成物（80 ℃196 時間加熱）のゲーサイトへの吸着（室温）を減衰全反射赤外分光法により測定した．この吸着過程は室温で数時間程度であり，60–80 ℃でゲーサイト添加により促進された褐変の時間スケール（数日程度）に比べて速い過程であった．このことは，ゲーサイトにより促進される褐変過程が，ゲーサイト表面に反応物・生成物が迅速に吸着した後の表面での反応過程により律速される可能性を示唆している．このような表面での反応過程は，新規開発中の水熱その場減衰全反射赤外分光セルによる室温から 80 ℃での追跡と解析により調べることができると期待される．

メイラード反応による腐植様物質の生成模擬過程の時間スケールを代表する指標として 420 nm の吸光度変化（褐変）の半増期を用い，実験結果をアーレニウスの式により低温

へ外挿し，15 ℃での半増期を見積もると，最小で 5 年，最大で 2000 年程度となった．これは英虞湾水底堆積物の蛍光強度増加（腐植様物質増加に対応）の数十年の時間スケールと調和的であった．今後は，本研究で開発した水熱その場分光測定システムを様々な反応条件でのメイラード反応に用いることができ，腐植様物質生成時間スケールのより良い理解につながると考えられる．

Acknowledgement

First of all, I would like to thank Prof. Satoru Nakashima of Osaka University for a lot of advices, encouragements and reading of this thesis. He taught me not only scientific knowledge and techniques but also pleasure of research life.

I would also like to thank Assistant Prof. M. Katsura of Osaka University for giving many advices and encouragement. I am grateful to Assistant Prof. O. Hisatomi of Osaka University for giving constructive advices and the use of a fluorescence spectrometer. I am also grateful to Assistant Prof. T. Yokoyama of Hiroshima University for giving lots of advices and encouragement on managing our chemical laboratory. I thank Assistant Prof. M. Moriizumi of Ryukoku University for scientific discussion and encouragement, and for the use of a size exclusion chromatographic apparatus and providing soil samples for developing fluorescence spectroscopy in solid phases. I also thank Dr. R. Tonoue, who gave me a lot of helpful advices and technical supports about spectroscopic data. Special thanks are paid to the colleagues at Nakashima Lab. for their helpful suggestions and encouragements.

I thank Drs. Y. Todokoro and N. Inazumi for NMR spectroscopy, Drs. A. Ito, R. Okamoto and Y. Kajihara for Mass Spectrometry. Center for Scientific Instrument Renovation and Manufacturing Support of Osaka University is also thanked for promptly and precisely making of new heatable liquid cells and their prototype models. I thank Dr. M. Igisu of JAMSTEC, who supported preparing the heatable liquid cell. Drs. M. Oguchi, S. Kashiwagi and N. Naka of HORIBA, Ltd. are thanked for technical supports in developing fluorescence spectroscopy for soils and sediments in solid phases. Mr. K. Okada and Mr. Y. Ikuno are also thanked for preparation and identification of iron hydroxides. I thank Ms. N. Yamaguchi for design of chapter headings. Part of this research was supported by JSPS KAKENHI Grant Number JP18J10249.

Table of contents

CHAPTER 1

General Introduction

1.1. Research background

Organic matter in living organisms such as proteins, carbohydrates, lipids, etc. are known to change to other organic molecules through enzymatic reactions, reactions between functional groups and metabolism of microorganisms. Most of the changes are continuous and non-uniform, therefore it is difficult to specify the products. “Humic substance” is a general term of such polymerized high molecular weight organic matter, whose structure is not well defined, present in Earth’s surface environments. While humic substances are sources of nutrients for microorganism, plants and some insects, and sources of fossil fuels, their abundant functional groups bring following environmental significances: complexation with toxic heavy metal ions using the functional groups as ligands; toxifying or detoxifying of heavy metal ions and organic chemicals; interactions with organic pollutants; producing CO_2 by decomposition of humic substances (Stevenson, 1994).

Humic substances are the major organic components in Earth’s surface environments and play key roles in interactions with environmental pollutants (Kördel et al., 1997). However, the processes and rates of formation of humic substances are complicated and poorly understood because of complexity of the formation processes and the products. After foundation of International Humic Substances Society (IHSS) in 1982, the term “humic substances” is often used based on analysis definition of IHSS by their extraction methods from natural samples and solubility in acid (Kuwatsuka et al., 1992). In this thesis, “humic-like substances” is used for samples which have similar properties to humic substances, but without using the analysis defined by IHSS.

Among various formation processes of humic substances, the Maillard reaction (browning reaction) is considered to be one of dominant formation processes of humic substances in aquatic or soil environments such as at the bottom of a deep lake where there is little dissolved oxygen and few microorganisms (Stevenson, 1994). In these environments, biogenic residues are considered to be major reactants of the Maillard reaction (Yamamoto and Ishiwatari, 1989). The Maillard reaction is a continuous reaction between an amino group in amino acids and a carbonyl group in saccharides producing various intermediates and their polymerized compounds, melanoidins (Maillard, 1912). They are brown-colored high molecular weight organic compounds, which have non-uniform structures. Their chemical similarities to natural humic substances provides a basis of the hypothesis of the Maillard reaction as a reaction forming humic substances in the natural environment (Ikan et al., 1996). Therefore, the Maillard reaction has been studied in a few geochemistry researches for understanding time scales, amounts and properties of the reaction and products (Abelson, 1978; Ikan et al., 1996).

Fig. 1.1.1 shows a schematic figure modified after Hodge (1953) for the Maillard reaction between glycine and ribose for forming brown products finally into melanoidins, where glycine and ribose are selected as representative reactants. Glycine is a simplest amino acid and ribose is a sugar compound

used in nucleotides forming RNA and DNA. The various pathways after the Amadori rearrangement (Fig. 1.1.1) include formation of an intermediate called (hydroxyl methyl) furfural, dehydration and fragmentation of the intermediates, the Strecker degradation of amino acids forming CO_2, and so on. (Hodge, 1953)

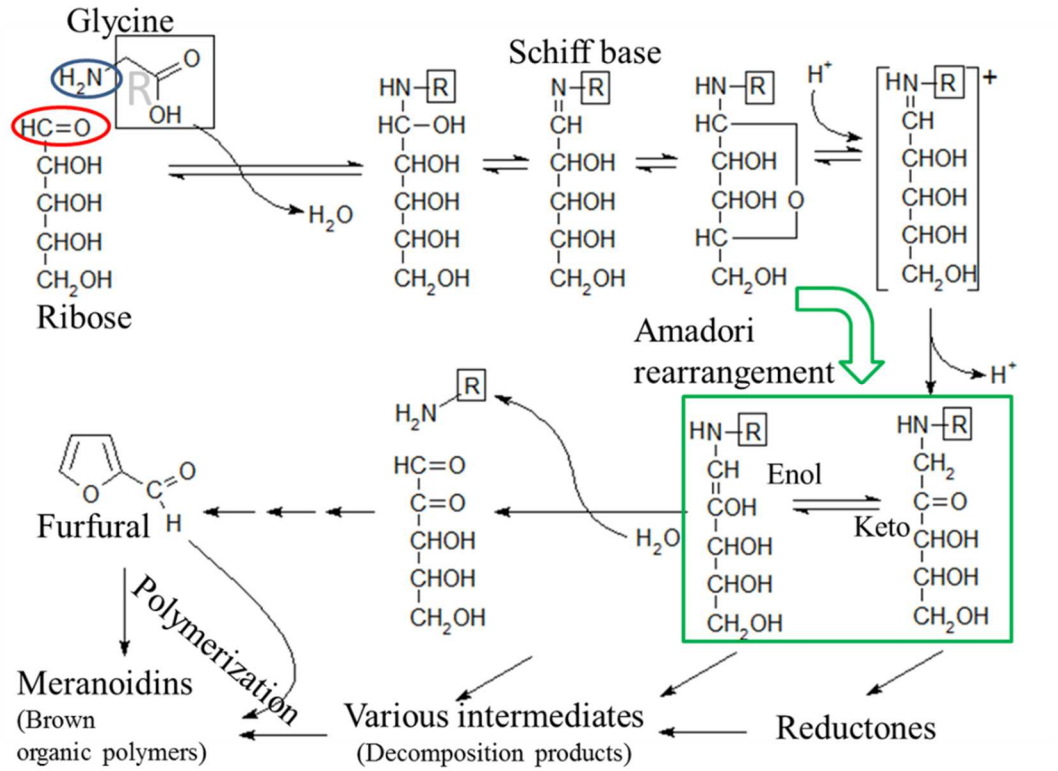

Fig. 1.1.1 A schematic figure modified after Hodge (1953) for the Maillard reaction between glycine and ribose for forming brown products finally into melanoidins. An amino group in glycine (blue circle) and a carbonyl group in ribose (red circle) are indicated by circles.

The Maillard reaction has been studied mainly in food chemistry for changes in colors, flavors and nutrition of foods (Finot, 2005). Since browning of foods is one of the most important problems in food chemistry, the progress of the Maillard reaction is often measured in terms of color formation by visible spectroscopy. For example, Stamp and Labuza (1983) followed the Maillard reaction between glucose and glycine as the zeroth order kinetics for increasing 420 nm absorbance by batch experiments and showed that the activation energy was 65 kJ/mol. Song et al. (1966) followed Maillard reaction between glucose and glycine focusing on increasing 490 nm absorbance by batch measurements. Van Boekel (2001) reviewed previous works on the Maillard reaction and showed that the activation energy of Maillard reaction in aqueous solutions ranged from 60 to 145 kJ/mol. However, these researches have been studied at relatively high temperatures simulating food cooking conditions and there is very little information on time scales of the Maillard reaction in geological environments,

except for some limited studies on reactions between amino acids and kerogens (high molecular weight insoluble organic matter) and analyses on dried products (Abelson, 1978; Yamamoto and Ishiwatari, 1989).

In this thesis, the formation process of humic-like substances was simulated by the Maillard reaction by glycine and ribose solution. Their thermal changes were traced by infrared (IR) and ultraviolet–visible (UV–Vis) spectroscopic methods and their time scales were evaluated by kinetic analyses for their spectroscopic changes.

1.2. Aims and contents of this study

This study aimes at:

- Developing in situ hydrothermal IR and UV–Vis spectroscopic measurement systems for the simulated Maillard reaction.
- Finding spectroscopic indicators which can represent progresses of the simulated Maillard reaction.
- Time scales evaluation for the simulated Maillard reaction by kinetic analyses for their spectral changes.

In Chapter 2, in situ hydrothermal spectroscopic measurement systems for the simulated Maillard reactions were first developed. In situ IR and UV–Vis spectroscopic measurements for the Maillard reaction of 0.5 mol l^{-1} glycine + ribose mixture solution at 60–80 °C were conducted.

In Chapter 3, for tracing UV spectral changes in detail, in situ UV–Vis spectroscopy for 0.1 mol l^{-1} glycine + ribose solutions at 60–80 °C was performed. Spectroscopic similarity between humic substances and the simulated Maillard reaction products was also discussed and validity of UV–Vis spectroscopy was suggested.

In Chapter 4, changes with time in absorbance at 420 nm (indicator of browning) were analyzed at 60–80 °C in the presence and absence of an iron hydroxide (goethite). Enhancement of reaction rates in the presence of goethite was recognized. Effects of initial concentrations (0.5 or 0.1 mol l^{-1}) were also noticed.

In order to examine surface processes on goethite during the simulated Maillard reaction, adsorption on goethite of reactants and products of the Maillard reaction at room temperature was studied by attenuated total reflection infrared (ATR-IR) spectroscopy (Chapter 5).

In Chapter 6, these results were summarized again and overall discussion and future perspectives were presented.

REFERENCE

Abelson, P. H. “Organic matter in the Earth's crust”. Annu. Rev. Earth Planet. Sci. 1978. 6. 325–351.

van Boekel, M. A. J. S. “Kinetic aspects of the Maillard reaction: a critical review”. Nahrung 2001. 45(3). 150–159.

Finot, P. A. “Historical perspective of the Maillard reaction in food science”. Ann. N. Y. Acad. Sci. 2005. 1043. 1–8.

Hodge, J. E. “Dehydrated foods, chemistry of browning reactions in model systems”. J. Agric. Food Chem. 1953. 1(15). 928–943.

Ikan, R., Y. Rubinsztain, A. Nissenbaum, I. R. Kaplan. “Geochemical aspects of the Maillard reaction” in R. Ikan (Ed.). “The Maillard reaction: consequences for the chemical, life sciences”. John Wiley & Sons. 1996. 1–25.

Kördel, W., M. Dassenakis, J. Lintelmann, S. Padberg. “The importance of natural organic material for environmental processes in waters and soils (Technical Report)”. Pure Appl. Chem. 1997. 69. 1571–1600.

Kuwatsuka, S., A. Watanabe, K. Ito, S. Arai. “Comparison of two methods of preparation of humic and fulvic acids, IHSS method and NAGOYA method”. Soil Sci. Plant Nutr. 1992. 38(1). 23–30.

Maillard, L. C. “Action of Amino Acids on Sugars. Formation of Melanoidins in a Methodical Way”. C. R. Hebd. Séances Acad. Sci. 1912. 154. 66–68.

Song, P. S., C. O. Chichester and F. H. Stadtman. “Kinetic behavior and mechanism of inhibition in the Maillard reaction. I. Kinetic behavior of the reaction between D-glucose and glycine”. J. Food Sci. 1966. 31(6). 906–913.

Stamp, J. A. and T. P. Labuza. “Kinetics of the Maillard reaction between aspartame and glucose in solution at high temperatures”. J. Food Sci. 1983. 48(2). 543–544.

Stevenson, F. J. Stevenson. “Humus Chemistry: Genesis, Composition, Reactions“. Wiley, 1994.

Yamamoto, S., R. Ishiwatari. “A study of the formation mechanism of sedimentary substances—ii. protein-based melanoidin model”. Org. Geochem. 1989. 14(5). 479–489.

CHAPTER 2

Development of in situ hydrothermal spectroscopic measurement systems for the simulated Maillard reaction

2.1. In situ infrared spectroscopy for the Maillard reaction by 0.5 mol l^{-1} glycine and ribose solution

This section has been modified from the following published paper in Chemistry Letters by the Chemical Society of Japan:

"In situ IR transmission spectroscopic observation and kinetic analyses of initial stage of the Maillard reaction as a simulated formation process of humic substances"

By Yuki Nakaya and Satoru Nakashima

Chemistry Letters, 2016. 45(10). 1204–1206.

2.1.1. Introduction

Kinetics of the Maillard reaction has been studied for long years by various researchers, especially in food chemistry (van Boekel, 2001). Since browning of food is one of the most important problems in food chemistry (Finot, 2005), progress of the Maillard reaction is often measured in terms of color formation by UV–Vis spectroscopy (e.g. Song et al., 1966; Stamp and Labuza, 1983; Ghazala et al. 1991; Baisier and Labuza, 1992; Ajandouz et al, 2008). However, most of amino acids and sugars as initial materials of the simulated Maillard reaction are neither colored nor UV–Vis active.

IR spectroscopy is one of useful methods for qualitative analyses of amino acids and sugars. Unlike their UV–Vis spectra, IR spectra have many characteristic absorption bands due to characteristic vibrations of polar functional groups such as hydroxyl (OH), carbonyl (C=O), ester (COO), carboxyl (COOH) groups, together with those of aliphatic and aromatic C-Hs and aromatic rings bound to polar components. Since IR transmission spectroscopy of aqueous solutions is very difficult because of strong absorption band of water, batch measurement of KBr pellets of well desiccated powders is often used. For the similar reason, in situ IR measurement on aqueous solutions has almost never been performed in the study of the Maillard reaction.

However, it is possible to measure IR transmission spectra of aqueous reactants and products of the Maillard reaction by adjusting appropriate concentrations and thicknesses of sample solutions. In this section, I aimed to establish a stable in situ IR measurement method of the Maillard reaction as a simulated formation process of humic-like substances and degradation process of reactants (Section 2.1) as well as the in situ UV–Vis spectroscopy (Section 2.2). In Section 2.1, a stable in situ IR transmission spectroscopic measurement method of Maillard reaction is established and the time scale for the decreases in initial materials is evaluated. In situ UV–Vis spectroscopic measurement of glycine + ribose mixture solutions for tracing intermediates and later products is described in later sections (Sections 2.2 and 3.2).

2.1.2. Methods

For in situ IR spectroscopic measurement of the aqueous Maillard reaction, I have designed and constructed a new heatable liquid cell (made by Center for Scientific Instrument Renovation and Manufacturing Support, Osaka Univ.). An overview and a schematic cross section of the cell is shown in Fig. 2.1.1. A sample solution stays in a thin space sandwiched by two CaF_2 (calcium fluoride) optical windows of 2 mm thick and 13 mm in diameter with a polytetrafluoroethylene (PTFE, Teflon) spacer of various thicknesses. And it is sealed by compression by upper and lower caps through rubber O-rings of 13 mm in diameter. The thickness of sample solution can be chosen approximately using a proper spacer. For in situ IR spectroscopic measurement in this section, PTFE spacers of 0.05 mm thick were used. They were hand-made from commercial PTFE sheets (7-358-07, AS ONE: chemically and thermally stable below 200 °C) of 0.05 mm thickness by piercing them with punches of 12 mm (outside diameter) and 8 mm (inside diameter) (Fig. 2.1.2).

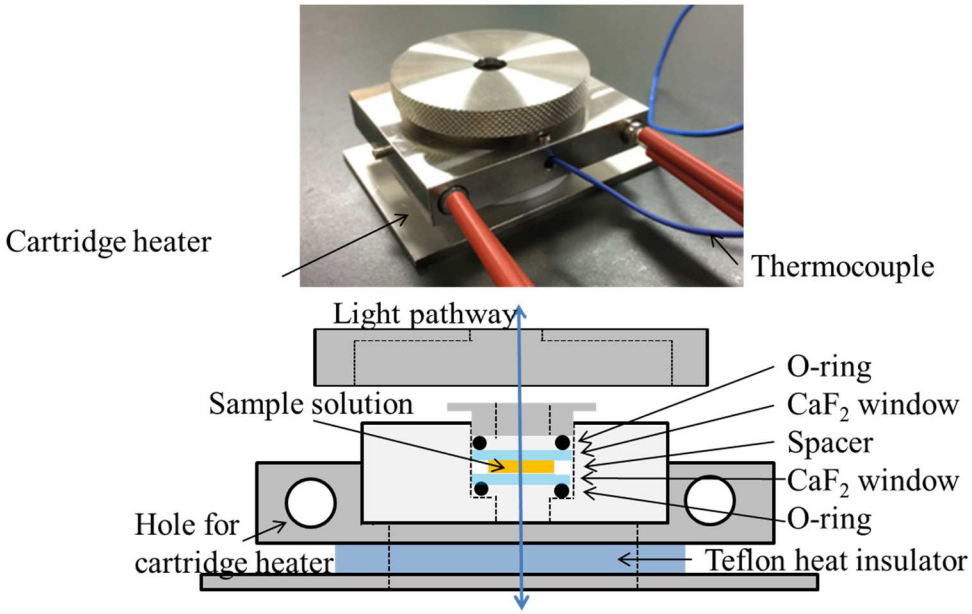

Fig. 2.1.1. An overview and a cross section of the new heatable liquid cell.

Fig. 2.1.2. A photograph of the punches, a PTFE sheet, and a hammer for punching.

As a starting solution of the Maillard reaction, a 0.5 mol l^{-1} glycine and ribose solution was selected here as representative amino acid and sugar components. 2.0 mol l^{-1} glycine and 2.0 mol l^{-1} ribose solutions were prepared by dissolving them in pure water (MilliQ: Resistance > 18.2 MΩ cm). These solutions and pure water were mixed to obtain 0.5 mol l^{-1} glycine + ribose mixture solutions, 0.5 mol l^{-1} glycine solutions and 0.5 mol l^{-1} ribose solutions. About 1 µl of the solution was injected in the sample chamber of the liquid cell.

Glycine + ribose mixture solutions (0.5 mol l^{-1}) were heated at 80, 75 and 70 °C for 48 hours (2 days) and at 65 and 60 °C for 96 hours (4 days) in an IR spectrometer (FTIR4100, Jasco) (Fig. 2.1.3). It has a single beam measurement system, in which light intensity (I) from the source through an interferometer passes through the sample compartment to be detected by a TGS detector. Intensity of reference (I_0) was measured without the cell and that for the sample (I) with the cell. Absorbance (*Abs.*) is expressed as a common logarithm of the ratio of transmitted light intensities of sample (I) and reference (I_0):

$$Abs. = -\log_{10}\frac{I}{I_0}$$

It should be noted that absorption by not only the sample solution but also two CaF_2 windows was measured in the single beam measurement system. A photograph of the sample compartment with the heatable liquid cell is shown in Fig. 2.1.4. IR spectra were measured every 2 minutes with a wavenumber resolution of 4 cm^{-1} and 64 scans in the 400-7800 cm^{-1} spectral range. As reference experiments, IR spectral changes for 0.5 mol l^{-1} glycine solution only and 0.5 mol l^{-1} ribose solution only were measured for 2 days heating at 80 °C. The other measurement conditions were the same as those of 0.5 mol l^{-1} glycine + ribose mixture solutions. Experimental procedures of the in situ IR spectroscopic observation are shown in Fig. 2.1.5.

Fig. 2.1.3. An overview of the IR spectrometer (FTIR4100, Jasco).

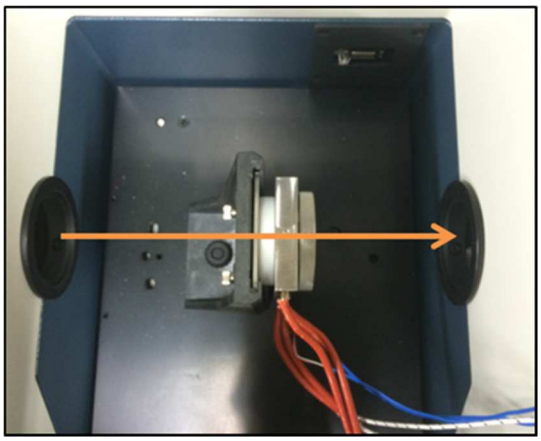

Fig. 2.1.4. A photograph of the sample compartment of the IR spectrometer (FTIR 4100, Jasco) with the heatable liquid cell.

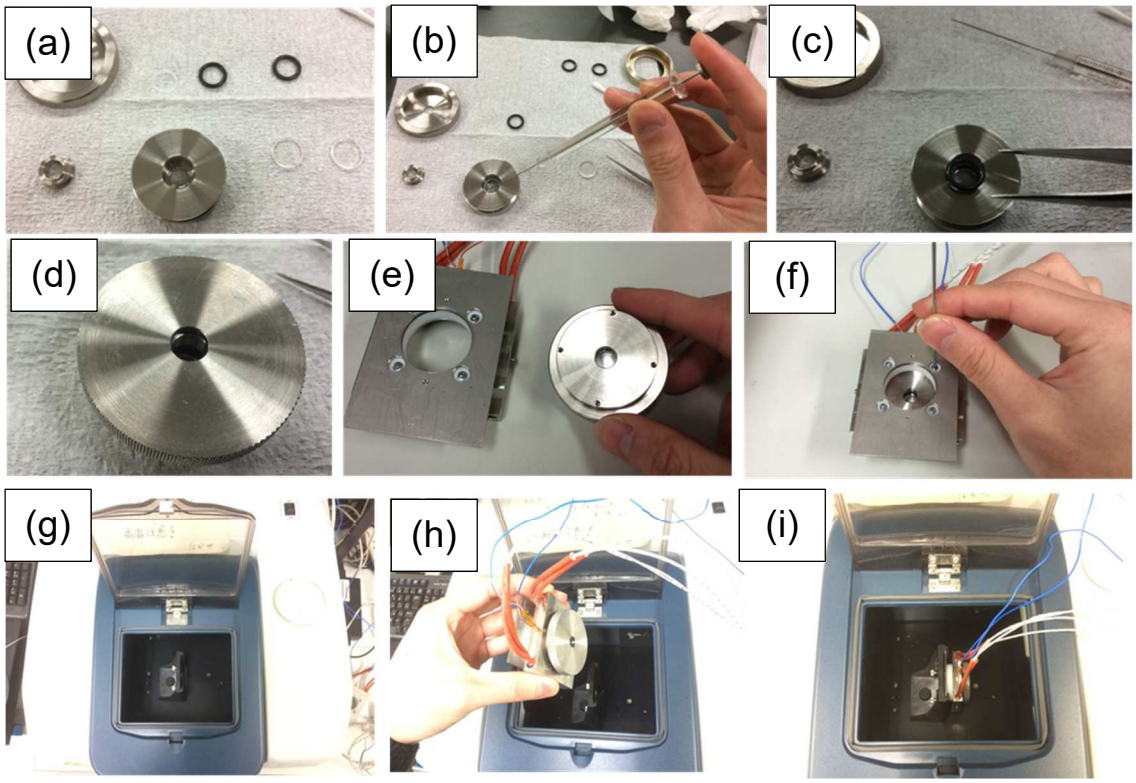

Fig. 2.1.5. Experimental procedures from (a) to (i) of the in situ IR spectroscopic observation of 0.5 mol l^{-1} glycine + ribose mixture solutions heated at 80, 75, 70, 65 and 60 °C in the heatable liquid cell.

2.1.3. Results

Representative in situ IR spectra of 0.5 mol l^{-1} glycine + ribose mixture solutions heated at 80 °C (0-48 hours) in the 400–7800 cm^{-1} spectral range are shown in Fig. 2.1.6. They show peaks around 1600, 3400, 5200 and 7000 cm^{-1} corresponding to vibrations of water molecules (Eizenberg and Kauzmann, 1969). The peaks around 1600 and 3400 cm^{-1} are saturated and their changes cannot be monitored quantitatively. This saturation of absorption by water in IR range occurred even in the measurements with PTFE spacers of 0.05 mm thick, and it prevented monitoring of IR absorbance in these regions. However, absorbance in the 900–1800 cm^{-1} spectral range were not saturated and it can be monitored quantitatively. The peaks around 5200 and 7000 cm^{-1} due to water were also not saturated, and they can be used for monitoring thickness of sample solutions.

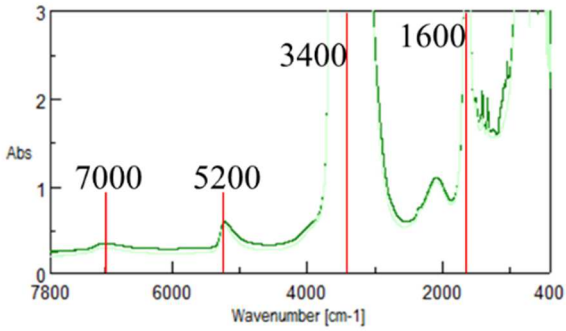

Fig. 2.1.6. Representative IR spectra of 0.5 mol l^{-1} glycine + ribose mixture solutions heated at 80 °C (0–48 hours) in the 400-7800 cm^{-1} spectral range.

Details of in situ IR spectra in the 900-1800 cm^{-1} spectral range of 0.5 mol l^{-1} glycine + ribose mixture solutions, 0.5 mol l^{-1} glycine solutions and 0.5 mol l^{-1} ribose solutions heated at 80 °C (0-48 hours) are presented in Fig. 2.1.7. They show peaks at 1044, 1088, 1120, 1156, 1220 and 1246 cm^{-1} corresponding to absorptions by ribose, and 1330, 1410, 1442 and 1510 cm^{-1} due to absorptions by glycine. These absorptions in the spectra of 0.5 mol l^{-1} glycine solutions alone and 0.5 mol l^{-1} ribose solutions alone showed no significant changes with heating time. Therefore, no significant changes occurred on IR active functional groups of glycine alone and ribose alone during their heating at 80 °C for 48 hours. On the other hand, in the spectra of 0.5 mol l^{-1} glycine + ribose mixture solutions, these absorptions decreased with heating time. This indicates that their functional groups were changed by the Maillard reaction. Assignments of IR absorption bands observed in Fig. 2.1.7 are listed in Table 2.1.1. It should be noted that no increasing absorption bands have been recognized.

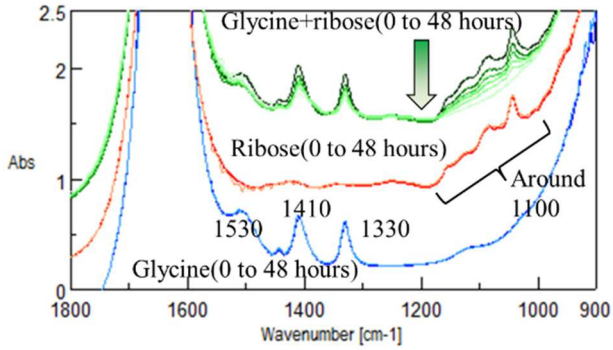

Fig. 2.1.7. Representative IR spectra of 0.5 mol l^{-1} glycine + ribose mixture solutions, 0.5 mol l^{-1} glycine solutions and 0.5 mol l^{-1} ribose solutions heated at 80 °C (0–48 hours) in the 900–1800 cm^{-1} spectral range. (They were shifted vertically for clarity.)

Table 2.1.1. Assignments of absorption bands observed in Fig. 2.1.7 based on the literatures ([1]Carmona and Molina, 1990; [2]Kumar et al., 2004; [3]Kitadai et al., 2010).

Wavenumber (cm^{-1})	Assignment (literature data of wavenumber (cm^{-1}))
1044	C-O stretching + C-C stretching + C-H bending of ribose (1030)[1]
1088	C-O stretching + C-C stretching of ribose (1078)[1]
1120	C-O stretching + C-C stretching of ribose (1112)[1]
1156	C-O stretching + C-C stretching of ribose (1155)[1]
1220	C-H bending + O-H bending of ribose (1215)[1]
1246	C-H bending + O-H bending of ribose (1240)[1]
1330	NH_2 bending+ CH_2 bending of glycine(1334)[2]
1410	COO^- symmetric stretching of glycine[3]
1442	CH_2 bending of glycine[3]
1510	NH_3^+ symmetric deformation of glycine[3]

2.1.4. Discussion

Changes with time in bands around 5200 and 7000 cm^{-1} (baselines of 4500–5500 cm^{-1} and 6500–7300 cm^{-1}, respectively) in the in situ IR spectroscopic measurements for 0.5 mol l^{-1} glycine + ribose mixture solution at 80, 75, 70, 65 and 60 °C are shown in Fig. 2.1.8. 5200 cm^{-1} band area was 70–77 and 7000 cm^{-1} band area was 20–22 for each measurement. It suggests that the thickness of sample solutions was almost the same and there was almost no escape of the sample solutions throughout each heating experiment.

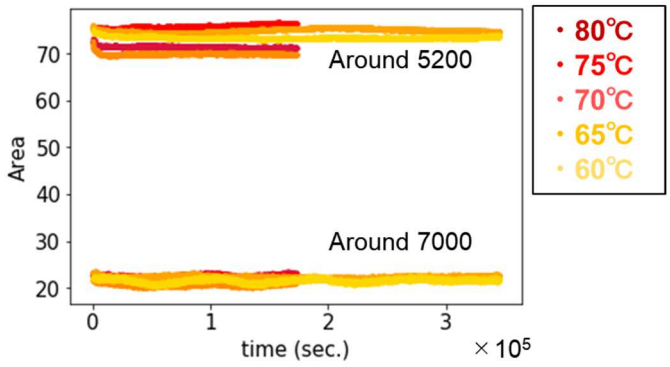

Fig. 2.1.8. Changes with time in band areas around 5200 and 7000 cm^{-1} during the in situ IR spectroscopic measurements for 0.5 mol l^{-1} glycine + ribose mixture solution at 80, 75, 70, 65 and 60 °C.

Small bands around 1156, 1120, 1088 and 1044 cm^{-1} correspond to C-O stretching vibrations of different C-O bonds in ribose (Carmona and Molina, 1990). Changes with time in these individual band areas around 1044, 1088, 1120, 1156 cm^{-1} (baseline: 1020–1060, 1075–1105, 1110–1145, 1145–1170 cm^{-1}, respectively) showed similar trends. Therefore, they can be regarded as one global C-O band of ribose and its band area was determined with a baseline of 1020–1170 cm^{-1}, because of its larger precision. This C-O stretching band around 1100 cm^{-1} is selected for further quantitative analyses of ribose. The 1100 cm^{-1} band areas (baseline: 1020–1170 cm^{-1}) were divided by the 1100 cm^{-1} band areas of the 0 second spectrum of 0.5 mol l^{-1} glycine + ribose mixture solutions heated at each temperature to normalize differences in the sample solution thickness. These normalized band areas showed exponential decreases at each heating temperature (Fig. 2.1.9a).

In order to perform kinetic analyses, the decreases in the normalized 1100 cm^{-1} band area with time were fitted by the following exponential equation, assuming the first order reaction:

$$IR_{1100} = C \ \exp(-k_{1100}t) \quad \text{(eq. 2.1.1)}$$

where IR_{1100} is the normalized 1100 cm^{-1} band area, t is the heating time (s), k_{1100} is the apparent first order rate constant (s^{-1}) and C is the intercept at time zero of the band area axis. Because the reaction

might have already proceeded to some extent during the increase in temperature and the time zero was taken when the target temperatures were attained, C is not set to 1.

Values of k_{1100}, C and correlation coefficient r values obtained by fitting of the experimental data by the above equation are listed in Table 2.1.2. Obtained C values were close to 1. The obtained apparent first order rate constants k_{1100} increased with temperature. They can be described by the following Arrhenius equation:

$$\ln k = \ln A - \frac{E_a}{RT} \quad \text{(eq. 2.1.2)}$$

, where A is the frequency factor (s^{-1}), E_a is the activation energy (kJ mol^{-1}), R is the gas constant (8.31 J mol^{-1} K^{-1}) and T is the absolute temperature (K).

The Arrhenius plots of k_{1100} and T (333–350 K) show a quasi-linear trend (Fig. 2.1.10). The fitting line of these experimental data gave E_a and A for the decreases in 1100 cm^{-1} band area during the heating of 0.5 mol l^{-1} glycine + ribose mixture solutions. The obtained E_a and A values were 98 kJ mol^{-1} and 4.8×10^9 s^{-1}, respectively.

The same kinetic analyses can be conducted on the bands due to glycine. Since similar changes with time were mostly obtained for these bands, the 1330 cm^{-1} band area (baseline: 1290–1360 cm^{-1}) was selected in this study as a representative band (NH_2 bending + CH_2 bending of glycine: Kumar et al., 2004) (Fig 2.1.9b). The normalized 1330 cm^{-1} band area decreases with time were fitted by the exponential equation assuming the first order reaction:

$$IR_{1330} = C_1 \exp(-k_{1330}t) + C_2 \quad \text{(eq. 2.1.3)}$$

where IR_{1330} is the normalized 1330 cm^{-1} band area of glycine, t is the heating time (s), k_{1330} is the apparent first order rate constant (s^{-1}), C_1 is the constant corresponding to the intercept at the normalized band area axis and C_2 is the vertical offset corresponding to glycine residues, which is unreacted or dissociated from intermediates (see later considerations). k_{1330}, C_1, C_2 and correlation coefficient r values obtained by fitting of the experimental data by the above equation are also listed in Table 2.1.2.

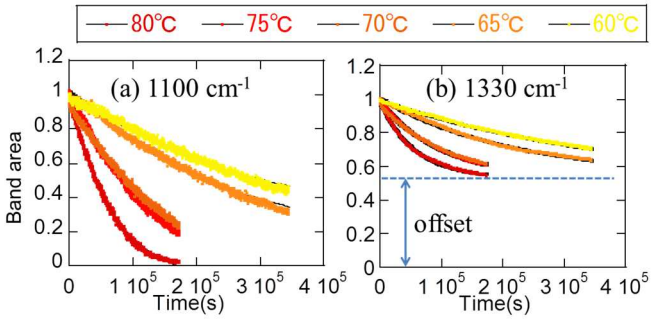

Fig. 2.1.9. Changes with time in the normalized (a) 1100 $cm^{-1}$and (b) 1330 cm^{-1} band areas during in situ IR spectroscopy of 0.5 mol l^{-1} glycine + ribose mixture solutions heated at 60, 65, 70, 75 and 80 °C with exponential fitting curves (the first order reaction).

Table 2.1.2. The values of k_{1100} (s^{-1}), k_{1330} (s^{-1}), C and r values of the apparent first order reactions for the normalized band areas of 1100 cm^{-1} and 1330 cm^{-1} in the heating experiments of 0.5 mol l^{-1} glycine + ribose mixture solutions at 60, 65, 70, 75 and 80 °C.

		80 °C	75 °C	70 °C	65 °C	60 °C
1100 cm^{-1}	k_{1100}	1.9×10^{-5}	9.2×10^{-6}	7.6×10^{-6}	3.3×10^{-6}	2.4×10^{-6}
	C	1.04	1.05	0.973	1.02	1.01
	r	0.996	0.997	0.996	0.998	0.996
1330 cm^{-1}	k_{1330}	1.8×10^{-5}	1.1×10^{-5}	9.2×10^{-6}	4.6×10^{-6}	2.5×10^{-6}
	C_1	0.45	0.46	0.44	0.46	0.50
	C_2	0.54	0.54	0.53	0.54	0.50
	r	0.999	0.999	0.999	0.999	0.999

NH_2 + CH_2 bending of glycine decreased almost simultaneously with C-O bonds of ribose. While C-O bonds of ribose continue to decrease until zero, about halves of NH_2 + CH_2 bonds of glycine decreased and the other halves remained (Fig. 2.1.9; C_2 ~ 0.5 in Table 2.1.2). In previous studies of the Maillard reaction, amino acids were considered to be separated from the reaction intermediates produced by combination of amino and carbonyl groups after Amadori rearrangement, and only sugar moieties were supposed to continue to be dehydrated (Hodge, 1953). Therefore, the above glycine residues observed in these experiments can correspond to these separated amino acids.

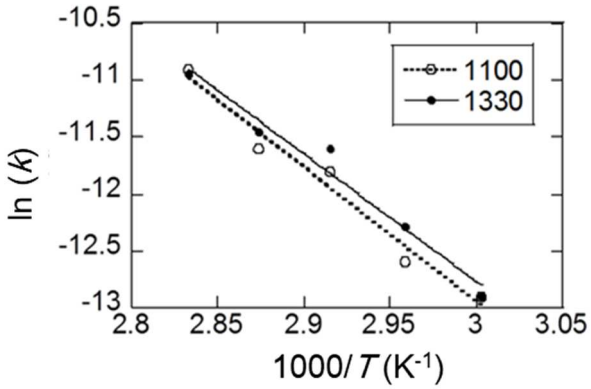

Fig. 2.1.10. The Arrhenius plots of k_{1100} and k_{1330} for the normalized band areas of 1100 cm^{-1} and 1330 cm^{-1} and the fitting lines.

The Arrhenius plots of k_{1100} and k_{1330} and T (333–350 K) for 1100 cm^{-1} band area of ribose and 1330 cm^{-1} band area of glycine show relatively good linear trends (Fig.2.1.10). The fitting lines of these experimental data gave E_a and A for the decreases in ribose and glycine bands during the heating of 0.5 mol l^{-1} glycine + ribose mixture solutions (E_a =98 kJ mol^{-1} and $A = 4.8\times10^9$ s^{-1} for ribose and E_a = 93 kJ mol^{-1} and $A = 1.2\times10^9$ s^{-1} for glycine, respectively). These values were on the same order

of magnitudes. These quasi-linear trends suggested the similar reaction mechanisms in this temperature range (60–80 °C).

In previous works, decreases in initial materials of the Maillard reaction have been fitted by either the first order or the second order reactions (van Boekel, 2001). The decrease with time of two starting materials can be usually fitted by the second order reaction. However, the second order fitting of the present experimental data were not good. On the other hand, their fittings by exponential equations were good with correlation coefficient $r > 0.996$ (Fig.2.1.9, Table 2.1.2). This indicates the validity of the first order reaction model. The collision of glycine and ribose in this study can be fast and the transformation of formed glycine-ribose composite might be the rate-limiting step following the first order reaction.

The obtained apparent first order rate constants k_{1100} and k_{1330} at 60–80 °C can be extrapolated to lower temperatures by the above Arrhenius equation (eq. 2.1.2). 15 °C was selected as a representative temperature of Earth's aquatic environment. The extrapolated k_1 values at 15 °C are 9.4×10^{-9} s^{-1} (= k_{1100}) for decrease in ribose (band area around 1100 cm^{-1}) and 1.4×10^{-8} s^{-1} (= k_{1330}) for decrease in glycine (band area around 1330 cm^{-1}) during the Maillard reaction of 0.5 mol l^{-1} glycine + ribose solution. In order to better represent time scales of these reaction rates at Earth's surface environments, their half-life $t_{1/2}$ can be calculated by $(\ln 2)/k_{1100\ (1330)}$ and the $t_{1/2}$ values at 15 °C are 2.3 years for decrease in ribose and 1.5 years for decrease in glycine.

In this section, decreases in starting materials were followed by the present in situ IR method. However, no significant increasing absorption bands corresponding intermediates and later products were recognized. Their concentrations or extinction coefficients were possibly too small to be detected in the IR range.

2.2. In situ ultraviolet–visible spectroscopy for the Maillard reaction by 0.5 mol l^{-1} glycine and ribose solution

2.2.1. Introduction

Humic substances are known to have broad and featureless UV–Vis absorption spectra (Wang et al, 1990), which are derived from presence of aromatic rings or conjugated C=C or C=O double bonds, in the ultraviolet (UV) (200–400 nm) and visible (Vis) (400–800 nm) regions (Stevenson, 1994). In spite of the featureless absorption spectra, UV–Vis spectroscopic measurements have been performed in various studies of humic substances because of ease of measurement, and some quantitative treatment of the spectra have been conducted. For example, slope in visible range, absorbance at 400 and 600 nm, their ratio and quotient of mass of organic matter (Kumada, 1965; Ghosh and Schnitzer, 1979; Ikeya and Watanabe, 2003).

UV–Vis spectroscopy is also employed in the study of the Maillard reaction. For example, Stamp and Labuza (1983) followed the Maillard reaction between aspartame, which has an amino group, and glucose by measuring absorbance at 420 nm at 70–100 °C, and obtained the activation energy of 65 kJ mol^{-1} assuming the zeroth order reaction. On the other hand, Song et al. (1966) followed the Maillard reaction between D-glucose and glycine by measuring absorbance at 490 nm. In fact, solution browning is typical for the Maillard reaction and is derived from a highly concentrated mixture of UV active species (Davies and Labuza, 1997) such as melanoidins, which are the final products of the Maillard reaction and have aromatic rings and conjugated C=C double bonds. Furthermore, furfural and hydroxymethyl furfural (HMF), which are the intermediates of the Maillard reaction (Hodge, 1953), has a broad absorption band around 280 nm. Since these intermediate products such as HMF show a yellowish color in the Maillard reaction, the coloration by HMF is called “secondary browning reaction” (Song et al. 1966).

Thus, UV–Vis spectroscopy has been often used in studies of humic substances and the Maillard reaction. However, in situ measurements have not been conducted for monitoring the reaction progress, except for Otsuka and Nakashima (2007) following the adsorption of a dissolved humic substances to goethite and subsequent oxidation to CO_2 by in situ UV–Vis spectroscopy mainly at 254 nm at 70 °C.

In order to monitor the formation of products by the Maillard reaction of 0.5 mol l^{-1} glycine + ribose mixture solution, in situ UV–Vis spectroscopic measurements for the solutions with the same types of heatable liquid cell were conducted. As an index of yellow-brownish compounds’ generation, absorbance at 420 nm with one-point base at 800 nm were employed after Stamp and Labuza (1983). For starting materials, glycine and ribose were selected in order to compare results with those by in situ IR spectroscopic measurement (Section 2.1). The heatable liquid cell and the PTFE spacers of 0.05 mm thickness were used.

2.2.2. Methods

By the same way as in IR measurements (Section 2.1), 0.5 mol l^{-1} glycine + ribose mixture solutions were prepared and about 1 µl of the solution was injected in the sample chamber of the same heatable liquid cell. 0.5 mol l^{-1} glycine + ribose mixture solutions were heated at 80, 75, 70, 65 and 60 °C for 144 hours (6 days) in an UV–Vis spectrometer (V530, Jasco) (Fig. 2.2.1). It has a double beam measurement system, in which light source is divided into two: one for sample and the other for reference, and detectors measure intensity of each light (I and I_0). The heatable liquid cell was mounted on the sample position of the UV–Vis spectrometer (Fig. 2.2.2). Therefore, absorption by not only the sample solution but also two CaF_2 windows was measured. In order to check reproducibility, 80 °C experiment was conducted 3 times. UV–Vis spectra were measured every 5 minutes at a scanning speed of 400 nm min^{-1} with a resolution of 1.0 nm in the 200–1100 nm spectral range. In order to check constancy of thickness of the sample solutions, IR spectra were also measured before and after the heating experiments with a wavenumber resolution of 4 cm^{-1} and 64 scans in the 400–7800 cm^{-1} spectral range.

Fig. 2.2.1. An overview of the UV–Vis spectrometer (V530, Jasco).

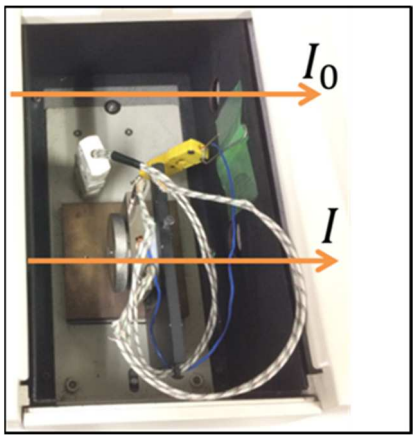

Fig. 2.2.2. A photograph of the sample compartment of the UV–Vis spectrometer (V530, Jasco).

2.2.3. Results

Representative visible spectra (400–1100 nm) for 0.5 mol l^{-1} glycine + ribose mixture solution heated at 80 °C for 0–144 hours (0–6 days) are shown in Fig. 2.2.3. Absorbance at shorter wavelength increased more for longer heating durations. It should be noted that spectral saturation occurred in UV region (200–400 nm) (not shown) because of strong absorption by UV active products.

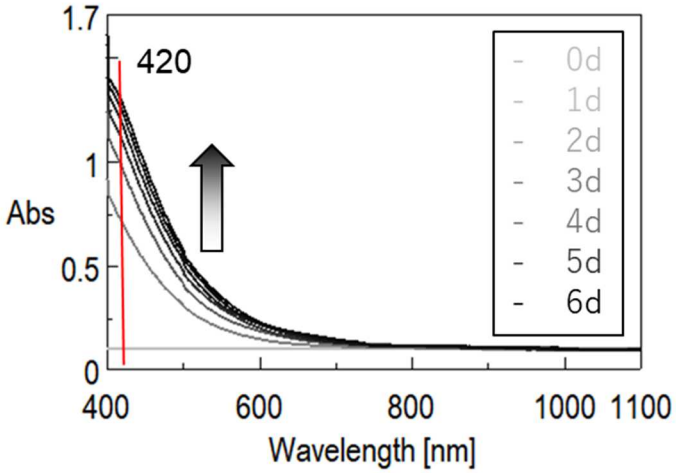

Fig. 2.2.3. Representative in situ visible spectra for the product solutions of 0.5 mol l^{-1} glycine + ribose mixture solutions heated at 80 °C for 0, 1, 2, 3, 4, 5 and 6 days.

On the other hand, water bands at 5200 and 7000 cm^{-1} in the near IR region were used for examining constancy of thickness of sample solutions. Fig. 2.2.4 shows IR spectra before and after in situ UV–Vis spectroscopy at 80 °C (before: 0 day; after: 6 days). 5200 cm^{-1} band area was 74–80 and 7000 cm^{-1} band area was 20–22 for each measurement. 5200 cm^{-1} band area (average value of before and after) were used for normalizing the experimental spectra in terms of the solution thickness.

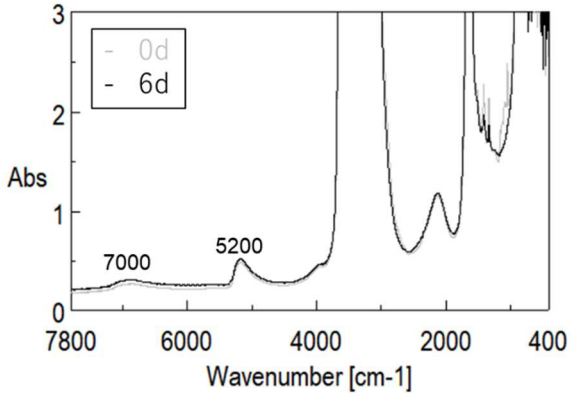

Fig. 2.2.4. IR spectra before and after in situ UV–Vis spectroscopy at 80 °C (before: 0 day; after: 6 days).

2.2.4. Discussion

Changes in absorbance at 420 nm with one-point base at 800 nm (Vis_{420}) with time during the in situ measurements at each heating temperature are plotted in Fig.2.2.5. The absorbance was corrected so as for sample thickness to be the same as the first experiment at 80 °C using 5200 cm^{-1} band area. These changes were fitted by the first order reaction model. The fittings of the data by

$$Vis_{420} = C(1 - k_{420}t) \quad \text{(eq.2.2.1)}$$

give apparent first order reaction rate constants k_{420} (fitting parameters: k_{420}, C). The fitting curves are shown in Fig. 2.2.5 on the Vis_{420} changes. k_{420}, C and correlation coefficient r values obtained by the first order fittings are listed in Table 2.2.1.

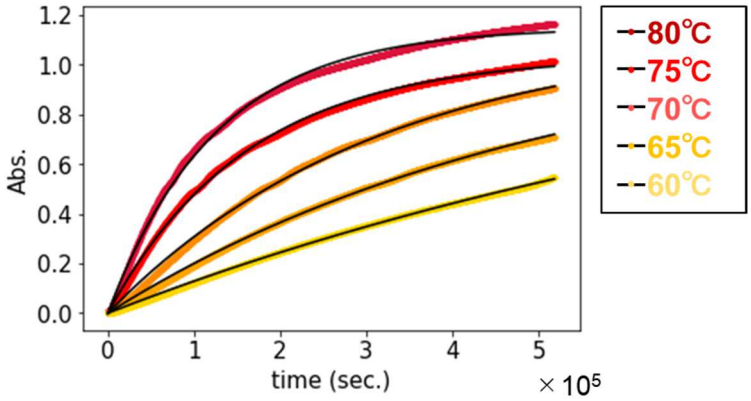

Fig. 2.2.5. Changes of Vis_{420} with time during the in situ measurements of 0.5mol l^{-1} glycine + ribose mixture solutions heated at 60, 65, 70, 75, and 80 °C with the fitting curves (the first order reaction). Changes at 80 °C are for the representative ones and changes for the other two experiments are not shown.

Table 2.2.1. The values of k_{420} (s^{-1}), C and correlation coefficient r values of the first order reaction fittings in the heating experiments of 0.5 mol l^{-1} glycine + ribose mixture solutions at 60, 65, 70, 75 and 80 °C.

	80 °C [1]	80 °C [2]	80 °C [3]	75 °C	70 °C	65 °C	60 °C
k_{420}	8.0×10^{-6}	7.0×10^{-6}	6.9×10^{-6}	6.2×10^{-6}	3.2×10^{-6}	1.9×10^{-6}	1.1×10^{-6}
C	1.15	1.15	1.20	1.03	1.13	1.14	1.27
r	0.999	0.999	0.999	0.999	0.999	0.999	0.999

The obtained apparent reaction rate constants increased with the heating temperature. They can be described by the Arrhenius equation (eq. 2.1.2).

$$\ln k = \ln A - \frac{E_a}{RT} \quad \text{(eq. 2.1.2)}$$

The Arrhenius plots of k_{420} and T (333–350 K) (Fig. 2.2.6) show relatively good linear trends, where average values of ln k_{420} at 80 °C are employed and their standard deviations (0.06) are indicated by error bars. The fitting lines of these experimental data gave E_a and A values for increase of 420 nm absorbance during the heating of 0.5 mol l^{-1} glycine + ribose mixture solutions (E_a = 98 kJ mol^{-1} and $A = 2.7\times10^9$ s^{-1}).

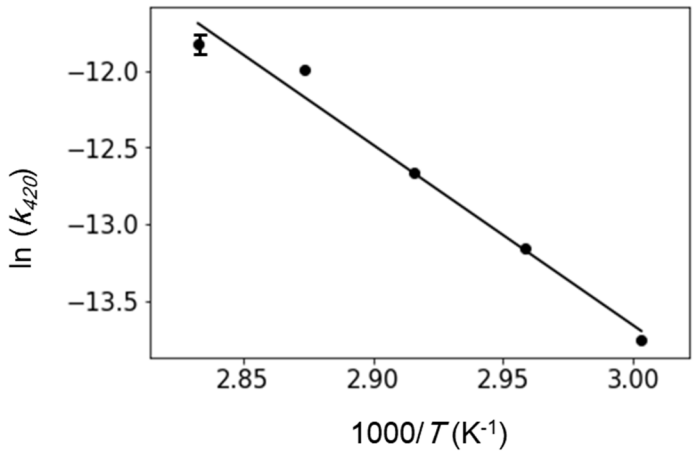

Fig. 2.2.6. The Arrhenius plot of the first order increase rate constant k_{420} values of Vis_{420} and their fitting line.

The obtained apparent first order rate constants k_{420} of Vis_{420} at 60–80 °C can be extrapolated to 15 °C by the above Arrhenius equation (eq. 2.1.2). The extrapolated k_{420} value at 15 °C was 4.5×10^{-9} s^{-1} for browning (absorbance at 420 nm) during the Maillard reaction of 0.5 mol l^{-1} glycine + ribose solution and the half-life ($t_{1/2}$) at 15 °C was 4.9 years.

Previous kinetic analyses of batch Maillard reactions reported wide ranges of activation energies (16–238 kJ mol^{-1}) possibly due to different experimental conditions and kinetic analyses (van Boekel, 2001). The present data by in situ IR and visible measurements with the activation energy of 90–100 kJ mol^{-1} can give constraints on the better understanding of the Maillard reaction.

On the other hand, spectrum in UV region (200–400 nm) could not be traced because of strong absorption by UV active products in the present experiments of 0.5 mol l^{-1} glycine + ribose mixture solution with 0.05 mm thickness PTFE spacer. For in situ UV spectroscopy, lower initial concentration should be examined (Chapter 3).

2.3. Conclusion

In order to examine formation rates of humic-like substances, I focused on the Maillard reaction by 0.5 mol l^{-1} glycine + ribose mixture solution as a reaction simulating a formation of humic substances.

First, for tracing degradation of the reactants by the Maillard reaction, in situ IR spectroscopic measurements using an original heatable liquid cell were conducted. In situ IR spectra of 0.5 mol l^{-1} glycine + ribose mixture solutions heated at 60–80 °C (0–96 hours) showed peaks at 1044, 1088, 1120, 1156, 1220, 1246, 1330, 1410, 1442 and 1510 cm^{-1}. Their band areas showed exponential decreases for most of the heating temperatures. From reference experiments, transformations of glycine alone and ribose alone did not occur in the present heating experiments of glycine + ribose mixture solutions. Constancy of bands around 5200 and 7000 cm^{-1} suggested thickness of sample solutions was almost the same and there was almost no escape of the sample solutions throughout each heating experiment.

The decreasing 1100 and 1330 cm^{-1} band areas (baseline: 1020–1170 and 1290–1360 cm^{-1}, respectively) were analyzed as indicators of amounts of ribose and glycine, respectively. The band area decreases with time were fitted by the exponential equation assuming the first order reaction and k_{1100}, k_{1330} and $t_{1/2}$ values were obtained, where k_{1100} and k_{1330} are the apparent first order rate constants for decreases in 1100 and 1330 cm^{-1} band area, $t_{1/2}$ is the half-life. The Arrhenius plots of k_{1100} and k_{1330} and T (333–350 K) gave linear trends and the fitted lines gave E_a and A to be E_a = 98 kJ mol^{-1} and $A = 4.8\times10^{9}$ s^{-1} for ribose decrease and E_a = 93 kJ mol^{-1} and $A = 1.2\times10^{9}$ s^{-1} for glycine decrease, respectively.

The obtained k_{1100} and k_{1330} at 60–80 °C were extrapolated to lower temperatures by the Arrhenius equation. The obtained k_{1100} and k_{1330} values at 15°C were 9.4×10^{-9} s^{-1} (= k_{1100}) for decrease of ribose (band area around 1100 cm^{-1}) and 1.4×10^{-8} s^{-1} (= k_{1330}) for decrease of glycine (band area around 1330 cm^{-1}), respectively. The half-life $t_{1/2}$ values at 15 °C were 2.3 years and 2.1 years, respectively.

Second, for tracing brown products by the reaction, in situ UV–Vis spectroscopic measurements of 0.5 mol l^{-1} glycine + ribose mixture solutions heated at 60–80 °C (0–144 hours) using the same heatable liquid cell were conducted. Constancy of the sample thickness was checked by IR spectroscopy before and after each in situ UV–Vis spectroscopic measurement and 5200 cm^{-1} band area (average value of before and after) was used for normalizing the experimental spectra in terms of the solution thickness. In situ UV–Vis spectra showed that absorbance at shorter wavelength increased more for longer heating durations. Spectral saturation occurred in UV region (200–400 nm) (not shown) because of strong absorption by UV active products.

Changes in absorbance at 420 nm with one-point base at 800 nm (Vis_{420}) with time during the in situ measurements at each heating temperature were fitted by the exponential equation assuming the first order reaction and k_{420} and $t_{1/2}$ values were obtained. The Arrhenius plots of k_{420} and T (333–350

K) gave linear trends and the fitted lines gave E_a and A to be E_a = 98 kJ mol^{-1} and $A = 2.7\times10^{9}$ s^{-1}. The obtained k_{420} at 60–80 °C was extrapolated to lower temperatures by the Arrhenius equation. The obtained k_{420} and half-life $t_{1/2}$values at 15 °C were 4.5×10^{-9} s^{-1} and 4.9 years.

REFERENCES

Ajandouz, E. H., V. Desseaux, S. Tazi and A. Puigserver. “Effects of temperature and pH on the kinetics of caramelization, protein cross-linking and Maillard reactions in aqueous model systems”. Food Chem. 2008. 107(3). 1244–1252.

Baisier, W. M. and T. P. Labuza. “Maillard browning kinetics in a liquid model system”. J. Agric. Food Chem. 1992. 40(5). 707–713.

van Boekel, M. A. J. S. “Kinetic aspects of the Maillard reaction: a critical review”. Nahrung 2001. 45(3). 150–159.

Carmona, P. and M. Molina. “Raman and infrared spectra of D-ribose and D-ribose 5-phosphate”. J. Raman Spectrosc. 1990. 21. 395–400.

Davies, C.G.A. and T. P. Labuza. “The Maillard reaction application to confectionery products” in G. Zeigler (Ed.). “Confectionery Science”. Pennsylvania State University Press. 1997. 35–66.

Eisenberg, D. and W. Kauzmann. “Structure and properties of water”. Oxford University Press. 1969.

Finot, P. A. “Historical perspective of the Maillard reaction in food science”. Ann. N. Y. Acad. Sci. 2005. 1043. 1–8.

Ghazala, S., H. S. Ramaswamy, F. R. van de Voort and T. Al-Kanani. “Kinetics of color development in aqueous systems at high temperatures”. J. Food Eng. 1991. 13(2). 79–89.

Ghosh, K. and M. Schnitzer. “UV and visible absorption spectroscopic investigations in relation to macromolecular characteristics of humic substances”. J. Soil Sci. 1979. 30(4). 735–745.

Hodge, J. E. “Dehydrated foods, chemistry of browning reactions in model systems”. J. Agric. Food Chem. 1953. 1(15). 928–943.

Ikeya, K. and A. Watanabe. “Direct expression of an index for the degree of humification of humic acids using organic carbon concentration”. Soil Sci. Plant Nutr. 2003. 49(1). 47–53.

Kitadai, N., T. Yokoyama amd S. Nakashima. “Temperature dependence of molecular structure of

dissolved glycine as revealed by ATR-IR spectroscopy". J. Mol. Struct. 2010. 981. 179–186.

Kumada. K. "Studies on the colour of humic acids". Soil Sci. Plant Nutr. 1965. 11(4). 151–156.

Kumar, S., A. K. Rai, V. B. Singh and S. B. Rai. "Vibrational spectrum of glycine molecule". Spectrochim. Acta Pt. A 2005. 61. 2741–2746.

Otsuka, T. and S. Nakashima. "The Formation of CO_2 by fulvic acid on the surface of goethite studied using ultraviolet and infrared spectroscopy". J. Mineral. Petrol. Sci. 2007. 102. 302–305.

Song, P. S., C. O. Chichester and F. H. Stadtman. "Kinetic behavior and mechanism of inhibition in the Maillard reaction. I. Kinetic behavior of the reaction between D-glucose and glycine". J. Food Sci. 1966. 31(6). 906–913.

Stamp, J. A. and T. P. Labuza. "Kinetics of the Maillard reaction between aspartame and glucose in solution at high temperatures". J. Food Sci. 1983. 48(2). 543–544.

CHAPTER 3

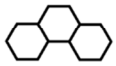

Spectroscopic similarity between humic substances and the simulated Maillard reaction products

This chapter has been modified from the following published paper:

"Non-destructive spectroscopic tracing of simulated formation processes of humic-like substances based on the Maillard reaction"

By Yuki Nakaya, Satoru Nakashima and Mihoko Moriizumi

Applied Spectroscopy, 2018. 72(8). 1189–1198.

3.1. Spectroscopic analyses for the batch solution of the simulated Maillard reaction products by 0.1 mol l^{-1} glycine and ribose solution

3.1.1. Introduction

In Chapter 2, in situ IR and UV–Vis spectroscopic measurements for the Maillard reaction of 0.5 mol l^{-1} glycine + ribose mixture solution at 60–80 °C simulating generation of humic substances were conducted, and kinetic analyses for decreases in the starting material and browning process suggested 90–100 kJ mol^{-1} of activation energies for their reactions. However, spectral changes for 0.5 mol l^{-1} glycine + ribose mixture solution in UV range could not be traced because of spectral saturation even using a 0.05 mm thickness spacer. Therefore, for tracing UV spectral changes, similar measurements at lower initial concentrations are needed. In this section, spectroscopic similarity between humic substances and the simulated Maillard reaction products by 0.1 mol l^{-1} glycine + ribose mixture solution is discussed and validity of UV–Vis spectroscopy is suggested.

UV–Vis spectroscopy has been commonly used not only in food chemistry concerning the Maillard reaction but also in humic substances researches. Although absorption spectra in UV and visible range of humic substances are often featureless (Wang et al, 1990), absorption intensities or their ratios at particular wavelengths were used as surrogate parameters of quantity and property of humic substances. For example, absorbance at 254 nm has been often used as a measure of dissolved organic matter (DOM) (Edzwald et al., 1985) and natural organic matter (NOM) (Korshin et al., 1997). Johnson et al. (2002) used specific UV absorbance per mass of carbon for examining transport behavior of humic substances in aquifer sediment.

On the other hand, three dimensional excitation emission matrix (3D-EEM) fluorescence spectroscopy and size exclusion liquid chromatography (SELC) are also important measurements monitoring humic substances in natural water. Nagao et al. (2003) used high-performance size exclusion chromatography for characterization of humic substances in natural water showing some fluorescence peaks in the range of 250–500 nm of excitation wavelength (Ex.) and 300–600 nm of emission wavelength (Em.). Since it is recently pointed out that destructive procedures such as alkaline extraction or drying for humic substances' analyses may limit precise examination of humic substances (Lehmann and Kleber, 2015), these non-destructive spectroscopic measurements are

expected to provide precise properties of humic substances.

In this section, spectroscopic data obtained by the following non-destructive direct measurements without any additional procedures including drying or extracting the solution is discussed: UV–Vis spectroscopy, 3D-EEM spectroscopy and SELC for batch samples including 0.1 mol l^{-1} glycine + ribose mixture solution heated at 80 °C for 0–168 hours (0–7 days).

In order to examine correlation among spectroscopic data and check validity of using UV–Vis spectra for monitoring progress of the Maillard reaction, generalized two-dimensional correlation spectroscopy (2D-COS) is used. It is a mathematical method to visualize correlation between bands in two series of spectra changing in response to a perturbation, for example time, temperature and composition. The two series of spectra can have the same or different spectral variables (Noda and Ozaki, 2004). Since the first proposal in 1986 (Noda, 1986), the use of 2D-COS in spectroscopy has been increasing (Noda, 2008). Recently in the humic substances' researches, 2D-COS has been introduced for examining the relationships among spectroscopic data concerning humic substances (Hur et al., 2011; Chen et al., 2014). For constructing generalized 2D-COS, dynamic spectra are calculated by subtracting the parent spectra from the reference spectrum (time-average spectrum in the present case). Then, the dynamic spectra measured in time domain are transformed in those in frequency domain by Fourier transform. Another series of dynamic spectra from the reference spectrum (time-average spectrum in the present case) is calculated in the same way. These two series of dynamic spectra are converted to 2D spectra by using a synthesized correlation function. The 2D spectra consist of real and imaginary components derived from the Fourier transform, and the real and imaginary components respectively give synchronous and asynchronous correlation intensity. In a synchronous spectrum, positive (or negative) peaks imply that the pairs of the spectral variable change corresponding to the perturbation in the same (or opposite) direction. In an asynchronous spectrum, if positive (negative) peaks appear at the same position as synchronous correlation peaks, that implies changes at the spectral variable on the horizontal axis occurring earlier (later) than those on the vertical axis.

In order to identify functional groups and chemical compositions of the reaction products, heteronuclear single quantum coherence nuclear magnetic resonance (HSQC-NMR) spectroscopy for products is conducted. HSQC-NMR spectrum is a 2D spectrum having horizontal and vertical axes for chemical shifts in two NMR spectra (in this study, ^{1}H-NMR and ^{13}C-NMR spectra) and indicating their correlation peaks. As another measurement for identification of functional groups, IR spectroscopy for dried products of the reaction is also conducted. In order to estimate molecular weight of the products, matrix assisted laser desorption/ionization time-of-flight mass spectroscopy (MALDI-TOF-MS) is also conducted.

3.1.2. Methods

Sample Preparation

Glycine and ribose solutions (0.2 mol l^{-1}) were prepared respectively by dissolving them in pure water (MilliQ: Resistance > 18.2 MΩ cm). These two solutions were mixed to obtain 0.1 mol l^{-1} glycine plus 0.1 mol l^{-1} ribose solution. This glycine + ribose mixture solution was subdivided into 16 polypropylene micro-tubes containing 1.5 ml of 0.1 mol l^{-1} glycine + ribose solutions. One of them was kept at room temperature (heated for 0 hour) and the others were heated at 80 °C in an electric oven for about 6, 12, 18, 24, 30, 36, 42, 48, 54, 60, 72, 96, 120, 144 and 168 hours in order to accelerate the reaction. After heating at 80 °C for each period, the solution bottles were taken out from the oven and stored in a refrigerator (6 °C). These batch solutions (0.1 ml) were diluted 100 times by pure water (MilliQ) in order to prevent spectral saturation and fluorescence quenching for the following measurements; (1) UV–Vis spectroscopy, (2) 3D-EEM spectroscopy, and (3) SELC. In order to obtain data for larger molecular weight components in the 168 hour heated products, another 0.1 mol l^{-1} glycine + ribose mixture solution heated at 80 °C for 168 hours was put into a dialysis tube (Molecular weight cutoff (MWCO): 3500 Da, in pure water buffer) for 24 hours and dialyzed to obtain fractions over 3500 Da. Here, it is called “dialyzed solution”.

UV–Vis Spectroscopy

UV–Vis spectra for the sample solutions heated for 0–168 hours and the dialyzed solution were measured in a quartz cell (optical pass length: 10 mm) by an UV–Vis spectrometer (V570, Jasco). Pure water was measured as a background spectrum, and then the diluted sample solutions were measured. UV–Vis spectra were measured at a scanning speed of 400 nm min^{-1} with a resolution of 1.0 nm in the 190–1100 nm spectral range.

3D-EEM Spectroscopy

Three dimensional excitation emission matrix spectra for the sample solutions heated for 0–168 hours and the dialyzed solution were measured in a fluorescence quartz cell (optical pass length: 2 mm, width: 10 mm) by a three-dimensional fluorescence spectrometer (F7000, HITACH). Excitation wavelength (Ex.) was 250–500 nm (excitation slit: 5 nm) and emission wavelength (Em.) was 300–600 nm (emission slit: 5 nm). Scanning speed was 2400 nm min^{-1} at 5 nm intervals and photomultiplier voltage was 400 V. All of the spectra were corrected based on rhodamine B spectrum.

SELC

SELC for the sample solutions heated for 0–168 hours was conducted by using a high performance size exclusion liquid chromatography (HPLC-SEC) unit (EXTREMA, Jasco) and a SEC column (YMC-Pack Diol 120, YMC, 35 °C). 50 mM sodium acetate/acetic acid solution (pH = 7) was used as a common eluent. The injection volume was 100 µl, the flow rate was 1 ml min^{-1}, and the analysis time was 30 min for each sample. The SEC column and experimental condition were the same as Moriizumi and Matsunaga (2011). Positions of void volume (V_0: retention time 5.5 minutes), total effective column volume (V_e: retention time 12.2 minutes) and retention time of molecular weight standards (ovalbumin: 42 kDa; myoglobin: 17 kDa) in their report are marked in the obtained chromatograms for reference. Because these protein standards and the Maillard reaction products are considered to have different molecular shapes and electrical properties, it should be noted that these values cannot be directly compared. Chromatograms were recorded with a UV detector (UV4070, Jasco) at 280 nm without baseline correction and a fluorescence detector (FP4025, Jasco) at Ex. 345 nm/Em. 430 nm. Obtained data were analyzed by a commercial software (Chromato-Pro, Runtime Instruments).

2D-COS

Generalized 2D-COS was conducted on UV–Vis spectra, emission spectra at a certain excitation wavelength in 3D-EEM spectra and SEC chromatograms for the batch solutions. The spectra were generated by using a free software available at https://sites.google.com/view/shigemorita/home/2dshige (last accessed date; February 4, 2019), 2DShige (Shigeaki Morita, Kwansei-Gakuin University, 2004–2005).

HSQC-NMR Spectroscopy

HSQC-NMR spectra for the product solutions (heated for 168 hours, undiluted) and controls (0.1 mol l^{-1} glycine and ribose solutions) were measured on AVANCE700 (Bruker) with 5 mm TCI Cryoprobe at 25 °C. The samples were diluted 10 times by D_2O and analyzed. Measurement times were 88 hours for the product solution and 11 hours for the controls.

IR Spectroscopy

In order to obtain IR spectra for the product solutions heated for 168 hours, the dialyzed solution and controls (0.1 mol l^{-1} glycine + ribose mixture solution), an FTIR micro-spectrometer

(FTIR620+IRT30, Jasco) was used. 10 µl of the sample solution were dried for 3 hours on an Al foil and transmission reflection (transflection) spectra of the dried samples were obtained. IR spectra were measured with a wavenumber resolution of 4 cm^{-1} and 64 scans in the 400–4000 cm^{-1} spectral range.

MALDI-TOF-MS

The MALDI-TOF mass spectra for the product solutions heated for 168 hours and the dialyzed solution were recorded in a positive mode on AXIMA-CFR (Shimadzu/Kratos) in a linear mode, controlled by the KOMPACT 2.3.5 software package. External calibration of MALDI mass spectra was carried out using the monoisotopic peaks of a mixture of Bradykinin 1–7 (*m*/*z* 757.40), Angiotensin II (*m*/*z* 1046.54), Angiotensin I (*m*/*z* 1296.68), Substance P (*m*/*z* 1347.74), Bombesin (*m*/*z* 1619.82), Renin Substrate (*m*/*z* 1758.93), ACTH clip 1–17 (*m*/*z* 2093.09), ACTH 18–39 (*m*/*z* 2465.20) and Somatostatin 28 (*m*/*z* 3147.47). In order to prepare the target sample, the product solution (heated for 168 hours, undiluted) and a matrix (1 mg ml^{-1} sinapinic acid methanol solution) were mixed at a ratio of 1:1 and they were air-dried.

3.1.3. Results

UV–Vis spectroscopy

Representative UV–Vis spectra for 0.1 mol l^{-1} glycine + ribose mixture solutions heated at 80 °C for 0, 24, 48, 72, 96, 120, 144 and 168 hours (diluted 100 times) are shown in Fig. 3.1.1a. A band around 280 nm increased with time. Moreover, absorbance at shorter wavelength increased more for longer heating durations. Fig. 3.1.1b shows a spectrum for the solution heated for 168 hours and that after dialysis (> 3500 Da). Absorption in the UV region generally decreased after dialysis, in particular around 280 nm. However, in the visible region, broad and featureless absorption remained.

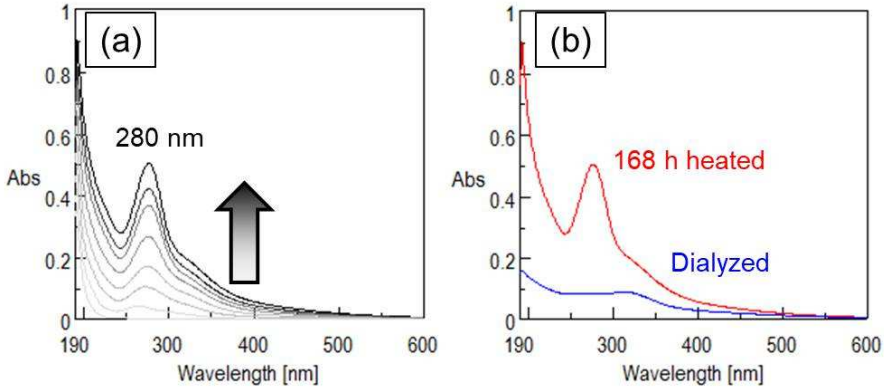

Fig. 3.1.1. (a) Representative UV–Vis spectra for the product solutions of 0.1 mol l^{-1} glycine + ribose mixture solutions heated at 80 °C for 0, 24, 48, 72, 96, 120, 144 and 168 hours (diluted 100 times) and (b) spectra for the 168 hours heated solution and for the dialyzed solution (> 3500 Da) (diluted 100 times).

3D-EEM Spectroscopy

Representative 3D-EEM spectra for 0.1 mol l^{-1} glycine + ribose mixture solutions heated at 80 °C for 0, 96 and 168 hours (diluted 100 times) and the dialyzed solution are shown in Fig. 3.1.2a, b, c and d respectively. Fluorescence maxima at Ex. 345 nm/Em. 430 nm can be recognized for spectra at 96 and 168 hours (Fig. 3.1.2b and c). 3D-EEM spectrum for the 168 hours heated solution after dialysis showed almost no fluorescence (Fig. 3.1.2 d).

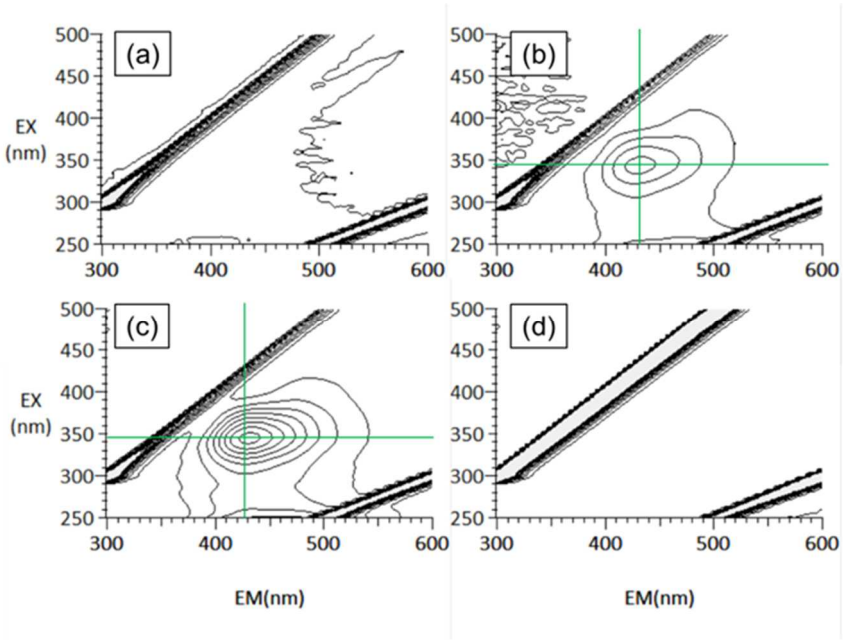

Fig. 3.1.2. Representative 3D-EEM spectra for the 0.1 mol l^{-1} glycine + ribose mixture solutions heated at 80 °C for (a) 0, (b) 96 and (c) 168 hours, and (d) the dialyzed solution. All the solutions were diluted 100 times. Contour intervals are 2.5 intensity units. Fluorescence intensity maximum positions at Ex. 345 nm/Em. 430 nm are indicated.

Size Exclusion Liquid Chromatography

Representative size exclusion liquid chromatograms by 280 nm absorbance on the product solutions show, from left to right, large (5.7 minutes), medium (10, 11 minutes) and small (18.8 minutes) molecular weight components based on markers (ovalbumin: 42 kDa; myoglobin: 17 kDa) (Fig. 3.2.2a). It should be noted that this chromatogram can include not only the peak around 280 nm but also a tail of broad absorption in the ultraviolet range because the detection was without baseline correction. On the other hand, representative chromatograms by fluorescence intensity at Ex. 345 nm/Em. 430 nm show peaks around retention time of 10 to 17 minutes (Fig. 3.1.3b), corresponding to medium molecular weights observed by 280 nm absorbance chromatograms (Fig. 3.1.3a).

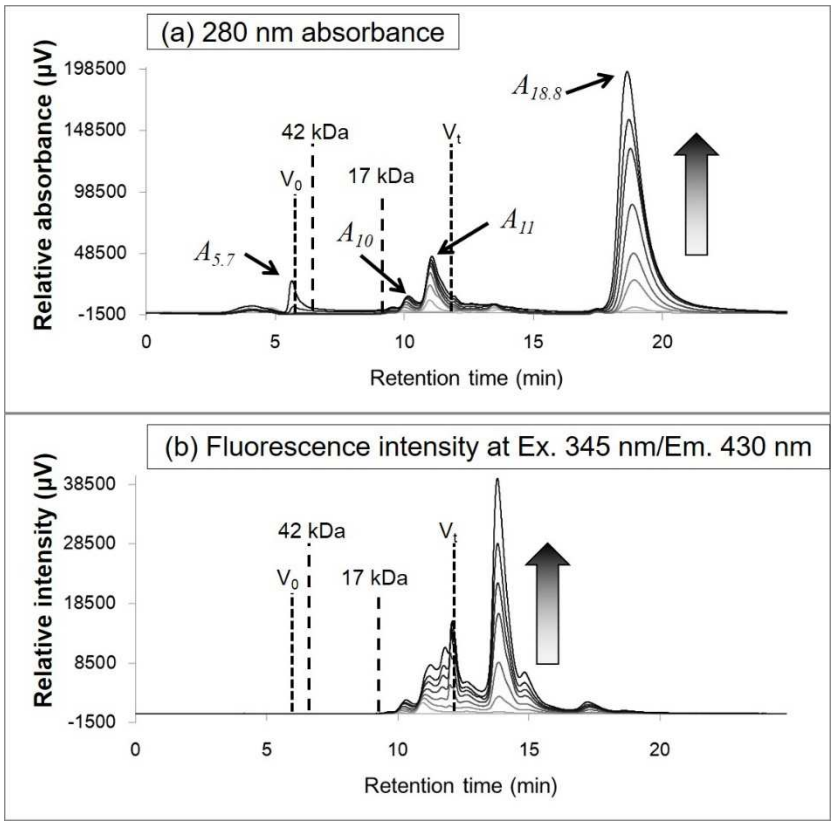

Fig. 3.1.3. Representative chromatograms by (a) 280 nm absorbance and (b) fluorescence intensity at Ex. 345 nm/Em. 430 nm on the product solutions of 0.1 mol l^{-1} glycine + ribose mixture solutions heated at 80 °C for about 0, 24, 48, 72, 96, 120, 144 and 168 hours (100 times diluted solutions further diluted 10 times by an eluent).

2D-COS

Generalized 2D synchronous and asynchronous spectra were generated from UV–Vis spectra, emission spectra at a certain excitation wavelength in 3D-EEM spectra and SEC chromatograms for the batch solutions by using 2DShige.

Generalized 2D synchronous correlation UV–Vis spectra for the product solutions of 0.1 mol l^{-1} glycine + ribose mixture solutions heated at 80 °C for 0–168 hours (batch solutions) show generally strong positive correlations around 200 and 280 nm (red portions in Fig. 3.1.4a). Asynchronous correlation spectra indicate sequential order of spectral changes: absorption around 320 nm firstly increased and 200, 280 and >350 nm absorption followed in this order (from reddish to bluish regions in Fig. 3.1.4b).

Fig. 3.1.4c and d show generalized 2D (c) synchronous and (d) asynchronous correlation spectra (horizontal axis: UV–Vis spectra, vertical axis: emission spectra excited at 345 nm), respectively. The fluorescence maxima around 430 nm has strong correlations to absorbance around 200 and 280 nm (Fig. 3.1.4c). This correlation extends to 500 nm in the visible region. In asynchronous correlation spectra, the fluorescence maxima around 430 nm increases at the same time as absorptions around 250 nm and 400 nm (white regions in Fig. 3.1.4d). Although changes in the emission spectra excited at 345 nm are assumed to have correlation with UV absorbance changes at 345 nm, Fig. 3.1.4c showed the relatively weak correlation among them. This is possibly because the fluorescent components less contributed to UV–Vis spectra than other UV absorbing components. In fact, the fluorescent components having chromatographic peaks around retention time of 10 to 17 minutes (Fig. 3.1.3b) show much weaker absorption at 280 nm than the components at retention time of 18.8 minutes (Fig. 3.1.3a) contributing mainly to changes in the 280 nm absorption band.

UV–Vis absorbances around 280 nm on the horizontal axis were determined as spectra above the baseline (245–315 nm) (Fig. 3.1.1a). Generalized 2D (e) synchronous and (f) asynchronous correlation spectra (horizontal axis: spectra around 280 nm above the baseline (245–315 nm), vertical axis: chromatograms by 280 nm absorbance) are shown in Fig. 3.1.4e and f. The chromatograms around retention time of 5.7, 10, 11 and 18.8 minutes ($A_{5.7}$, A_{10}, A_{11} and $A_{18.8}$) show synchronous correlations around 260-300 nm (Fig. 3.1.4e). A_{10} and A_{11} increase earlier than UV–Vis spectral changes and $A_{5.7}$ and $A_{18.8}$ increase later (blue and red regions in Fig. 3.1.4f, respectively). The spectra around 280 nm above the baseline show strong and simultaneous correlations with $A_{18.8}$ (red region in Fig. 3.1.4e and white region in Fig. 3.1.4f, respectively).

Generalized 2D synchronous correlation spectra (horizontal axis: UV–Vis spectra, vertical axis: chromatograms by fluorescence intensity at Ex. 345 nm/Em. 430 nm) indicate that the components with 10–17 minutes retention time show strong correlation with 200-300 nm absorbance (red regions in Fig. 3.1.4g). Asynchronous correlation spectra indicate earlier increases than UV–Vis spectral

changes for the components with retention times at 10 and 11 minutes (blue regions in Fig. 3.1.4h). The components with longer retention time (12–17 minutes) show later changes (red regions in Fig. 3.1.4h).

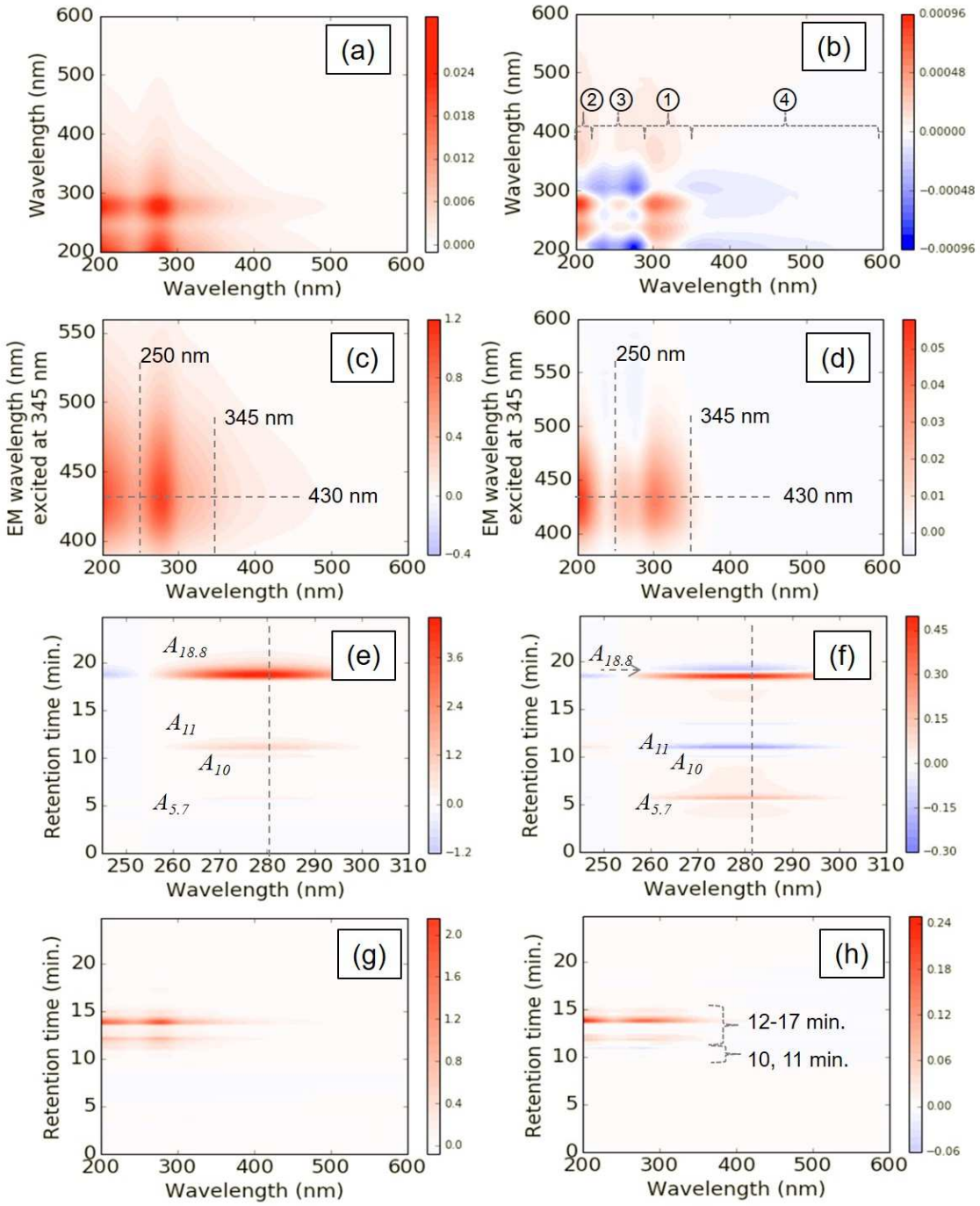

Fig. 3.1.4. Generalized 2D (a) synchronous and (b) asynchronous correlation UV–Vis spectra for the product solutions of 0.1 mol l^{-1} glycine + ribose mixture solutions heated at 80 °C for 0–168 hours. Numbers of the regions in (b) corresponds to the order of spectral changes. Generalized 2D (c)

synchronous and (d) asynchronous correlation spectra (horizontal axis: UV–Vis spectra, vertical axis: emission spectra excited at 345 nm) for the product solutions of 0.1 mol l^{-1} glycine + ribose mixture solutions heated at 80 °C for 0–168 hours. Generalized 2D (e) synchronous and (f) asynchronous correlation spectra (horizontal axis: spectra around 280 nm above the baseline (245–315 nm), vertical axis: chromatograms by 280 nm absorbance). Generalized 2D (g) synchronous and (h) asynchronous correlation spectra (horizontal axis: UV–Vis spectra, vertical axis: chromatograms by fluorescence intensity at Ex. 345 nm/Em. 430 nm). Color scale bars are indicated for each figure. These scales are variation ranges of each correlation and cannot be compared each other.

HSQC-NMR Spectroscopy

HSQC-NMR spectra for 0.1 mol l^{-1} solutions of (a) glycine, (b) ribose and (c) 0.1 mol l^{-1} glycine + ribose mixture solution heated at 80 °C for 168 hours are shown in Fig. 3.1.5. The spectrum for 168 hours heated solution (Fig. 3.1.5c) shows peaks of glycine (light green) and ribose (red) together with some new peaks. Circles indicate characteristic areas for aliphatic CH_2 and CH_3 and aromatic CH (Stevenson, 1994). The other peaks with gray arrows are folded peaks for the products; chemical shift for ^{13}C are 170 and 185 ppm, respectively. Peaks forming vertical (^{1}H: 3.5 ppm) and horizontal (^{13}C: 40 and 60 ppm) lines are noise peaks.

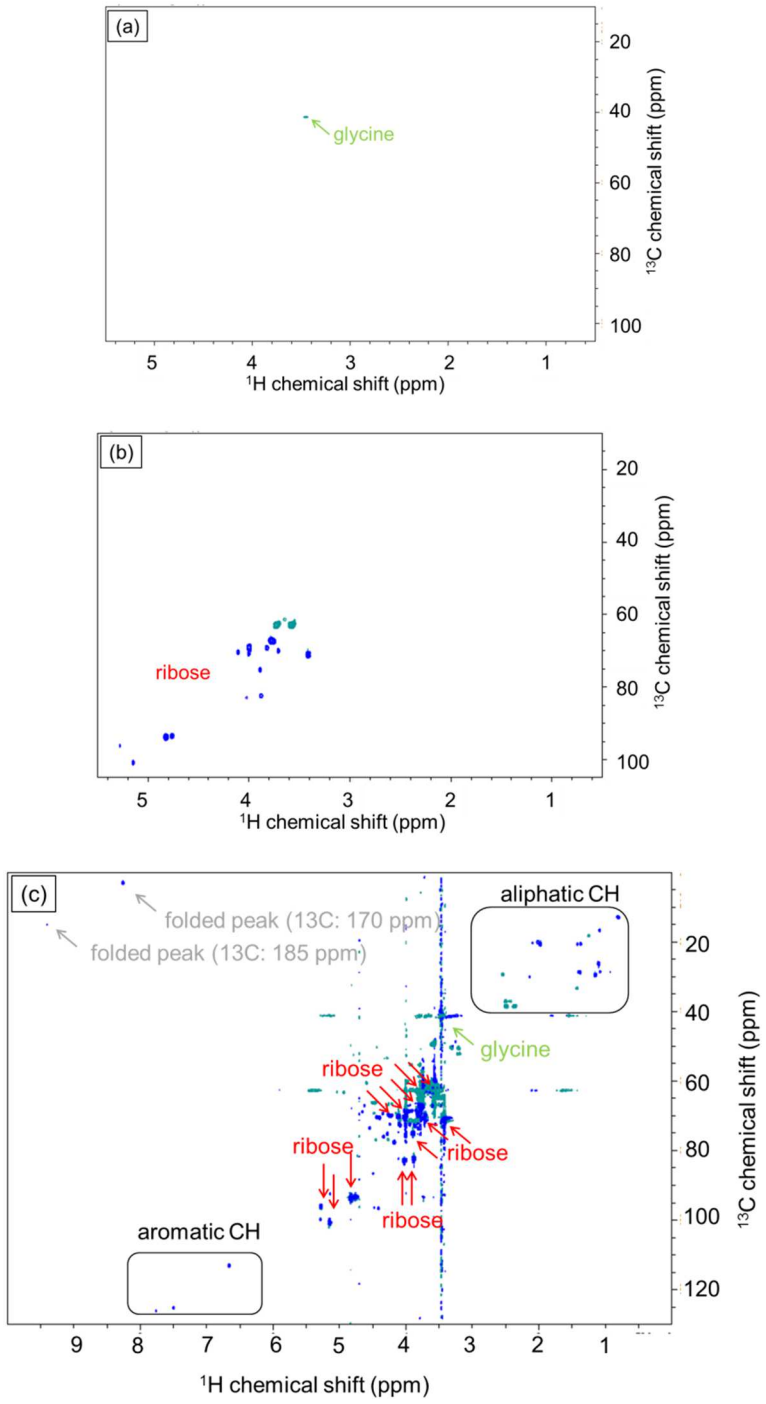

Fig. 3.1.5. HSQC-NMR spectra for 0.1 mol l^{-1} solutions of (a) glycine, (b) ribose and (c) 0.1 mol l^{-1} glycine + ribose mixture solution heated at 80 °C for 168 hours. Peak positions of glycine and ribose are indicated. Circled areas are for aliphatic CH_2 and CH_3 and aromatic CH. Folded peaks for the products are indicated by gray arrows.

IR Spectroscopy

IR spectrum for the dried sample of glycine + ribose mixture solution (heated for 0 hours: before the reaction) (Fig. 3.1.6a) showed ribose bands around 1100 cm^{-1} and glycine bands at 1248, 1322, 1405, 1504 and 1620 cm^{-1} (Section 2.1). The absorption band at 1620 cm^{-1} is considered to correspond to COO^- asymmetric stretching of glycine (Kitadai et al., 2010). IR spectrum for the dried sample of 168 hours heated solution (Fig. 3.1.6b) showed peaks mainly from glycine and ribose. Because of relatively strong absorptions of glycine and ribose, almost no significant peak of the products could be recognized. IR spectrum for the dried sample of the dialyzed solution (Fig. 3.1.6c) showed almost no glycine and ribose absorptions around 1100, 1248, 1322, 1405, 1504 and 1620 cm^{-1}. This can be explained by escape of glycine and ribose due to dialysis of small components (>3500 Da). On the other hand, this spectrum showed an absorption at 1728 cm^{-1} corresponding to COOR groups, and absorptions at 2848, 2915 and 2954 due to aliphatic CH stretching (Stevenson, 1994).

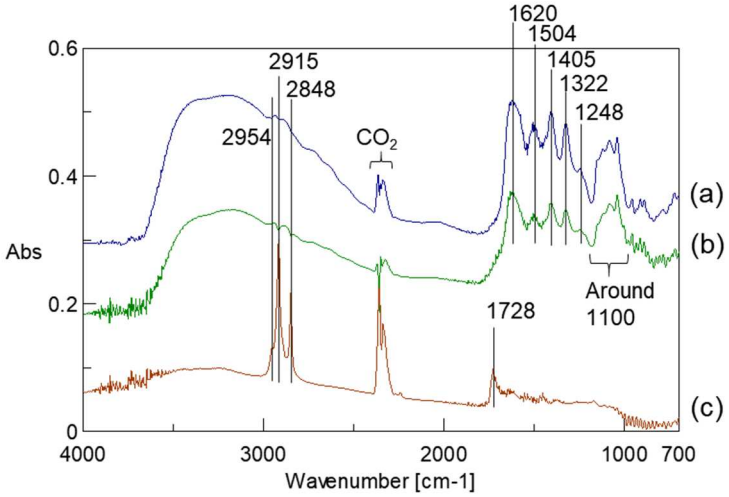

Fig. 3.1.6. IR spectra for the dried samples of (a) 0.1 mol l^{-1} glycine + ribose mixture solution (heated for 0 hour), (b) the product solution heated at 80 °C for 168 hours and (c) the dialyzed solution. Absorptions around 2350 cm^{-1} are considered to be due to CO_2 in the optical path of the spectrometer.

MALDI-TOF-MS

Mass spectra for the 0.1 mol l^{-1} glycine + ribose mixture solution heated at 80 °C for 168 hours (red) and its dialyzed solution (> 3500 Da) (blue) are shown in Fig. 3.1.7a *m/z*: 0–1000, and b *m/z*: 0–300). Weak peaks at *m/z* at 97.77 and 172.71 (indicated in Fig.3.1.7a and b) were considered to be due to sodium adducted ions of glycine (calculated value: 98.02) and ribose (calculated value: 173.04). Strong peaks at *m/z* at 224.44 and 206.45 (indicated in Fig. 3.1.7a) are due to the matrix of sinapinic acid and its dehydrate, respectively. The other peaks can be due to products and their fragment ions. Peaks at *m/z*: 66–69 are indicated in Fig. 3.1.7b, which can be due to fragment ions of furfural (NIST Chemistry WebBook, NIST Standard Reference Database 69: http://webbook.nist.gov/cgi/cbook.cgi?ID=C98011&Units=SI&Mask=200#Mass-Spec (last accessed date: February 4, 2017)), one of reported intermediates of the Maillard reaction (Hodge, 1953). In spite of the presence of medium and high molecular weight components indicated by SEC measurements (Fig. 3.1.3), mass spectrum for 168 hours heated solution showed no significant peaks in higher *m/z* region (>1000).

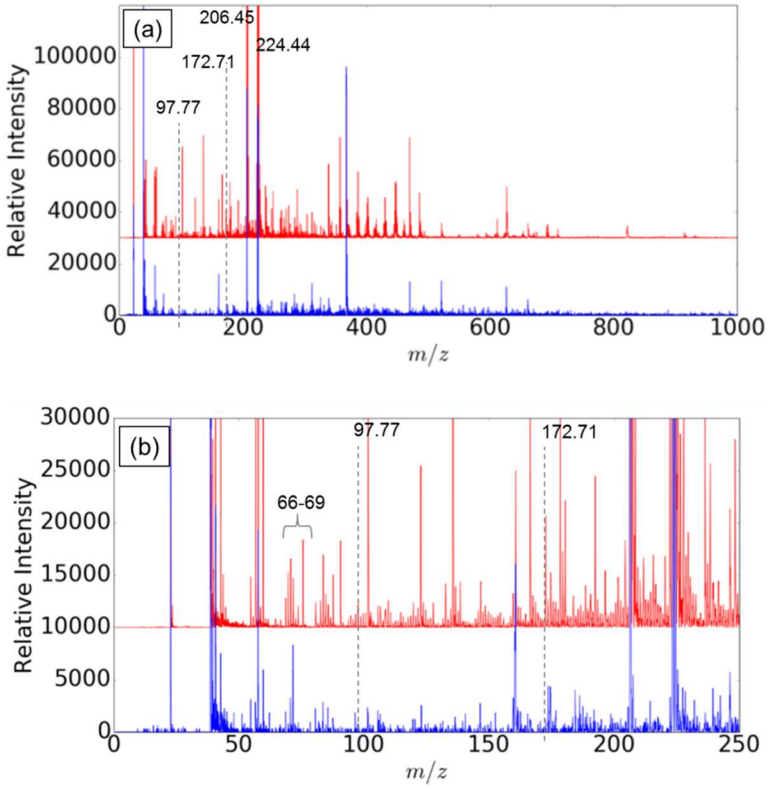

Fig. 3.1.7. Mass spectra ((a) *m/z*: 0–1000, (b) *m/z*: 0–300) for 0.1 mol l^{-1} glycine + ribose mixture solutions heated at 80 °C for 168 hours (red) and the dialyzed solution (> 3500 Da) (blue).

3.1.4. Discussion

Increases in the products during the heating of glycine and ribose mixed solution (0.1 mol l^{-1}) were quantitatively traced by UV–Vis and 3D-EEM spectroscopy and SELC (Figs. 3.1.1–3). These measurements did not require any additional procedures including drying or extracting the solution. In the following, implications of these spectral changes including their 2D correlation spectroscopic analyses are discussed.

UV–Vis spectra (Fig. 3.1.1a) and chromatograms by 280 nm (Fig. 3.1.3a) suggested the formation with time of small components with 280 nm absorption. These are considered to include furfural, which has an absorption peak around 280 nm (Martinez et al., 2000). The disappearance of peak at 280 nm in the spectrum of the dialyzed solution (> 3500 Da) (Fig. 3.1.1b) can be understood by the small size of furfural.

By 2D correlation spectroscopic analyses, a band around 280 nm above the baseline of 245–315 nm was suggested to be taken as a measure of the intermediates including furfural (Fig. 3.1.4e and f). Spectral changes in the visible region (> 350 nm: browning) followed after the 280 nm increases (Fig. 3.1.4d). Therefore, in this study, the band area around 280 nm with a baseline of 245–315 nm (UV_{280}) is used for kinetic analyses of the formation of furfural-like intermediates in Section 3.2.

On the other hand, humic-like products were indicated by UV–Vis spectra (Fig. 3.1.1), 3D-EEM spectra (Fig. 3.1.2) and chromatograms by fluorescence intensity at Ex. 345 nm/Em. 430 nm (Fig. 3.1.3b). The fluorescence maxima in Figs. 3.1.3a, b and c resembled to those of natural humic solutions reported in a previous research (Nagao et al., 2003). Therefore, humic-like fluorescent products are considered to be produced from glycine and ribose by heating them at 80 °C. HSQC-NMR spectra (Fig. 3.1.5c) indicated the humic-like products might include aliphatic and aromatic components. Although size exclusion liquid chromatograms (Fig. 3.1.3b) indicated medium and high molecular weight components, the dialyzed solution (> 3500 Da) did not show fluorescence (Fig. 3.1.2d) and mass spectra did not indicate products larger than 3500 Da. This can be due to supramolecular property of the humic-like products: aggregations of some smaller products via intermolecular interactions such as hydrogen bonding and Van der Waals forces (Piccolo, 2001; Sutton et al., 2005).

By 2D correlation spectroscopic analyses, it was suggested that 250 nm absorbance and visible absorbance can be employed as a measure of the humic-like products with fluorescence. In this study, 254 nm absorption with a one-point base at 600 nm (UV_{254}) is used for kinetic analyses of the formation of humic-like products in Section 3.2. It should be noted that UV_{254} include not only tails of 280 nm absorption band but also broad UV tails (Fig. 3.1.1).

Other components at retention times at 5.7 and 10–17 minutes (Fig. 3.1.4e, f, g and h) could not be assigned to UV–Vis spectral changes. It should be noted that changes in chromatograms at retention time 5.7 and 12–17 minutes were later than UV–Vis spectral changes and those at 10 and 11 minutes

were earlier. Moreover, no shift in the chromatographic peaks (no shift in the molecular weight) may imply increases with time in similar molecular weight components (Fig. 3.1.3a and b).

Since the Maillard reaction has many pathways and products possibly including non-UV-active and non-fluorescent products (Hodge, 1953), some components in the Maillard reaction cannot be traced by UV–Vis and fluorescence spectroscopy.

In order to characterize the products, we tried additional HSQC-NMR spectroscopy, IR spectroscopy and MALDI-TOF-MS (Figs.3.1.6–8). The batch experiments indicated that some reactions occurred generating new products including aliphatic and/or aromatic compounds and furfural. IR, NMR and MS analyses showed that starting glycine and ribose still remained in the 168 hours heated solution. HSQC-NMR spectra (Fig. 3.1.6) could not determine precise structures of products since the sample solution was mixture of the reactants, products and fragments. However, they indicated that the Maillard reaction of glycine and ribose produced aliphatic and/or aromatic compounds. Strong IR absorptions from glycine and ribose prevented detection of products in IR spectra. Mass spectra could not provide clear *m*/*z* values of products because of very complex multiple peaks. In particular, products with an *m*/*z* larger than 1000 could not be identified in the mass spectra. Moreover, the mass spectrum of the dialyzed solution (> 3500 Da) also did not show the larger products. Despite these difficulties, mass spectra (Fig. 3.1.7) indicated at least the production of furfural. IR, NMR and MS analyses thus indicated the presence of aliphatic, aromatic components and furfural together with residual glycine and ribose. To summarize, many components and residual reactants, glycine and ribose in the product solution prevented accurate measurements and they provided little information on details of products, except for the results that the products may include aliphatic and aromatic components. These are difficulties of characterizing complex products of simulated geochemical processes.

3.2. In situ ultraviolet–visible spectroscopy for the Maillard reaction by 0.1 mol l^{-1} glycine and ribose solution

3.2.1. Introduction

In the above section (Section 3.1), the formation processes of humic-like substances were simulated by heating glycine and ribose mixed solution (0.1 mol l^{-1}) at 80 °C through the Maillard reaction. Increases in the products during the heating of glycine and ribose mixed solution (0.1 mol l^{-1}) were quantitatively traced by UV–Vis and 3D-EEM spectroscopy and SELC. Two-dimensional correlation spectroscopic analyses suggested that a band area around 280 nm (UV_{280}) and 254 nm absorbance (UV_{254}) can be used as measures of the formation of furfural-like intermediates and humic-like products, respectively.

In order to evaluate precise kinetic data for the progress of the Maillard reaction by using 280 nm and 254 nm absorbances, in situ UV–Vis spectroscopy with the original heatable liquid cell (Sections 2.1 and 2.2) was conducted on 0.1 mol l^{-1} glycine + ribose mixture solutions heated at 60, 65, 70, 75 and 80 °C for 0–144 hours, for accelerating the reaction. Changes with time in UV_{280} and UV_{254} were fitted by the first order reaction equation and their kinetic parameters were estimated.

3.2.2. Methods

In order to prevent spectral saturation in UV region, PTFE spacers of 0.1 mm thick were selected for in situ UV–Vis spectroscopy of 0.1 mol l^{-1} glycine + ribose mixture solutions heated at 60, 65, 70, 75 and 80 °C for 0–144 hours. They were made from commercial PTFE sheets (AS ONE, 7-358-02) by piercing them with punches of 12 mm (outside diameter) and 8 mm (inside diameter). 0.2 mol l^{-1} glycine and 0.2 mol l^{-1} ribose solutions were prepared by dissolving them in pure water (MilliQ). These solutions and pure water were mixed to obtain 0.1 mol l^{-1} glycine + ribose mixture solutions. About 3 µl of the solution was injected in the sample chamber of the liquid cell.

The glycine + ribose mixture solutions (0.1 mol l^{-1}) were heated at 80, 75, 70, 65 and 60 °C for 144 hours (6 days) in an UV–Vis spectrometer (V530, Jasco). In order to examine reproducibility, 80 °C measurement was conducted three times. The heatable liquid cell was mounted on the sample position of the UV–Vis spectrometer and the reference position was left blank. UV–Vis spectra were measured every 5 minutes at a scanning speed of 400 nm min^{-1} with a resolution of 1.0 nm in the 200–1100 nm spectral range.

3.2.3. Results

Representative UV–Vis spectra for 0.1 mol l^{-1} glycine + ribose mixture solutions heated at 80 °C for 0–144 hours are shown Fig. 3.2.1. The intensity of a band around 280 nm increased with time, in the same way as the batch experiments.

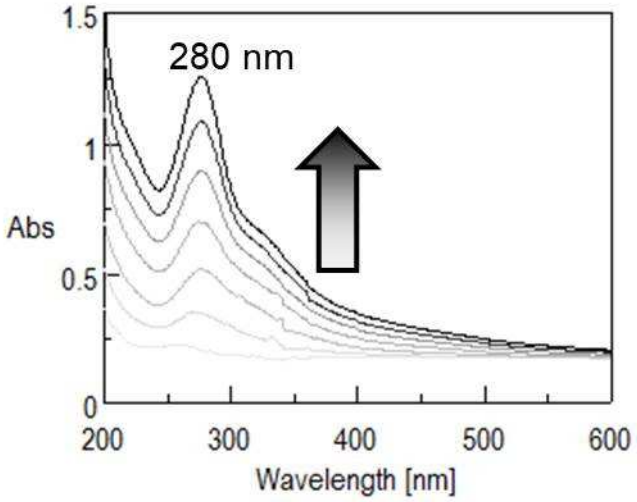

Fig. 3.2.1. Representative in situ UV–Vis spectra for the product solutions of 0.1 mol l^{-1} glycine + ribose mixture solutions heated at 80 °C for about 0, 24, 48, 72, 96, 120 and 144 hours.

It should be noted that the batch measurements in Section 3.1 were done on 10 mm cell for 100 times diluted solutions, while the in situ measurements were on about 0.1 mm thickness with initial solutions. Therefore, absorbance values by the both methods can be expected to be in the same order. However, 280 nm absorbance on the 144 hours spectrum in the in situ measurements at 80 °C (Fig. 3.2.1) are about 2.5 times larger than those in the batch experiments (Fig. 3.1.1). These differences are considered to be due to thicker solution thicknesses than the spacer of the in situ cell and the different references (blank for in situ vs. pure water for batch). The solution escape from the same in situ cell were considered to be minor by the IR spectroscopy showing the stable absorbance of water around 5200 and 7000 cm^{-1} (Chapter 2). Unfortunately, absorption by water at 960 nm in the near-IR range was too weak to be monitored for the water loss. It should be also noted that glycine only and ribose only solutions showed almost no absorption increase in the UV–Vis range at 80 °C.

3.2.4. Discussion

UV–Vis spectra of 0.1 mol l^{-1} glycine + ribose mixture solutions heated at 60, 65, 70, 75 and 80 °C for 0-144 hours were obtained. The continuous measurements at a short time interval (5 minutes) and the stability of temperature (±1 °C) of the present in situ spectroscopy enable detailed quantitative analyses of kinetic data. Changes with time (t (s)) in band area around 280 nm with baseline of 245–315 nm (UV_{280}) and absorbance at 254 nm with one point base at 600 nm (UV_{254}) were calculated. To simplify kinetic analyses, their starting values (t = 0) were respectively subtracted from all of UV_{280} and UV_{254} values. Changes in (a) UV_{280} and (b) UV_{254} with time during the in situ measurements at each heating temperature are plotted in Fig. 3.2.2a, b. These changes can be divided into the early induction stage and the later progress stage (van Boekel, 2001). In this study, the later stage where UV_{280} >1 or UV_{254} > 0.05 were fitted as steady changing states for kinetic analyses. The changes in the later stage were fitted by the first order fittings after the kinetic analyses for changes in 420 nm absorbance by the Maillard reaction of 0.5 mol l^{-1} glycine + ribose mixture solutions (Section 2.2) for possible comparison of rate constant values (unit: s^{-1}) and easiness of using half-life values.

The preliminary fittings of the data were firstly conducted on the changes at 80 °C by

$$UV_{280} = C_1\left(1 - \exp\left(-k_{280}(t-\tau)\right)\right) \quad \text{(eq. 3.2.1)}$$

$$UV_{254} = C_1(1 - \exp\left(-k_{254}(t-\tau)\right)) \quad \text{(eq. 3.2.2)}$$

where fitting parameters were C_1, apparent first order reaction rate constants k_{280} and k_{254} and τ. Since 80 °C in situ measurement was conducted three times for replicability, the parameters were optimized as for all three data to be fitted. The values of C_1 were 47.0 for UV_{280} and 11.5 for UV_{254}. The values of τ were 7880 s for UV_{280} and 29400 s for UV_{254}. Secondly, the changes at 80 °C were fitted by eq. 3.2.1 and 3.2.2 using the fixed C_1 and τ, and k_{280} and k_{254} were obtained for each changes at 80 °C. For fittings on the changes at 60, 65, 70 and 75 °C, eq. 3.2.1 and 3.2.2 with the fixed C_1 and fitting parameters of k_{280}, k_{254} and τ were used. The fitting curves are shown in Fig. 3.2.2 on the UV_{280} and UV_{254} changes. k_{280}, k_{254}, τ and correlation coefficient r values obtained by the first order fittings are listed in Table 3.2.1.

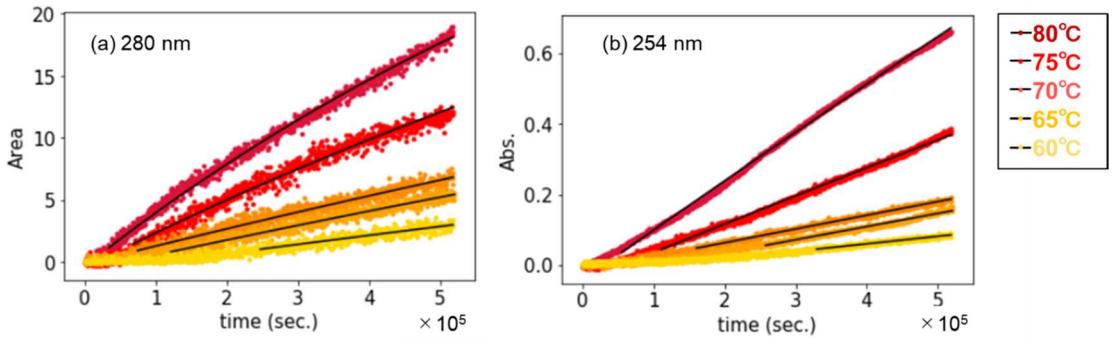

Fig. 3.2.2. Changes in (a) UV_{280} and (b) UV_{254} with time during the in situ measurements of 0.1 mol l^{-1} glycine + ribose mixture solutions heated at 60, 65, 70, 75, and 80 °C with the fitting curves (the first order reaction).

Table 3.2.1. The values of k_{280}, k_{254}, τ and correlation coefficient r values of the first order reaction fittings in the heating experiments of 0.1 mol l^{-1} glycine + ribose mixture solutions at 60, 65, 70, 75 and 80 °C.

		80 °C[1]	80 °C[2]	80 °C[3]	75 °C	70 °C	65 °C	60 °C
(a)	k_{280}	9.55×10^{-7}	1.02×10^{-6}	1.01×10^{-6}	6.13×10^{-6}	3.09×10^{-6}	2.64×10^{-6}	1.61×10^{-6}
280	τ	(7880)	(7880)	(7880)	16700	10600	55000	110000
nm	r	1.00	1.00	1.00	1.00	0.998	0.999	0.970
(b)	k_{254}	1.23×10^{-7}	1.21×10^{-7}	1.16×10^{-7}	7.02×10^{-8}	3.39×10^{-8}	3.25×10^{-8}	1.85×10^{-8}
254	τ	(29400)	(29400)	(29400)	55500	36700	107000	115600
nm	r	1.00	1.00	1.00	1.00	1.00	0.999	0.993

The obtained apparent reaction rate constants increased with heating temperatures. They can be described by the Arrhenius equation (eq. 2.1.2).

$$\ln k = \ln A - \frac{E_a}{RT} \quad \text{(eq. 2.1.2)}$$

The Arrhenius plots of k_{280} and k_{254} and T (333–350 K) (Fig. 3.2.3) show relatively good linear trends, where average values of ln k at 80 °C are employed and their standard deviations (0.027 for ln k_{280} and 0.024 for ln k_{254} at 80 °C) are indicated by error bars. The fitting lines of these experimental data gave the E_a and A values for the reactions in the first reaction stages of 280 nm band area and 254 nm absorbance during the heating of 0.1 mol l^{-1} glycine + ribose mixture solutions (Table 3.2.2). The absorbance at 254 nm with one point base at 600 nm can reflect not only the shoulder of 280 nm peak but also a tail of broad UV absorptions. In fact, the first order rate constants for increases in the band area around 280 nm (k_{280}) are larger than those for the 254 nm absorbance (k_{254}) with a slight difference

in the activation energy values (E_a) (Tables 3.2.1 and 2, and Figs.3.2.2 and 3). The obtained E_a and A values enabled extrapolation of k_{280} and k_{254} values to lower and higher temperatures by the Arrhenius equation (Eq. 2.1.2). For example, k_{280} and k_{254} values at 15 °C were estimated to be 1.1×10^{-9} s^{-1} and 1.3×10^{-10} s^{-1}, respectively. They also gave 20 and 174 years of half-lives for k_{280} and k_{254} values at 15 °C.

In addition, the induction time τ can be also a kinetic parameter determining time scales of the reaction. Assuming that τ values reflect periods of the induction stage, pseudo reaction rate constants in the induction stage (k^{ind}_{280} and k^{ind}_{254}) can be defined by $1/\tau$. Their Arrhenius plots and fitting by the Arrhenius equation (Eq. 2.1.2) (Fig. 3.2.3) gave E_a and A values for reactions in the induction stage (Table 3.2.2). From extrapolation of k^{ind}_{280} and k^{ind}_{254} values to 15 °C by the Arrhenius equation (Eq. 2.1.2), the periods in the induction stage were estimated to be 2.57 and 0.11 years for UV_{280} and UV_{254}, respectively. These are much shorter than in the later apparent first order reaction progress stage and time scales of the whole reaction may be controlled by the later stage. The present spectroscopic method and obtained kinetic parameters can be used in evaluating time scales of the Maillard reaction both in Earth surface environment and food chemistry with further detailed studies.

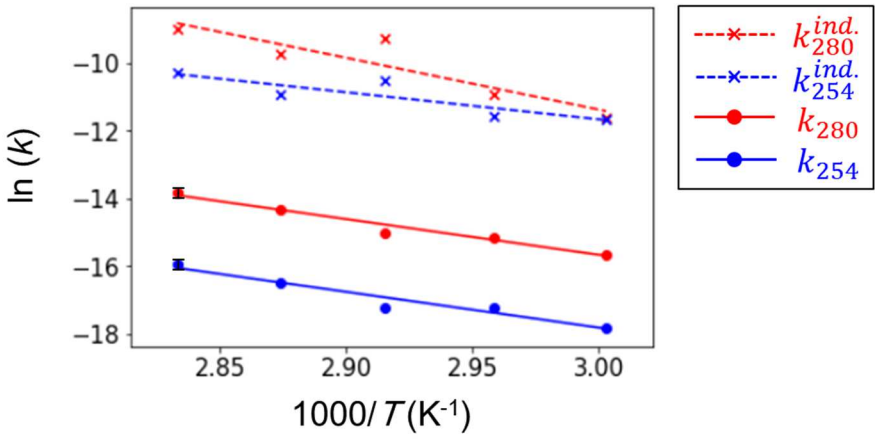

Fig. 3.2.3. The Arrhenius plots of k_{280}, k^{ind}_{280}, k_{254} and k^{ind}_{254} values and their fitting lines.

Table 3.2.2. The obtained E_a and A values for the reactions in the induction and the first reaction stages of (a) 280 nm band area and (b) 254 nm absorbance in the heating experiments of 0.1 mol l^{-1} glycine + ribose mixture solutions at 60, 65, 70, 75 and 80 °C.

		E_a (kJ mol^{-1})	A (s^{-1})
(a) 280 nm	Later 1st order stage	87	8.1×10^{6}
	Early induction stage	127	8.9×10^{14}
(b) 254 nm	Later 1st order stage	88	1.0×10^{6}
	Early induction stage	66	2.2×10^{5}

On the other hand, changes with time in 420 nm absorbance can be compared with ones during in situ measurement for 0.5 mol l^{-1} glycine + ribose mixture solutions. Fig. 3.2.4 shows changes with time in 420 nm absorbance with one point base at 800 nm during in situ measurement for (a) 0.5 mol l^{-1} (Section 2.2) and (b) 0.1 mol l^{-1} (this section) glycine + ribose mixture solutions at 80 °C. In both of their measurements, 0.1 mm thickness spacers were used. Changes for (b) 0.1 mol l^{-1} are increased by 5 times for visibility in Fig. 3.2.4. Because of weak absorption in visible range, these changes at 60–75 °C could not be traced quantitatively. (a) Changes for 0.1 mol l^{-1} solution show the induction stage while (b) changes for 0.5 mol l^{-1} solution showed almost no induction stage (Fig. 3.2.4). This suggests that pseudo reaction rates in the induction stage are inversely proportional to concentration of the reactants and/or intermediates. In order to examine effects of concentration of the reactants on the reaction time scales, additional experiments are needed. Because spectral changes in UV range for 0.5 mol l^{-1} solution could not be traced due to strong absorption even using a thin spacer, comparing changes in 420 nm absorption can be a measure for comparison. A thicker spacer may enable tracing of changes in 420 nm absorption for 0.1 mol l^{-1} solution. These points concerning concentration effects are discussed in Chapter 4 in addition to effects of minerals on the Maillard reaction.

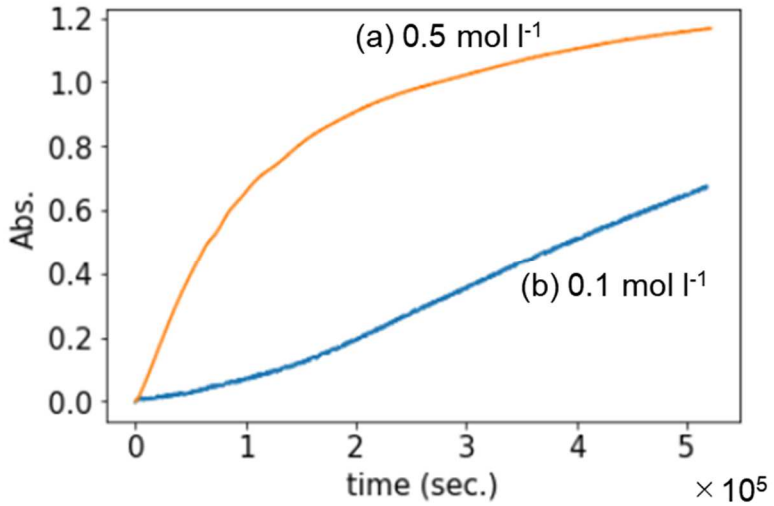

Fig. 3.2.4. Changes in 420 nm absorbance (one point base at 800 nm) with time during the in situ measurements of (a) 0.5mol l^{-1} and (b) 0.1mol l^{-1} glycine + ribose mixture solutions heated at 80 °C. Changes for (b) 0.1 mol l^{-1} are increased by 5 times for visibility.

3.3. Conclusion

In order to evaluate the progress of the Maillard reaction, I first conducted batch heating experiments of 0.1 mol l^{-1} glycine + ribose solutions at 80 °C directly in solution states. The product solutions were analyzed by (1) UV–Vis spectroscopy, (2) 3D-EEM fluorescence spectroscopy, (3) SELC, (4) IR spectroscopy, (5) HSQC-NMR spectroscopy and (6) MALDI-TOF-MS. Generalized 2D-COS were also used to examine correlations among some of the above spectroscopic data.

a) UV–Vis spectra and chromatograms by 280 nm suggested the formation with time of small molecular weight components with 280 nm absorption. These were considered to include furfural, one of reported intermediates of the Maillard reaction having an absorption peak around 280 nm. By 2D correlation spectroscopic analyses, a band around 280 nm above the baseline of 245–315 nm was suggested to be taken as a measure of the formation of furfural-like intermediates.
b) Larger products were indicated by UV–Vis spectra, 3D-EEM spectra and chromatograms by fluorescence intensity at Ex. 345 nm/Em. 430 nm. The fluorescence maxima resembled to those of natural humic solutions reported in a previous research. By 2D correlation spectroscopic analyses, it was suggested that 254 nm absorbance with a one-point base at 600 nm (UV_{254}) can be employed as a measure of the humic-like products.
c) IR and HSQC-NMR spectra for 0.1 mol l^{-1} glycine + ribose mixture solutions heated at 80 °C for 168 hours showed peaks of glycine and ribose together with some new peaks of the products including aliphatic and aromatic components.
d) Mass spectra for the 0.1 mol l^{-1} glycine + ribose mixture solution heated at 80 °C for 168 hours and the dialyzed solution (> 3500 Da) showed no significant peaks in high mass number region (>1000) after dialysis. Although details of mass characteristics of the products were not specified, furfural was identified.
e) The absence of high mass components in the mass spectra and the absence of fluorescent components in the dialyzed solution (> 3500 Da) were possibly due to the supramolecular characters of humic-like products.

In order to evaluate precise kinetic data for the progress of the Maillard reaction by using 280 nm and 254 nm absorbances, in situ UV–Vis spectroscopy with an original heatable liquid cell was conducted on 0.1 mol l^{-1} glycine + ribose mixture solutions heated at 60, 65, 70, 75 and 80 °C for 0–144 hours. Changes with time in band area around 280 nm and absorbance at 254 nm were divided into an early induction stage and a later apparent first order reaction stage. Kinetic analyses of the obtained data gave the activation energies of 66–127 kJ mol^{-1}. The obtained apparent reaction rate constants at 60–80 °C was extrapolated to 15 °C by the Arrhenius equation and the reaction time scale was estimated to be more than 20 and 147 years for increases in 280 and 254 nm absorbance, respectively.

These non-destructive measurements by in situ spectroscopic method did not require any additional procedures including drying or extracting the solution and they can be effectively used for direct tracing of the reaction progress and/or decomposition.

REFERENCES

Chen, W., C. Qian, X. Liu, H. Yu. “Two-dimensional Correlation Spectroscopic Analysis on the Interaction between Humic Acids and TiO_2 Nanoparticles”. Environ. Sci. Technol. 2014. 48(19). 11119–11126.

Edzwald, J. K., W. C. Becker and K. L. Wattier. “Surrogate parameters for monitoring organic matter and THM precursors”. J. Am. Wat. Works Assoc. 1985. 77. 122-132.

Hodge, J. E. “Dehydrated Foods, Chemistry of Browning Reactions in Model Systems”. J. Agric. Food Chem. 1953. 1(15). 928–943.

Hur, J., K. Jung, Y. M. Jung. “Characterization of Spectral Responses of Humic Substances upon UV Irradiation Using Two-dimensional Correlation Spectroscopy”. Wat. Res. 2011. 45(9). 2965–2974.

Johnson, W. P., G. Bao, W. W. John. “Specific UV Absorbance of Aldrich Humic Acid: Changes during Transport in Aquifer Sediment”. Environ. Sci. Technol. 2002. 36(4). 608–616.

Kitadai, N., T. Yokoyama amd S. Nakashima. “Temperature dependence of molecular structure of dissolved glycine as revealed by ATR-IR spectroscopy”. J. Mol. Struct. 2010. 981. 179–186.

Korshin, G. V., C. W. Li, M. M. Benjamin. “Monitoring the Properties of Natural Organic Matter through UV Spectroscopy: A Consistent Theory”. Wat. Res. 1997. 31(7). 1187–1795.

Lehmann, J., M. Kleber. “The Contentious Nature of Soil Organic Matter”. Nature 2015. 528. 60–68.

Martinez, A., M. E. Rodriguez, S. W. York, J. F. Preston, L. O. Ingram. “Use of UV Absorbance to Monitor Furans in Dilute Acid Hydrolysates of Biomass”. Biotechnol. Prog. 2000. 16(4). 637–641.

Moriizumi, M., T. Matsunaga. “Molecular Weight Separation of Hot-water Extractable Soil Organic Matter Using High-performance Size Exclusion Chromatography with Chemiluminescent Nitrogen Detection”. Soil Sci. Plant Nutr. 2011. 57(2). 185–189.

Nagao, S., T. Matsunaga, Y. Suzuki, T. Ueno, H. Amano. “Characteristics of Humic Substances in the Kuji River Waters as Determined by High-performance Size Exclusion Chromatography with Fluorescence Detection”. Wat. Res. 2003. 37(17). 4159–4170.

Noda, I. “Two-dimensional Infrared Spectroscopy”. Bull. Am. Phys. Soc. 1986. 31. 520–524.

Noda, I. “Recent Advancement in the Field of Two-dimensional Correlation Spectroscopy”. J. Mol. Struct. 2008. 883-884. 2–26.

Noda, I., Y. Ozaki. “Two-Dimensional Correlation Spectroscopy: Applications in Vibrational and Optical Spectroscopy”. John Wiley & Sons. 2004.

Piccolo, A. “ The Supramolecular Structure of Humic Substances”. Soil Sci. 2001. 166. 810–832

Stevenson, F. J. Stevenson. “Humus Chemistry: Genesis, Composition, Reactions“. Wiley. 1994.

Sutton, R., G. Sposito. “Molecular Structure in Soil Humic Substances: The New View”. Environ. Sci. Technol. 2005. 39(23). 9009–9015.

Wang, Z., B. C. Pant, C. H. Langford. “Spectroscopic and Structural Characterization of a Laurentian Fulvic Acid: Notes on the Origin of the Color”. Anal. Chim. Acta 1990. 232. 43–49.

Appendix: Kinetic analyses in a published paper by YN

In Section 3.2, UV changes were divided into the early induction stage and the later progress stage. Their kinetic analyses suggested the activation energies of 66–127 kJ mol^{-1}. On the other hand, in a published paper (Nakaya et al., 2018), kinetic analyses were conducted only for the later stage in order to avoid complicated explanation. Here, these analyses are presented as an appendix.

From UV–Vis spectra of 0.1 mol l^{-1} glycine + ribose mixture solutions heated at 60, 65, 70, 75 and 80 °C for 0–144 hours, changes in (a) UV_{280} and (b) UV_{254} with time during the in situ measurements at each heating temperature were traced (Fig. I.1.a, b). It should be noted that substraction of their starting values (t = 0) from all of UV_{280} and UV_{254} values were not conducted in the published paper. The later stage where UV_{280} >1 or UV_{254} > 0.095 were fitted as steady changing states for kinetic analyses. The fittings of the data by

$$UV_{280} = C_1\left(1 - \exp\left(-k_{280}(t-\tau)\right)\right) + 0.095 \quad \text{(eq. I.1)}$$

$$UV_{254} = C_1(1 - \exp\left(-k_{254}(t-\tau)\right)) + 1 \quad \text{(eq. I.2)}$$

give apparent first order reaction rate constants k_{280} and k_{254}, where τ is a **starting time** of each later stage when UV_{280} = 1 and UV_{254} = 0.095, and C_1 is a fixed parameter determined by preliminary fittings. The preliminary fittings were conducted on the changes at 80 °C by eq. 3.2.1 and 2 (fitting parameters: k, C_1). Since 80 °C in situ measurement was conducted three times for replicability, average value of C_1 was employed. The values of C_1 were 49.2 for UV_{280} and 3.23 for UV_{254}. The fitting curves are shown in Fig. I.1 on the UV_{280} and UV_{254} changes. The values of k_{280}, k_{254} and correlation coefficient r values obtained by the first order fittings are listed in Table I.1.

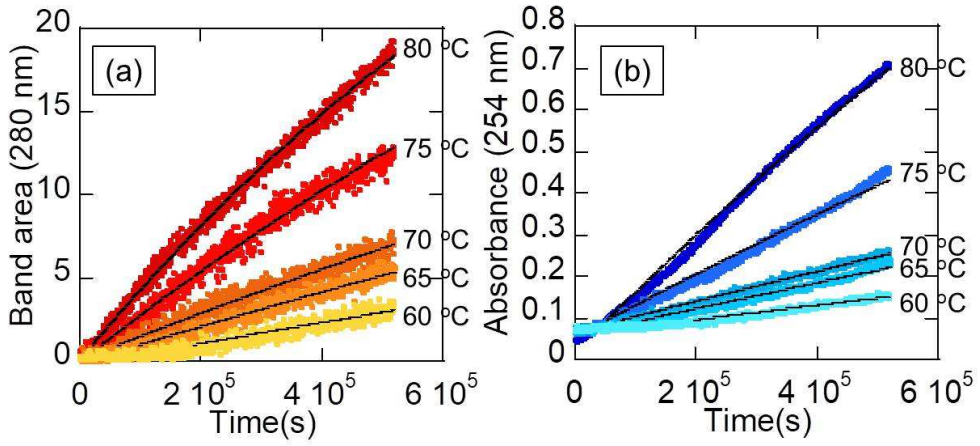

Fig. I.2. Changes in UV_{280} and UV_{254} with time during the in situ measurements of 0.1 mol l^{-1} glycine + ribose mixture solutions heated at 60, 65, 70, 75, and 80 °C with the fitting curves (the first order reaction).

Table I.1. The values of k_{280}, k_{254} and correlation coefficient r values of the first order reaction fittings in the heating experiments of 0.1 mol l^{-1} glycine + ribose mixture solutions at 60, 65, 70, 75 and 80 °C.

		80 °C[1]	80 °C[2]	80 °C[3]	75 °C	70 °C	65 °C	60 °C
(a)	k_1 (10^{-7} s^{-1})	8.73	9.59	6.90	5.72	2.88	2.21	1.29
280 nm	r	0.997	0.998	0.997	0.990	0.979	0.976	0.927
(b)	k_1 (10^{-7} s^{-1})	4.45	4.57	3.64	2.35	1.14	0.978	0.547
254 nm	r	0.997	0.999	0.993	0.993	0.993	0.987	0.967

The obtained apparent reaction rate constants increased with heating temperatures. They can be described by the Arrhenius equation (eq. 2.1.2).

$$\ln k = \ln A - \frac{E_a}{RT} \qquad \text{(eq. 2.1.2)}$$

The Arrhenius plots of k_{280} and k_{254} and T (333–350 K) (Fig. I.3) show relatively good linear trends, where average values of ln k at 80 °C are employed and their standard deviations (0.14 for k_{280} and 0.10 for k_{254} at 80 °C) are indicated by error bars. The fitting lines of these experimental data gave E_a and A values for the reactions in the first reaction stages of 280 nm band area and 254 nm absorbance during the heating of 0.1 mol l^{-1} glycine + ribose mixture solutions (Table I.2). The absorbance at 254 nm with one point base at 600 nm can reflect not only the shoulder of 280 nm peak but also a tail of broad UV absorptions. In fact, the first order rate constants for increases in the band area around 280 nm (k_{280}) were larger than those for the 254 nm absorbance (k_{254}) with a slight difference in the activation energy values (E_a) (Tables I.1 and 2, and Figs. I.2 and 3). The obtained E_a and A values enabled extrapolation of k_{280} and k_{254} values to lower and higher temperatures by the Arrhenius equation (Eq.2.1.2). For example, half-lives for k_{280} and k_{254} values at 15 °C were 30 and 98 years.

These values obtained from the kinetic analyses in the published paper are generally similar to those in Section 3.2. In Section 3.2, kinetics in the induction stage were additionally considered by using τ value as a fitting parameter of the fitting for the later first order reaction stage. This enables estimation of whole time scales of the reaction, and is possibly a more improved kinetic analyses of the whole processes.

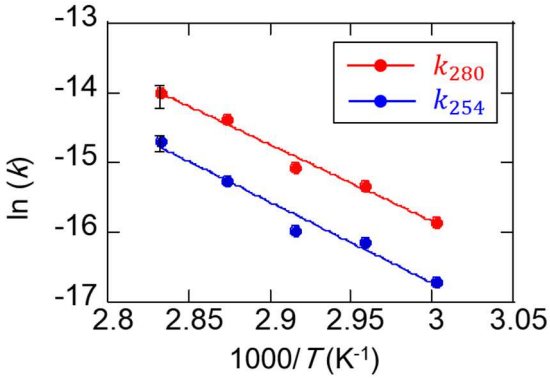

Fig. I.3. The Arrhenius plots of k_{280} and k_{254} values and their fitting lines.

Table I.2. The obtained E_a and A values for the reactions in the induction and the first reaction stages of (a) 280 nm band area and (b) 254 nm absorbance in the heating experiments of 0.1 mol l^{-1} glycine + ribose mixture solutions at 60, 65, 70, 75 and 80 °C.

	E_a (kJ mol^{-1})	A (10^8 s^{-1})
(a) 280 nm	91.4	2.79
(b) 254 nm	96.6	7.68

CHAPTER 4

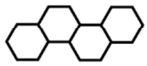

Effects of goethite on the simulated Maillard reaction

This chapter has been modified from the following published paper:

"Spectroscopic study of effects of goethite surfaces on the simulated Maillard reaction forming humic-like substances"

By Yuki Nakaya, Katsuya Okada, Yudai Ikuno and Satoru Nakashima

e-Journal of Surface Science and Nanotechnology, 2018. 16. 411-418.

4.1. General introduction about effects of minerals on the geochemical reaction

Solid-liquid interfaces determine chemical and physical properties of organic and inorganic materials' surfaces in contact with liquids in various fields. In Earth sciences, solid-liquid interfaces are crucial for dynamic behavior of Earth systems, because most of reactions and transport of materials occur at mineral-water interfaces (Nakashima et al., 2004). Moreover, mineral surfaces have been reported to act as catalytic sites for various geochemical reactions (e.g. Hoffmann, 1990; Wehrli, 1990; Sulzberger, 1990; Otsuka and Nakashima, 2007).

Otsuka and Nakashima (2007) reported that humic substances decomposed faster in the presence of goethite. They suggested adsorption and oxidation of humic substances on goethite surfaces. Some experimental works studied changes in bulk solution chemistry during the Maillard reaction in the presence of clay minerals (e.g. Taguchi and Sampei, 1986; Arfaioli et al., 1999). They reported that reaction products and their formation rates were modified by clay minerals.

Adsorption of humic substances onto clay minerals is also important because it is responsible for stability and mobility of humic substances (Weng et al., 2006), thus concerning to those of the pollutants. However, various types of complex clay minerals are present in natural environments and characterization of their surfaces are not easy (Hillier, 2000). Some studies have simulated adsorption of humic substances to clay minerals by using iron hydroxide, goethite (α-FeOOH) (e.g. Weng et al., 2006; Otsuka and Nakashima, 2007).

In order to examine effects of minerals on kinetic parameters of the Maillard reaction between glycine and ribose forming humic-like substances (Chapters 2 and 3), batch experiments of 0.1 mol l^{-1} glycine + ribose mixture solution heated at 60–80 °C in the presence and absence of an iron hydroxide, goethite, was conducted in this study. Goethite is one of representative inorganic soil constituents giving yellow-brownish colors of soils, and is the most stable phase in humid environments (Cornell and Schwertmann, 1996). Its surface is positively charged at acidic to neutral pH conditions (Zeltner and Anderson, 1988). Goethite is playing important roles in the environment as an adsorbent and a catalyst (Liu et al., 2014).

4.2. Preparation and identification of goethite

4.2.1. Introduction

Goethite can be synthesized in laboratory by oxidation and reduction of iron compounds. For example, Schwertsmann and Cornell (2000) and Otsuka and Nakashima (2007) used $Fe(NO_3)_3$ solution and KOH solution to make ferrihydrite precipitate, and heated the suspension to obtain goethite precipitate. Ferrihydrite is red-brownish metastable iron hydroxides, which ages to goethite. While they used $Fe(NO_3)_3$ and KOH in the methods, in this study, goethite was prepared by using $FeCl_3$ and NaOH for avoiding remaining nitrate adsorbed on goethite surfaces and for possible future comparison with different ionic strength conditions. In this section, the preparation and identification of goethite by visible, Raman and IR spectroscopy and X-ray diffractometry are also presented.

4.2.3. Methods

A mixture solution of 100 mL of 0.1 mol l^{-1} $FeCl_3$ solution and 180 mL of 5 mol l^{-1} NaOH solution were diluted to 2 l with pure water (MilliQ: Resistance > 18.2 MΩ cm). This solution with rapid precipitation of brownish suspension was subdivided into two polypropylene vessels (1 l each) and incubated at 70 °C for 60 hours. Then yellowish-brown precipitates were filtered using 0.2 μm Millipore filter. They were washed by pure water three times and dried in an electric oven at 50 °C for 4.5 hours.

In order to identify the obtained precipitates, small amounts of them were hand pressed on Al foil and measured by visible, Raman and IR micro-spectroscopy. For visible and Raman micro-spectroscopy, a home-built micro-spectrometer was used (Onga and Nakashima, 2014). Visible spectra were obtained in the wavelength region of 380–850 nm by using a 150 lines mm^{-1} grating with the following conditions: 5 seconds of integration time; accumulation numbers of 12; with a dark field type objective lens (5×). Raman spectra were obtained in the 50–1950 cm^{-1} range by using a 1200 lines mm^{-1} grating with the following conditions: 5 seconds of integration time; accumulation numbers of 12; with a 50× objective lens. IR micro-spectroscopic measurements were conducted by using an FT-IR micro-spectrometer (FTIR620 + IRT30, Jasco) (Tonoue at al., 2014; Hamamoto et al., 2015; Kudo et al., 2017). IR spectral measurements were accumulated for 64 scans with a wavenumber resolution of 4 cm^{-1} in the 700–4000 cm^{-1} spectral range. The precipitates were also measured by X-ray diffractometry using MiniFlex (Rigaku). X-ray patterns were measured at a scanning speed of 2.0° per minute with a measurement interval of 0.1° in the 6.0°–50.0° angle range.

4.2.3. Results and discussion

A representative visible reflectance spectrum of the obtained iron hydroxide sample is shown in Fig. 4.2.1a. Three absorption bands around 420, 500 and 680 nm (indicated in Fig. 4.2.1a) were recognized in all the obtained visible spectra. These bands were similar to reported absorption bands of goethite by Onga and Nakashima (2014).

Raman spectra of the same sample showed peaks at 392 and 687 cm^{-1} (Fig. 4.2.1b) (Onga and Nakashima, 2014). They correspond to reported peaks of goethite at 392 and 682 cm^{-1}. The other peaks at 239, 298, 477, 988, 1128, 1214 and 1330 cm^{-1} were not assigned but did not correspond to reported peaks of ferrihydrite, lepidocrocite and hematite (Onga and Nakashima, 2014). Therefore, the obtained iron hydroxides were mainly composed of goethite.

An IR transflection (transmission-reflection) spectrum of the obtained iron hydroxide sample is shown in Fig. 4.2.1c. Absorption bands at 652, 780, 895 and 3125 cm^{-1} can be recognized in all of the IR spectra obtained in the present study and correspond to those for goethite reported by Nagano et al. (1992). Weaker bands at 1200–1900 cm^{-1} (e.g. 1307, 1560 and 1780 cm^{-1}) are considered to be due to overtones and combinations of the goethite fundamental bands such as 652, 780 and 895 cm^{-1}.

X-ray diffraction pattern of the iron hydroxide showed six dominant peaks at 2θ = 21.3°, 26.4°, 33.2°, 34.7°, 36.7°, 39.2°, 40.1° and 41.3° (Fig. 4.2.1d). They correspond to reported peaks of goethite by Nagano et al. (1992). The other weaker peaks at 2θ = 11.1°, 15.8°, 18.0° and 43.4° could not be assigned.

Based on these results by visible, Raman and IR micro-spectroscopy and X-ray diffraction, the obtained precipitates are mainly composed of goethite but contain some unidentified impurities.

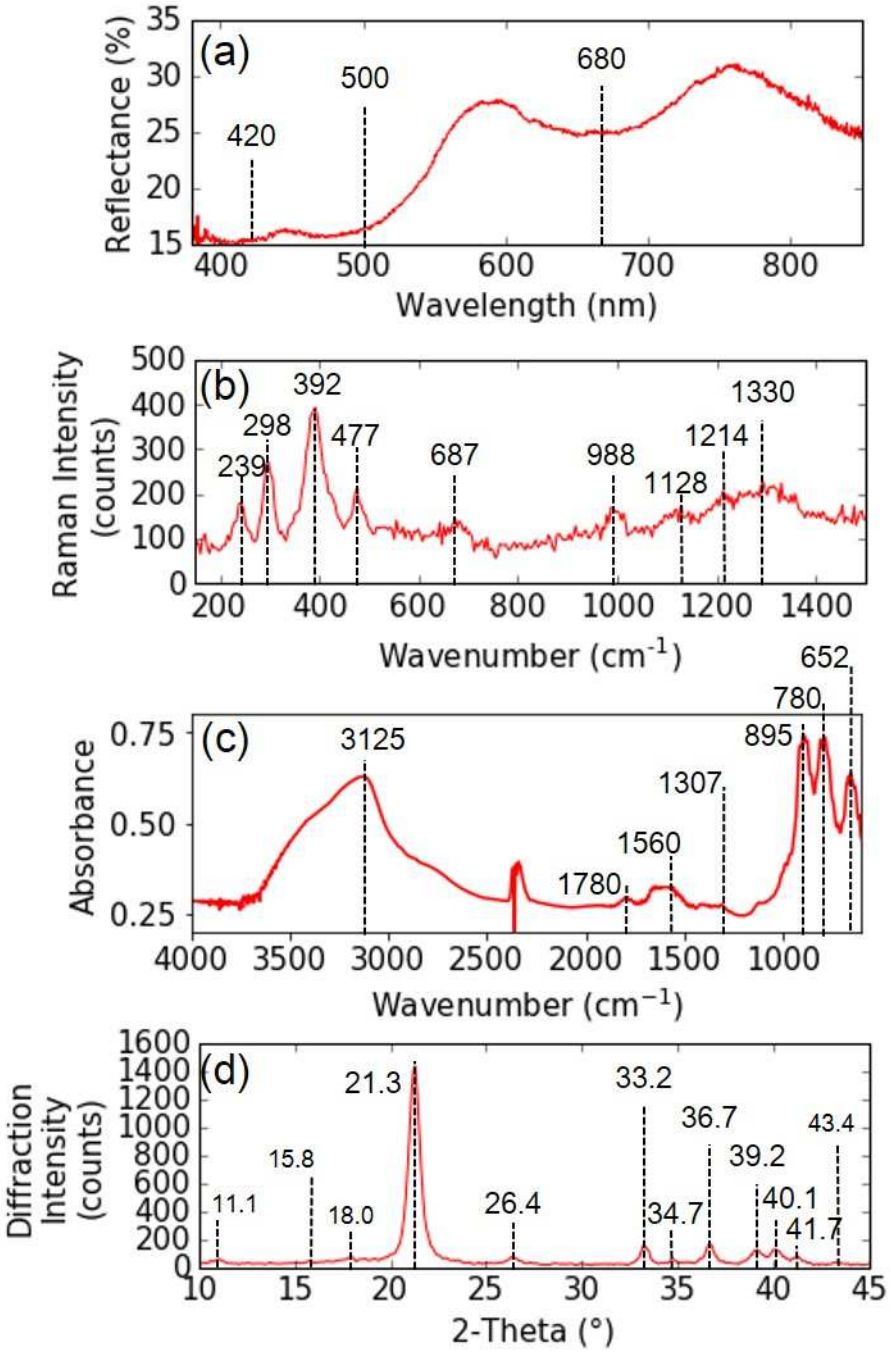

Fig. 4.2.1. (a) A representative visible reflectance spectrum, (b) a representative Raman spectrum, (c) a representative IR transflection (transmission-reflection) spectrum and (d) X-ray diffraction pattern, for the obtained iron hydroxide sample indicating mainly goethite.

4.3. Kinetic analyses for effects of goethite on the simulated Maillard reaction by 0.1 mol l^{-1} glycine and ribose solution

4.3.1. Introduction

In order to examine effects of goethite on the kinetic parameters of the Maillard reaction between glycine and ribose forming humic-like substances, batch experiments of 0.1 mol l^{-1} glycine + ribose mixture solution heated at 60, 70 and 80 °C with/without goethite were conducted. As indicators for the reaction progress, absorptions at 254 and 420 nm can be used. They have been often used as quantitative indicators for amounts of dissolved organic matter in water (254 nm) (Edzwald et al., 1985) and browning degree in the Maillard reaction processes (420 nm) (Stamp and Labuza, 1983).

4.3.2. Methods

For batch heating experiments of 0.1 mol l^{-1} glycine + ribose mixture solution, polypropylene micro-tubes containing 1.0 ml of the solution were prepared. For an experimental group including goethite (7 × 3 polypropylene micro-tubes), 5 mg of goethite samples were added to 0.1 mol l^{-1} glycine + ribose solutions. The three sets (7 × 3) were heated at 60, 70 and 80 °C in an electric oven for 24, 48, 72, 96, 120, 144 and 168 hours (1–7 days) in order to accelerate the reaction. Other three sets (7 × 3) without goethite were also prepared for control group, and heated at 60, 70 and 80 °C in an electric oven for 24, 48, 72, 96, 120, 144 and 168 hours (1–7 days) After heating for each period, they were taken out from the oven and stored in a refrigerator (6 °C). Another set of 0.1 mol l^{-1} glycine + ribose solutions with and without goethite was kept at room temperature (heated for 0 hour). The supernatants of the product solutions were diluted 10 times by pure water (MilliQ) in order to prevent spectral saturation.

The diluted solutions (3 ml) were measured in a quartz cell (optical pass length: 10 mm) by an UV–Vis spectrometer (V570, Jasco). UV–Vis spectra were measured at a scanning speed of 400 nm min^{-1} with a wavelength resolution of 1.0 nm in the 200–1100 nm spectral range.

4.3.3. Results

A photograph of 0.1 mol l^{-1} glycine + ribose solutions heated at 80 °C for 0–7 days with goethite suspensions (the experimental group) is shown in Fig. 4.3.1a. A photograph of those without goethite (the control group) is also shown in Fig. 4.3.1b. The product solutions became more yellow-brownish with increasing heating duration. The product solutions show darker colors than the control group for all the heating durations.

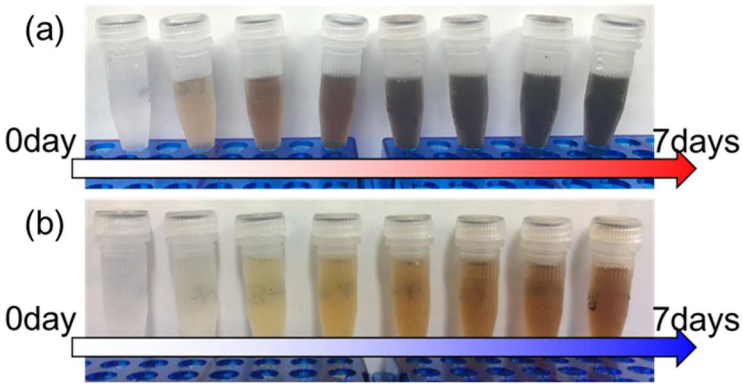

Fig. 4.3.1. Photographs of (a) 0.1 mol l^{-1} glycine + ribose mixture solutions heated at 80 °C for 0–7 days with goethite suspensions (the experimental group) and (b) 0.1 mol l^{-1} glycine + ribose mixture solutions heated at 80 °C for 0–7 days without goethite (the control group).

UV–Vis spectra for the product solutions heated at 80 °C (diluted 10 times) are shown in Fig. 4.3.2. Absorbance at shorter wavelength increased more for longer heating durations. These spectral changes suggest progress of the simulated Maillard reaction. For the experimental group (Fig. 4.3.2a), the absorption intensities in the ultraviolet to visible wavelength region are generally larger than the control group (Fig. 4.3.2b). It should be noted that larger absorbances more than 2 do not have linear correlations with concentration due to spectral saturation. Therefore, absorption in the visible wavelength range was mainly analyzed in this study.

In order to show quantitative differences in absorption intensities with and without goethite, absorption intensities at 420 nm (Vis_{420}) were determined as peak heights with a one-point base at 800 nm. Vis_{420} has been often used as a quantitative indicator for browning degree in the Maillard reaction processes (Section 2.2). Fig. 4.3.3 shows changes with time in Vis_{420} for 0.1 mol l^{-1} glycine + ribose mixture solutions with/without goethite (the experimental/control group) heated at 60, 70 and 80 °C for 0–7 days. The higher heating temperatures gave the larger increases in Vis_{420}. The values of Vis_{420} for the experimental group (with goethite) were consistently larger than those without goethite. These results indicate enhancement of formation of brown products by the presence of goethite.

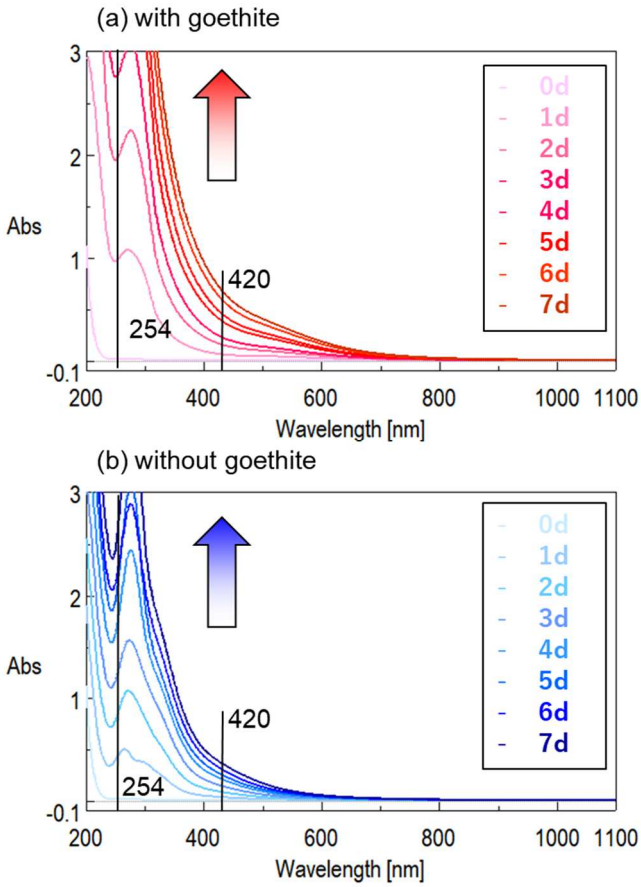

Fig. 4.3.2. UV–Vis spectra for (a) product solutions with goethite (experimental group) and (b) product solutions without goethite (control group) heated at 80 °C for 0–7 days (diluted 100 times). 0, 1, 2, 3, 4, 5, 6 and 7 days spectra are shown.

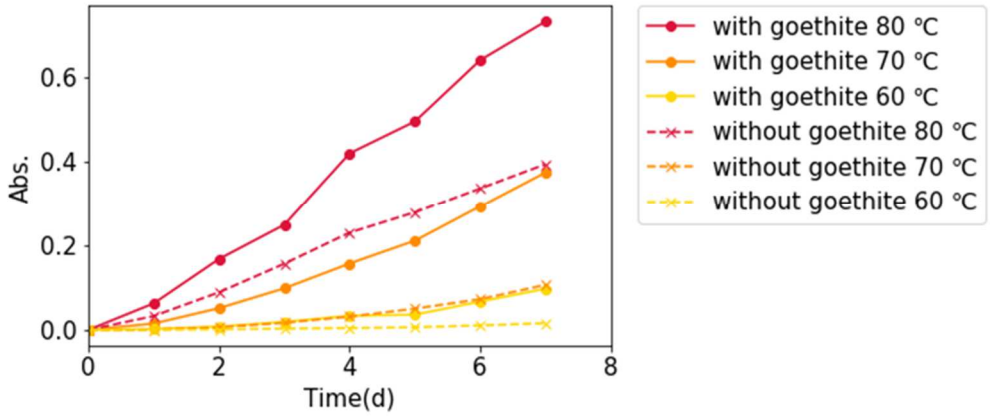

Fig. 4.3.3. Changes with time (0–7 days) in absorption intensities at 420 nm with a one-point base at 800 nm (Vis_{420}) for product solutions with/without goethite (experimental/control group) heated at 60, 70 and 80 °C (diluted 100 times).

4.3.4. Discussion

In Section 2.2, changes with time in Vis_{420} for 0.5 mol l^{-1} glycine + ribose mixture solutions without goethite were fitted by the first order reaction model and the apparent reaction rate constant were obtained. In this section, similar analyses for the batch samples of 0.1 mol l^{-1} glycine + ribose mixture solutions with/without goethite heated at 60–80 °C are presented (Fig. 4.3.3). Since UV–Vis spectral changes at 60–80 °C are considered to consist of the early induction stage and the later progress stage (Section 3.2), the fitting was conducted by the following equation:

$$Vis_{420} = C\left(1 - \exp\left(-k_{420}(t - \tau)\right)\right) \quad \text{(eq. 4.3.1)}$$

First, in order to fix C value, changes with time in Vis_{420} in "in situ" UV–Vis spectroscopy for 0.1 mol l^{-1} glycine + ribose mixture solutions heated at 80 °C (without goethite) (Section 3.2) were fitted by eq. 4.3.1 with fitting parameters of C, k_{420} and τ as preliminary values. Since in situ measurement at 80 °C was conducted three times for replicability, the parameters were determined by average values of the three fittings (C = 0.670). The fittings were conducted again by eq. 4.3.1 with the fixed C (= 0.670). Fig. 4.3.4 shows changes in Vis_{420} with time for the in situ measurements of 0.1 mol l^{-1} glycine + ribose mixture solutions without goethite heated at 80 °C with the fitting curves (the first order reaction) by eq. 4.3.1 (C = 0.670). Obtained apparent first order reaction rates k_{420} and induction periods τ are listed in Table 4.2.1.

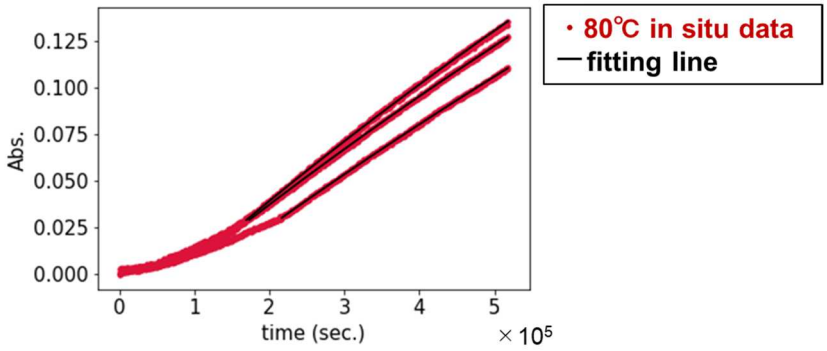

Fig. 4.3.4. Changes in Vis_{420} with time for the in situ measurements of 0.1 mol l^{-1} glycine + ribose mixture solutions without goethite heated at 80 °C with the fitting curves (the first order reaction).

However, this C cannot be used in fitting of the batch experiments because Vis_{420} values in the in situ UV–Vis spectroscopy (Fig. 4.3.4) were smaller than those in the batch experiments (Fig. 4.3.3) and scaling factors were needed. This is possibly due to difference in optical path length and dilution factor between in situ measurements with a heatable liquid cell and batch measurements with a quartz cell. The scaling factors for C_1 were determined as follows: (1) Vis_{420} values at 0, 1, 2, 3, 4, 5 and 6 days were extracted from whole Vis_{420} values in the in situ experiments. (2) They were multiplied by the same scaling factor and subtracted from those in the batch experiments (Fig. 4.3.4), where the scaling factor was optimized so as the residuals to be minimum by a least square method. Since in situ measurement at 80 °C was conducted three times, determination of the scaling factor were also conducted three times, and an average value was employed. Finally, the preliminary value of C (= 0.670) was multiplied by the scaling factor, and a new fixed parameter C' for fitting of the batch experiments was obtained to be 1.86.

Second, changes with time in Vis_{420} for the batch samples of 0.1 mol l^{-1} glycine + ribose mixture solutions with goethite heated at 60–80 °C and those without goethite heated at 70 and 80 °C for 2–7 days were fitted by the following equation:

$$Vis_{420} = C'\left(1 - \exp\left(-k_{420}(t - \tau)\right)\right) \quad \text{(eq. 4.3.2)}$$

where fitting parameters were k_{420} and τ with the fixed C' = 1.86. It should be noted that the fitting for the sample without goethite heated at 60 °C was not conducted because of few changes with time. The fitting curves are shown in Fig. 4.3.5 on the Vis_{420} changes. Obtained apparent first order reaction rates k_{420} and induction periods τ are listed in Table 4.2.1.

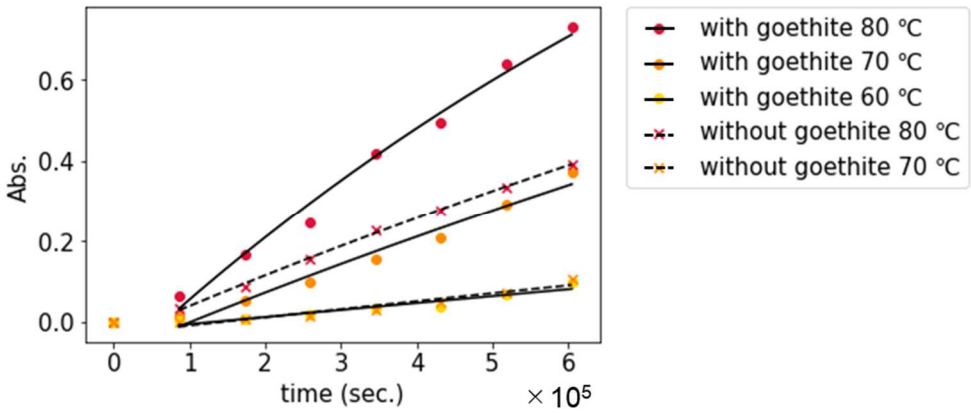

Fig. 4.3.5. Changes in Vis_{420} with time for the batch samples of 0.1 mol l^{-1} glycine + ribose mixture solutions with goethite heated at 60, 70 and 80 °C (red, orange and yellow filled circles) and those without goethite heated at 70 and 80 °C (red and orange crosses). The fitting curves (the first order reaction) are overlaid.

Table 4.2.1. The values of k_{420}, τ and correlation coefficient r values of the first order reaction fittings in the heating experiments of 0.1 mol l^{-1} glycine + ribose mixture solutions.

	In situ spectroscopy			Batch experiments				
	Without goethite			With goethite			Without goethite	
	80 °C [1]	80 °C [2]	80 °C [3]	80 °C	70 °C	60 °C	80 °C	70 °C
k_{420} ($\times 10^{-7}$ s^{-1})	5.30	4.89	4.52	8.99	4.06	0.950	4.28	1.09
τ (s)	85300	82200	113900	66200	101200	128800	49600	141300
r	1.00	1.00	1.00	1.00	0.999	0.991	1.00	0.996

Third, k_{420} for the samples with/without goethite are plotted in an Arrhenius diagram (Fig. 4.3.6). The values of k_{420} for the batch and in situ experiments for 0.1 mol l^{-1} and 80 °C are almost similar. Therefore, the above fitting procedure is considered to be reasonable. The values of k_{420} for in situ experiments for 0.5 mol l^{-1} at 60–80 °C and the fitting lines by the Arrhenius equation (eq. 2.1.2) (Section 2.2)

$$\ln k = \ln A - \frac{E_a}{RT} \qquad \text{(eq. 2.1.2)}$$

are also shown in Fig. 4.3.6. Table 4.2.2 lists E_a and A values obtained from the fitting by the Arrhenius equation, together with k_{420} values and half-lives of the first order reaction stage at 15 °C estimated by extrapolation of the Arrhenius equation.

Fig. 4.3.6 shows larger reaction rate constants (apparent first order reaction) for 0.5 mol l^{-1} samples than 0.1 mol l^{-1} samples for 60–80 °C heating temperature range. The first order reaction rate is in principle independent of initial concentration of the reactants. However, in this case, the reaction rate constants can include some factors related to initial concentrations of the reactants. Therefore, Vis_{420} changes can be considered to be described by the higher order reaction than the first one. Fig. 4.3.6 also suggests that Vis_{420} changes for 0.1 mol l^{-1} glycine + ribose mixture solutions can be accelerated by the presence of goethite. These initial concentration effects and reaction enhancement by goethite are considered to determine reaction time scales in the real environment.

Since the number of data points on the fittings by the Arrhenius equation were small (3 points for k_{420} values for 0.1 mol l^{-1} samples with goethite and 2 points for those without goethite, Fig. 4.3.6), large errors for the obtained E_a and A values can be included. However, they show the similar activation energy values. For better understanding of effects of goethite and initial concentrations on the reaction, longer experimental duration and more data points are needed.

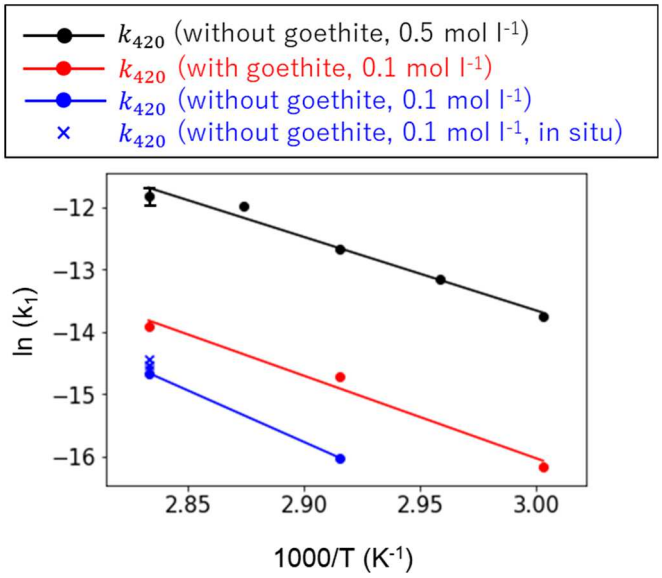

Fig. 4.3.6. The Arrhenius plots of k_{420} values in the in situ heating experiments for 0.5 mol l^{-1} glycine + ribose mixture solutions without goethite (black filled circles) and 0.1 mol l^{-1} glycine + ribose mixture solution without goethite (blue cross) and the batch experiments for 0.1 mol l^{-1} glycine + ribose mixture solutions with/without goethite (red/blue filled circles) with their fitting lines.

Table 4.2.2. The E_a, A values obtained from the fitting by the Arrhenius equation and k_{420} values and half-lives of the first order reaction stage at 15 °C estimated by extrapolation of the Arrhenius equation.

	E_a (kJ mol^{-1})	A (s^{-1})	k_{420} at 15 °C (s^{-1})	Half-life at 15 °C (y)
0.5 mol l^{-1} (in situ without goethite)	98	2.7×10^{9}	4.5×10^{-9}	4.9
0.1 mol l^{-1} (batch with goethite)	110	2.0×10^{10}	2.1×10^{-10}	105
0.1 mol l^{-1} (batch without goethite)	137	9.1×10^{13}	1.1×10^{-11}	1990

4.4. Conclusion

In order to examine effects of goethite on spectral changes with time during the Maillard reaction between glycine and ribose forming humic-like substances, batch heating experiments of 0.1 mol l^{-1} glycine + ribose mixture solution with/without goethite was conducted at 60, 70 and 80 °C.

First, iron hydroxide was prepared by using $FeCl_3$ and NaOH for avoiding remaining nitrate adsorbed on goethite surfaces and for possible future comparison with different ionic strength conditions. The product was analyzed by visible, Raman and IR spectroscopy and X-ray diffractometry. The results indicated that the obtained precipitates were mainly composed of goethite but contained some unidentified impurities.

Second, UV–Vis spectroscopy was conducted on the batch samples heated at 60, 70 and 80 °C. Spectral saturation occurred in UV region (200–400 nm) (not shown) because of strong absorption by UV active products. Therefore, absorption in visible range was mainly analyzed. Changes in absorbance at 420 nm with one-point base at 800 nm (Vis_{420}) with time at each heating temperature were fitted by the exponential equation assuming the first order reaction. Obtained apparent first order reaction constants k_{420} were larger in the presence of goethite, indicating reaction enhancement by goethite. The reaction rates at 0.1 mol l^{-1} were smaller than those for 0.5 mol l^{-1} glycine + ribose mixture solution heated at 60–80 °C without goethite, suggesting that higher initial concentration of the reactants can make the reaction faster. The fitting by the Arrhenius equation for k_{420} and T (333–350 K) gave the E_a and A values. These values can include errors due to few data points. Although further studies are needed, reaction enhancement by goethite and initial concentration effects should be considered in evaluating reaction time scales in the real environment.

REFERENCES

Arfaioli, P., O. L. Pantini, M. Bosetto, G. G. Ristori. “Influence of clay minerals and exchangeable cations on the formation of humic-like substances (melanoidins) from D-glucose and L-tyrosine”. Clay Miner. 1999. 34. 487–497.

Cornell, R. M., U. Schwertmann. “The Iron Oxides: Structure, Properties, Reacions, Occurrences and Uses”. VCH. 1996.

Edzwald, J. K., W. C. Becker and K. L. Wattier. “Surrogate parameters for monitoring organic matter and THM precursors”. J. Am. Wat. Works Assoc. 1985. 77. 122–132.

Hamamoto, M., M. Katsura, N. Nishiyama, R. Tonoue, S. Nakashima. “Transmission IR micro-spectroscopy of interfacial water between colloidal silica particles”. e-J. Surf. Sci. Nanotech. 2015. 13. 301–306.

Hillier, S. “Accurate quantitative analysis of clay and other minerals in sandstones by XRD: comparison of a Rietveld and a reference intensity ratio (RIR) method and the importance of sample preparation”. Clays Miner. 2000. 35. 291–302.

Kudo, S., H. Ogawa, E. Yamakita, S. Watanabe, T. Suzuki, S. Nakashima. “Adsorption of water to collagen as studied using infrared (IR) microspectroscopy combined with relative humidity control system and quartz crystal microbalance”. Appl. Spectrosc. 2017. 71. 1621–1632.

Liu, H., T. Chen, R. L. Frost. “An overview of the role of goethite surfaces in the environment”. Chemosphere. 2014. 103. 1–11.

Nagano, T., S. Nakashima, S. Nakayama, K. Osada, M. Senoo. “Color variations associated with rapid formation of goethite from proto-ferrihydrite at pH 13 and 40 °C”. Clays Clay Miner. 1992. 40. 600–607.

Nakashima, S., C. J. Spiers, L. Mercury, P. Fenter, M. H. Hochella, Jr. ”Physicochemistry of thin film water in geological and biological systems –current issues and new developments–”. in S. Nakashima, C. J. Spiers, L. Mercury, P. Fenter and M. H. Hochella, Jr. (Eds.) “Physicochemistry of Water in Geological and Biological Systems: Structures and Properties of Thin Aqueous Films”. Universal Academy Press, Inc. 2004. 1–15.

Onga, C., S. Nakashima. “Darkfield reflection visible microspectroscopy equipped with a color mapping system of a brown altered granite”. Appl. Spectrosc. 2014. 68. 740–748.

Otsuka, T. and S. Nakashima. “The Formation of CO_2 by fulvic acid on the surface of goethite studied using ultraviolet and infrared spectroscopy”. J. Mineral. Petrol. Sci. 2007. 102. 302–305.

Schwertmann, U., R. M. Cornell. “Iron oxides in the laboratory: preparation and characterization”. Wiley-VCH. 2000.

Stamp, J. A. and T. P. Labuza. “Kinetics of the Maillard reaction between aspartame and glucose in solution at high temperatures”. J. Food Sci. 1983. 48(2). 543–544.

Sulzberger, B. “Photoredox reactions at hydrous metal oxide surfaces: a surface speciation”. in W. Stumm Ed. “Aquatic chemical kinetics: reaction rates of processes in natural waters”. John Wiley & Sons. 1990. 401–429.

Taguchi, K., Y. Sampei. “The formation, and clay mineral and $CaCO_3$ association reactions of melanoidins”. Org. Geochem. 1986. 10. 1081–1089.

Tonoue, R., M. Katsura, M. Hamamoto, H. Bessho, S. Nakashima. “A method to obtain the absorption coefficient spectrum of single grain coal in the aliphatic C–H stretching region using infrared transflection microspectroscopy”. Appl. Spectrosc. 2014. 68. 733–739.

Weng, L., W. H. van R iemsdijk, L. K. Koopal, T. Hiemstra. “Adsorption of humic substances on goethite: comparison between humic acids and fulvic acids”. Environ. Sci. Technol. 2006. 40. 7494–7500.

Wehrli, B. “Redox reactions of metal ions at mineral surfaces”. in W. Stumm Ed. “Aquatic chemical kinetics: reaction rates of processes in natural waters”. John Wiley & Sons. 1990. 311–336

Zeltner, W. A., M. A. Anderson. “Surface charge development at the goethite/aqueous solution interface: effects of CO_2 adsorption”. Langmuir. 1988. 4. 469–474.

CHAPTER 5

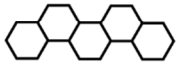

Adsorption of the simulated Maillard reaction reactants and products on goethite studied by in situ attenuated total reflection infrared (ATR-IR) spectroscopy

5.1. In situ attenuated total reflection infrared (ATR-IR) spectroscopy for adsorption of the simulated Maillard reaction reactants and products on goethite

This section has been modified from the following published paper:
"Spectroscopic study of effects of goethite surfaces on the simulated Maillard reaction forming humic-like substances"
By Yuki Nakaya, Katsuya Okada, Yudai Ikuno and Satoru Nakashima
e-Journal of Surface Science and Nanotechnology, 2018. 16. 411–418.

5.1.1. Introduction

In Chapter 4, enhancement of the Maillard reaction by goethite was suggested. Some works also reported that the Maillard reaction products and their formation rates were modified by clay minerals (Taguchi and Sampei, 1986; Arfaioli et al., 1999). These modifications of the Maillard reaction are generally supposed to take place at mineral surfaces. However, surface processes on minerals during the Maillard reaction have not been experimentally examined. In this section, adsorption on goethite of reactants and products of the Maillard reaction at room temperature is studied by attenuated total reflection infrared (ATR-IR) spectroscopy.

ATR-IR spectrum is an absorption-like IR spectrum obtained from absorption by a sample of evanescent waves penetrating at the interface between the ATR crystal and the sample on it. Kitadai et al. (2009a, b) used ATR-IR spectroscopy for examining adsorption of L-lysine on montmorillonite and amorphous silica in their colloidal suspensions. On the other hand, Hug and Sulzberger (1994) and Hug (1997) directly observed adsorption of some oxalates and sulfate on minerals by making thin mineral layers on the ATR crystal. In this study, thin goethite layers were made on an ATR crystal in reference to Hug (1996) and Luengo et al. (2006), and in situ ATR-IR spectral changes for the reactants and products of the Maillard reaction were monitored at room temperature.

5.1.2. Methods

In order to examine adsorption on goethite of the reactants of the simulated Maillard reaction, ATR-IR measurements were conducted by an FT-IR spectrometer (VIR9500, Jasco) with an ATR attachment (horizontal ATR with a ZnSe crystal, Specac: about 5 times reflection) (Fig. 5.1.1). In the ATR-IR method, IR beam (evanescent waves) penetrates in the order of several hundreds of nm at the interface between the ATR crystal and the sample on it (Fig. 5.1.2) and an absorption-like IR spectrum can be obtained from the sample (Hug and Sultzberger, 1994). Since penetration depth depends on wavenumber and optical path length is difficult to be normalized, ATR-IR signals at different wavenumbers cannot be compared in the same way as absorbance spectra. In this study, pATR = $-\log_{10} I/I_0$ (I: reflection intensity, I_o: incident intensity) values ("p" means "- log") was employed for the vertical axis of ATR-IR spectra following Masuda et al. (2003). In this study, thin layers of goethite were made on the ATR crystal (ZnSe), and IR spectral changes with time for the reactant solution on the goethite layer were measured.

The thin layer of goethite was made on the ATR crystal (ZnSe) in reference to Hug (1996) and Luengo et al. (2006), as follows: pure water (1.0 ml) was pipetted onto the crystal, and 0.8 ml was removed to obtain thin water layer on the crystal. Then 0.8 ml of a 10 g l^{-1} goethite suspension was pipetted onto the crystal and mixed by using the pipette tip. After air-drying at room temperature for 2 hours, the ATR surface was rinsed by pure water twice in order to remove excess goethite. After the second air-drying, thin layer of goethite was obtained on the ZnSe crystal (Fig. 5.1.2).

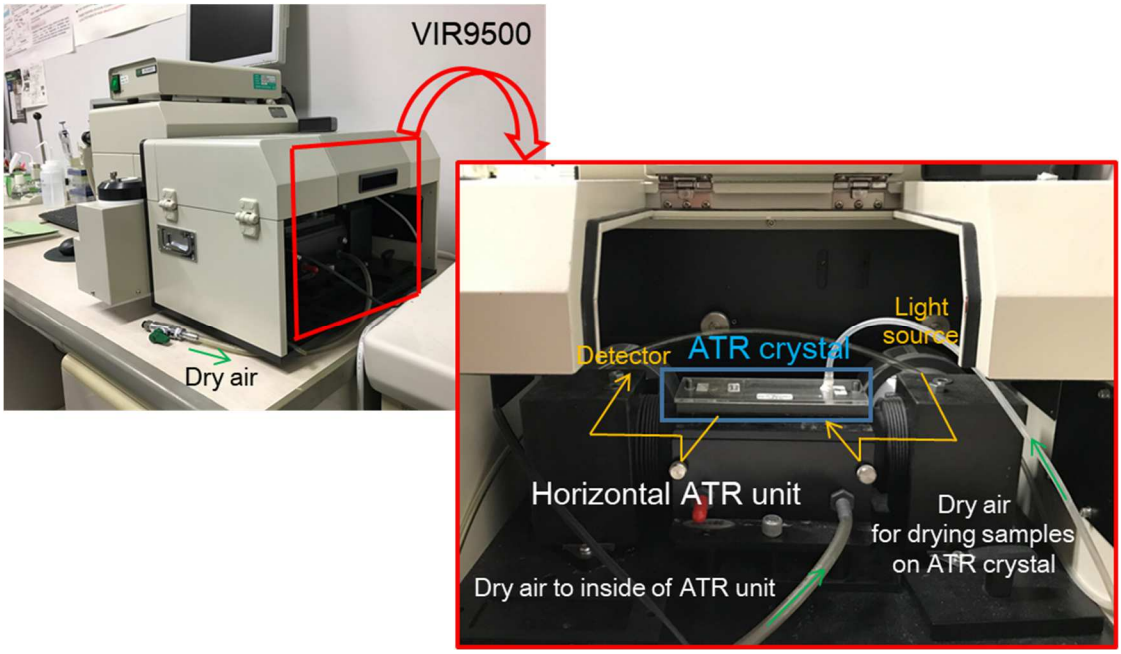

Fig. 5.1.1. An overview of the FTIR spectrometer (VIR9500, Jasco) and the sample compartment with the horizontal ATR unit (horizontal ATR with a ZnSe crystal, Specac).

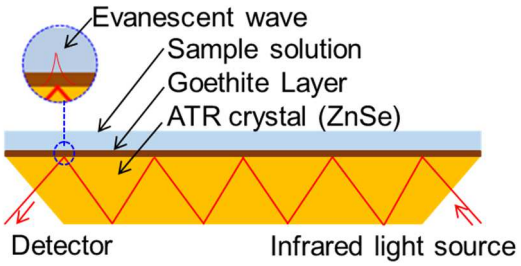

Fig. 5.1.2. A schematic figure of the attenuated total reflection (ATR) crystal (ZnSe) with thin layers of goethite used in ATR-IR measurements.

The deposited goethite layer on the ATR crystal was observed by laser scanning confocal microscopy (LSCM). A line profile for surface heights of the goethite layer on the ATR crystal (line A–B in Fig. 5.1.3a) show height differences of 200 to 500 nm corresponding to thin layers of a few hundred nm (< 1 μm) (Fig. 5.1.3b). Some large particle aggregates of 10–50 μm in size with heights of about 3 μm can also be recognized (Fig. 5.1.3). The goethite layer was mostly thinner than the penetration depth of evanescent waves in the order of several hundred nm. Therefore, ATR-IR spectra can include both solutes dissolved in water nearby the goethite surface and those adsorbed on goethite surfaces besides goethite layer itself.

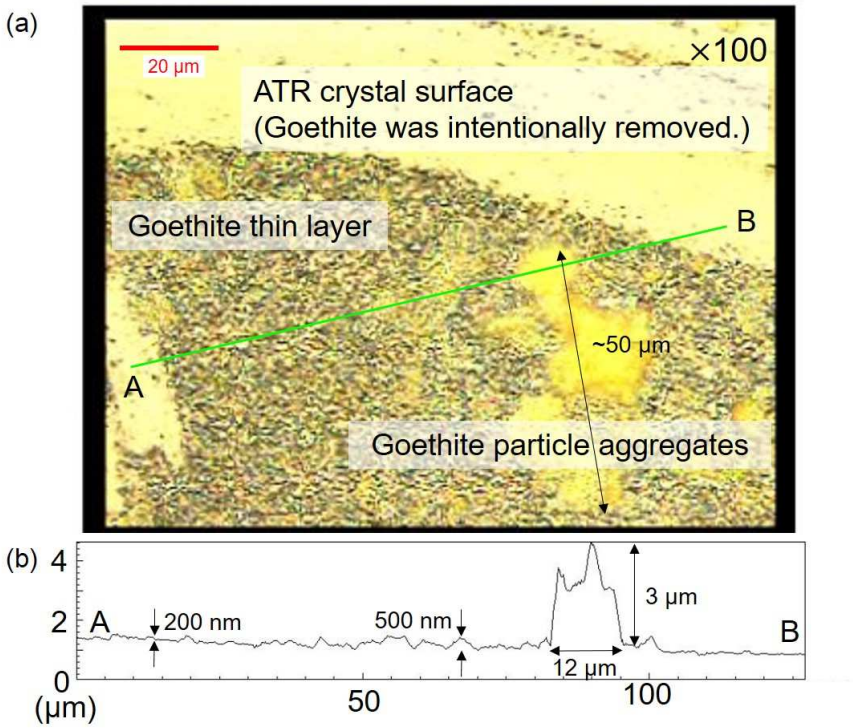

Fig. 5.1.3 (a) A representative laser scanning confocal microscope (LSCM) image of goethite layer on ATR crystal (ZnSe) (objective lens: ×100) and (b) height profile on a line segment A–B. Particle aggregates of about 3 μm thick and a thinner layer of a few hundred nm are recognized.

As reactants for the simulated Maillard reaction forming humic-like substances, glycine and ribose were selected here based on my previous researches in Chapters 2, 3 and 4. The reactant solution (0.1 mol l^{-1} glycine plus 0.1 mol l^{-1} ribose solution) were heated at 80 °C in the electric oven for 196 hours to obtain a product solution. In the ATR-IR measurements, these product (experimental) and reactant (control) solutions were used.

The reactant solution and the product solution (1.0 ml) were pipetted onto the ATR crystal with the goethite layer and their IR spectral changes with time were measured every 150 seconds for 10800 seconds (3 hours) at room temperature (25 ± 3 °C). As control experiments, IR spectral changes with time for the reactant and product solutions on the ATR crystal without goethite layer were also measured every 150 seconds for 10800 seconds (3 hours). All the IR spectral measurements were accumulated for 64 scans with a wavenumber resolution of 4 cm^{-1} in the 650–4000 cm^{-1} spectral range. It should be noted that amount of water vapor on the optical path in the spectrometer can change depending on ambient humidity giving small fine peaks on measured spectra in the 1300–1800 cm^{-1} region. In this study, these peaks were removed from sample spectra by subtracting an spectrum for water vapor so as for a representative vapor peak height at 1845 cm^{-1} (baseline: 1839–1853 cm^{-1}) to become zero.

It should be noted that pHs of the sample solutions were 5.8 for the reactant solution and 4.0 for the product solution. This acidification in the reaction for 196 hours is possibly due to generation of -COOH groups (Ikan et al., 1996; Chung et al., 2012). In order to examine IR absorption bands of the reactants and products including such pH dependent groups, ATR-IR spectra for the reactant (pH = 5.8, 4.1 and 3.5) and product (pH = 4.0 and 3.5) solutions were observed, where pHs were adjusted by adding several μl of 1 mol l^{-1} HCl solution.

5.1.3. Results

ATR-IR spectra were measured for the reactant and product solutions (0.1 mol l^{-1} glycine + ribose solutions and those heated at 80 °C for 196 hours) with/without the goethite layer. Raw pATR spectra (pATR = - log I/I_0; I: reflection intensity, I_o: incident intensity) for (a) the reactant solution without the goethite layer, (b) pure water without the goethite layer and (c) goethite thin layer (dried) are shown in Fig. 5.1.4. The spectra for aqueous solution (Fig. 5.1.4a and b) showed water absorptions around 772, 1635, 2110 and 3340 cm^{-1} (Masuda et al., 2003; Hamamoto et al., 2015). The goethite absorptions at 652 and 3125 cm^{-1} (Fig. 4.2.1c) were possibly masked by the strong absorptions by water. Smaller peaks around 1000-1600 cm^{-1} on the spectrum (a) were by the reactants. A raw pATR spectrum for goethite thin layer (dried) is shown in Fig. 5.1.4c. Peaks at 795, 890 and 3155 cm^{-1} were mostly similar to those in IR transflection (transmission-reflection) spectrum of goethite (Fig. 4.2.1c). However, the peak position for goethite by ATR-IR was slightly different from that by transflection method (895 cm^{-1} for Fig. 4.2.1c vs 890 cm^{-1} in Fig. 5.1.4a). These differences are originated from distortion of absorption bands by ATR-IR due to differences with wavenumber in penetration depths of evanescent waves (Masuda et al., 2003). An absorption around 2350 cm^{-1} is due to CO_2 on the optical path in the spectrometer. Small fine peaks in the 1300–1800 cm^{-1} region are due to water vapor, whose amount on the optical path in the spectrometer can be changed by ambient humidity. In the following, these peaks were removed from sample spectra by subtracting an spectrum for water vapor so as for a representative vapor peak height at 1845 cm^{-1} (baseline: 1839–1853 cm^{-1}) to become zero.

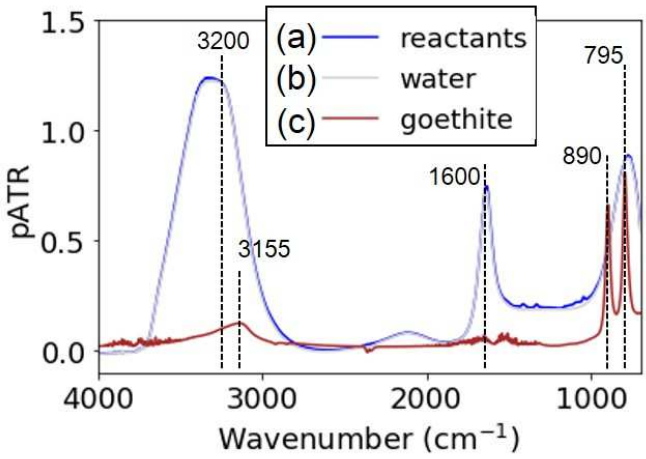

Fig. 5.1.4. Raw pATR-IR spectra for (a) the reactant solution (0.1 mol l^{-1} glycine + ribose solution), (b) pure water and (c) dried goethite thin layer.

Subtracting the water spectrum from an aqueous solution spectrum can provide an ATR-IR spectrum of solutes. In the following, solution spectra subtracted by pure water are presented.

The spectra for the reactants solution (pH = 5.8) shows absorption peaks at 1010, 1044, 1088, 1120, 1156, 1226, 1246, 1330, 1410, 1442, 1510, 1630 and 1780 cm^{-1} (Fig. 5.1.5$R_{5.8}$). Those for the reactant solutions at pH= 4.1 and 3.5 also show the same peaks (Fig. 5.1.5$R_{4.1}$ and $R_{3.5}$). Those for the reactant solution on the goethite layer showed peaks at 1010, 1044, 1088, 1120, 1156, 1226, 1246, 1330, 1410, 1442, 1510, 1630 and 1780 cm^{-1} (Fig. 5.1.5R+g).

Fig 5.1.5 $R_{5.8}$, $R_{4.1}$, $R_{3.5}$ and R+g show the glycine peak at 1510 cm^{-1} originated from amino group ($-NH_3^+$) and the peaks at 1330 and 1442 cm^{-1} originated from methyl group ($>CH_2$) (Kumar et al., 2005; Kitadai et al., 2010). The peaks at 1410 and 1630 cm^{-1} (Fig 5.1.5$R_{5.8}$, $R_{4.1}$, $R_{3.5}$ and R+g) can be due to symmetric and asymmetric stretching of COO^- of glycine, and the later possibly includes a reported peak by amino groups of glycine at 1600 cm^{-1} (Kitadai et al., 2010). The peak at 1740 cm^{-1} (Fig 5.1.5$R_{5.8}$, $R_{4.1}$ and $R_{3.5}$) can be due to C=O stretching of COOH group (Silverstein et al., 1991; Max et al., 1998). The larger intensities at 1740 cm^{-1} in the lower pH spectra (Fig 5.1.5$R_{5.8}$, $R_{4.1}$ and $R_{3.5}$) indicate protonation of COO^- of glycine by acidification of the reactant solution (Silverstein et al., 1991; Max et al., 1998). The peaks at 1044, 1088, 1120 and 1156 cm^{-1} (Fig 5.1.5$R_{5.8}$, $R_{4.1}$, $R_{3.5}$ and R+g) can be possibly originated from C-O bonds of ribose (Carmona and Molina, 1990). Some reported peaks by ribose can be recognized at 1010, 1226 1246 and 1442 cm^{-1} (Fig 5.1.5$R_{5.8}$, $R_{4.1}$, $R_{3.5}$ and R+g) (Huang et al., 2016).

The spectra for the product solutions (0.1 mol l^{-1} glycine + ribose solution heated at 80 °C for 196 hours without goethite, pH = 4.0 and 3.5) show similar peaks to the reactant solutions at 1010, 1044, 1088, 1120, 1156, 1226, 1246, 1330, 1410, 1442, 1510, and 1630 cm^{-1} (Fig. 5.1.5$P_{4.0}$ and $P_{3.5}$), originating from the residual reactants (Section 3.1). The bands around 1710 cm^{-1} in $P_{4.0}$ and $P_{3.5}$ spectra are broader and larger than those at 1740 cm^{-1} in $R_{5.8}$, $R_{4.1}$ and $R_{3.5}$ spectra. These broad bands around 1710 cm^{-1} can include a lower wavenumber component such as COOR group together with a contribution from COOH species around 1740 cm^{-1}. These COOH and COOR groups can be formed in intermediates and products of the Maillard reaction (Ikan et al., 1996).

The goethite spectrum in Fig. 5.1.4c is also shown in Fig. 5.1.5gt after removal of a water vapor spectrum. Several bands at 1200–1900 cm^{-1} (e.g. 1780 and 1685 cm^{-1}) are considered to be due to overtones and combinations of goethite fundamental bands such as 890 and 795 cm^{-1} (Fig. 5.1.4c). It should be noted that the other overtones and combinations of the goethite fundamental bands such as 652, 780 and 895 cm^{-1} can overlap the reactants' bands around 1200–1700 cm^{-1}.

Smaller fine peaks in the 1400–1800 cm^{-1} region are due to water vapor which remained after subtraction of pure water spectrum.

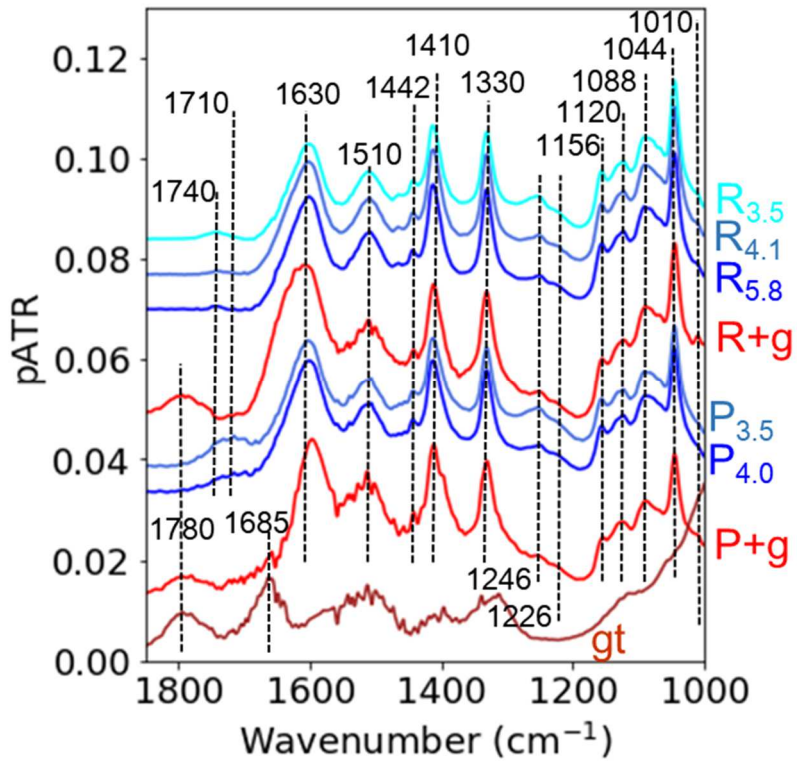

Fig. 5.1.5. Difference IR spectra from the pure water spectrum for the reactants without goethite with pHs of 5.8 ($R_{5.8}$), 4.1 ($R_{4.1}$) and 3.5 ($R_{3.5}$). (R+g): the reactants on goethite. The products without goethite with pHs of 4.0 ($P_{4.0}$) and 3.5 ($P_{3.5}$). (P+g): the products on goethite. (gt): goethite layer.

5.1.4. Discussion

In order to examine changes with time in the ATR-IR spectra for the reactant and product solutions with/without goethite layer, they are shown as difference spectra from the starting spectra (t = 0 second) for showing only time dependent changes removing contribution from the goethite layer (Fig. 5.1.5gt).

Representative difference spectra from t = 0 spectrum for (R) the reactant solution without goethite (Fig. 5.1.6R) at t = 0, 1, 2 and 3 hours show only a few changes due to water vapor. On the other hand, representative difference spectra from t = 0 spectrum for (R+g) the reactant solution with goethite (Fig. 5.1.6R+g)) show larger increases in bands at 1410 cm^{-1} (a) and 1630 cm^{-1} (b) than that without goethite. The peak at 1410 cm^{-1} (a) is due to asymmetric stretching of COO^- of glycine (Fig. 5.1.5R), and the peak at 1630 cm^{-1} (b) is due to symmetric stretching of COO^- of glycine (Fig. 5.1.5R).

Representative difference spectra from t = 0 spectrum for the product solution without goethite (Fig. 5.1.6P) show also increases in bands at 1410 cm^{-1} (A) and 1630 cm^{-1} (B). Those for the product solution with goethite (Fig. 5.1.5P+g) show larger increases in bands at 1390 cm^{-1} (A') and 1630 cm^{-1} (B) than that without goethite (Fig. 5.1.5P). Moreover, a band at 1710 cm^{-1} (C) appeared and increased with time. It should be noted that the peak at 1410 cm^{-1} shifted with time toward 1390 cm^{-1}.

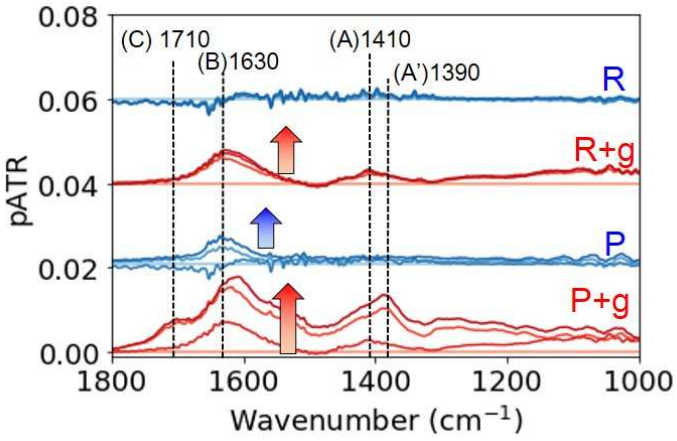

Fig. 5.1.6. Representative difference IR spectra (t = 0, 1, 2 and 3 hours) from t = 0 spectrum for (R) the reactant solution without goethite, (R+g) the reactant solution on goethite, (P) the product solution without goethite and (P+g) the product solution on goethite.

In order to show quantitatively these increases, changes with time in peak heights at (A) 1410, (B) 1630 and (C) 1710 cm^{-1} (baselines: 1325–1443, 1500–1800 and 1500–1800 cm^{-1} for each) in the R, P, R+g and P+g spectra are plotted in Fig. 5.1.7. The peaks and baselines were selected so that fluctuations of water vapor peaks affect as less as possible.

Increases in the intensities of peaks at 1410 and 1630 cm^{-1} without goethite (R and P) can correspond to increases in the concentration of components with COO^- functional groups (symmetric and asymmetric vibrations) due to water evaporation (Fig. 5.1.7A and B). However, larger increases in these intensities with goethite (R+g and P+g) than in those without goethite (R and P) cannot be explained by this evaporation effect. These might be due to adsorption of COO^--bearing components onto the goethite layer. The increases in these intensities at 1410 and 1630 cm^{-1} are about twice as large for the products (P+g) than for the reactants (R+g) (Fig. 5.1.7A and B). COO^--bearing components in the products can be more strongly adsorbed on goethite. It should be noted that these increases can be larger for P+g because of the band shift from 1410 to 1390 cm^{-1} for P+g.

The peak height at 1710 cm^{-1} with a linear baseline at 1500–1800 cm^{-1} remained mostly unchanged for the reactants and the products without goethite (Fig. 5.1.7C). The negative peak heights can be due to increases in broad 1630 cm^{-1} band affecting the inclination of baselines. This 1710 cm^{-1} peak increased only for the products with goethite (P+g) (Fig. 5.1.7C). Since this peak is due to either COOH or COOR groups, these carboxyl or ester components can be adsorbed on goethite.

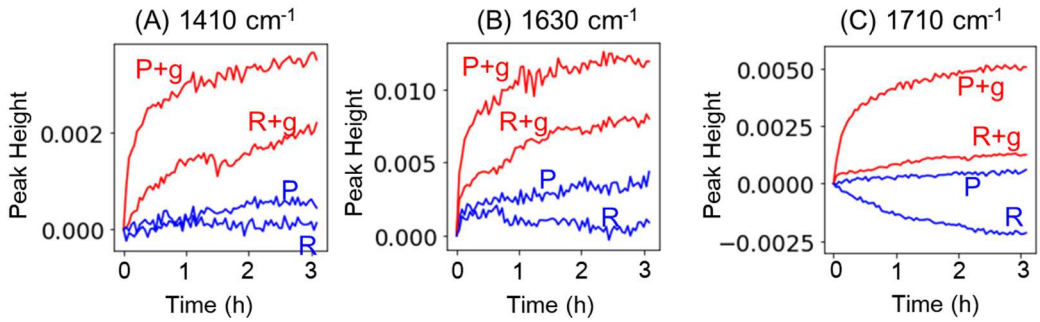

Fig. 5.1.7. Changes with time (0-3 hours) in IR peak heights at (A) 1410, (B) 1630 and (C) 1710 cm^{-1} (baselines: 1325–1443, 1500–1800 and 1500–1800 cm^{-1}, respectively) in the R, R+g, P and P+g spectra of Fig. 5.1.6.

From the above observation, oxygenated components in both the reactants and products are considered to be adsorbed onto goethite in a few hours at room temperature. Adsorbed amounts onto goethite were generally larger for the product solution than for the reactant solution.

In Section 4.3, the time scales for the simulated Maillard reaction progress are suggested to be more than several days at 60–80 °C (Fig. 4.3.3) and can be far much longer at room temperature. It should be noted that the enhancement of reaction progress in the presence of goethite occurred already within a day (Fig. 4.3.3). On the other hand, adsorption of the reactant glycine and products onto goethite occurred within a few hours at room temperature (Fig. 5.1.7). Therefore, later processes on the goethite surface after the fast adsorption are necessary for the reaction enhancement. They can be possibly due to acceleration of association of glycine, ribose and reaction intermediates with COOH

or COOR groups by their higher concentrations on the goethite surface.

The goethite surface is reported to be charged positively with mainly surface Fe-OH_2^+ groups under pH conditions of this study (pH = 4.0–5.8) (Zeltner and Anderson, 1988). Therefore, negatively charged COO^- groups can be easily attracted on the goethite surface and adsorption of glycine and the Maillard reaction products on goethite is suggested to be driven by electrostatic interaction of these charged groups. Electrostatic interaction has also been suggested in some previous studies using silica (Vlasova and Golovkova, 2004; Kitadai et al., 2009b) and montmorillonite (Kitadai et al., 2009a), whose surfaces are negatively charged and can interact with positively charged amino acids such as lysine. On the other hand, COOH or COOR groups can also be adsorbed by hydrogen bonding between oxygen molecules of these groups and hydrogenated goethite surface. Olsson et al. (2011) suggested adsorption of glucose on goethite via hydrogen bonding interaction. Since the pH of the product solution became more acidic (pH = 4.0) than the reactant solution (pH = 5.8), the surface positive charge of goethite possibly increased (Zeltner and Anderson, 1988) resulting in larger adsorption of these components (Fig. 5.1.7A and B).

For the better understanding of mechanism of these adsorption processes, kinetic analyses for increase in adsorbed components are needed. Strauss et al. (1997) and Luengo et al. (2006) conducted adsorption experiments of phosphate on goethite for more than a week and suggested that the adsorption could be described by combination of faster initial and slower secondly processes. Therefore, in the future study, adsorption experiments for longer duration should be conducted.

5.2. Development of in situ hydrothermal ATR-IR spectroscopic measurement systems

In order to understand detail surface processes, kinetic ATR-IR measurements at goethite surfaces at different temperatures (20–80 °C) for longer duration are necessary. We have designed and constructed a new in situ heatable ATR-IR cell without solvent evaporation, for precise quantitative monitoring of surface processes (made by Center for Scientific Instrument Renovation and Manufacturing Support, Osaka Univ.). An overview and a schematic cross section of the cell is shown in Fig. 5.2.1. A sample solution stays in a space sandwiched by an ATR crystal (ZnSe), an o-ring and an upper CaF_2 (calcium fluoride) optical window of 2 mm thick and 20 mm in diameter. And it is sealed by compression by upper and lower caps through rubber O-rings of 20 mm in diameter.

The in situ heatable ATR-IR cell can be set on a commercial variable angle ATR unit (VeeMAX, PIKE). The ATR unit can be set in the sample compartment of the IR spectrometer (FTIR4100, Jasco) (Fig. 5.2.2). These apparatuses are arranged so as for IR signal to be as strong as possible by using a designed pedestal. A plastic plate on the ATR unit (Fig. 5.2.2b) enables the sample compartment including the ATR unit to be sealed.

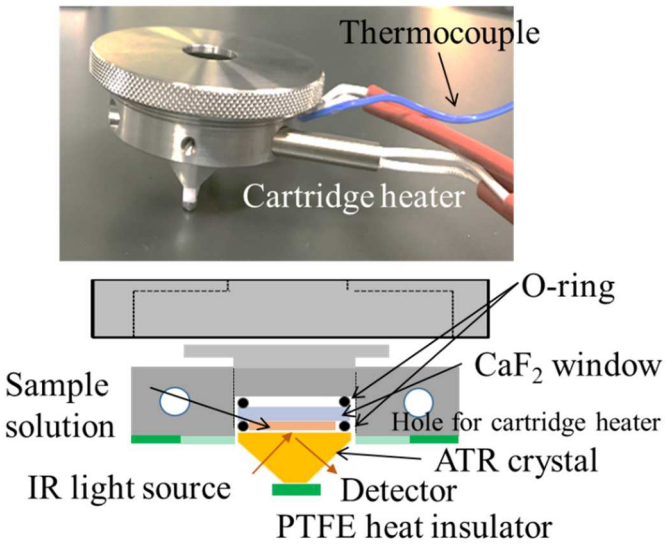

Fig. 5.2.1. An overview and a cross section of the new heatable cell for ATR-IR spectroscopy.

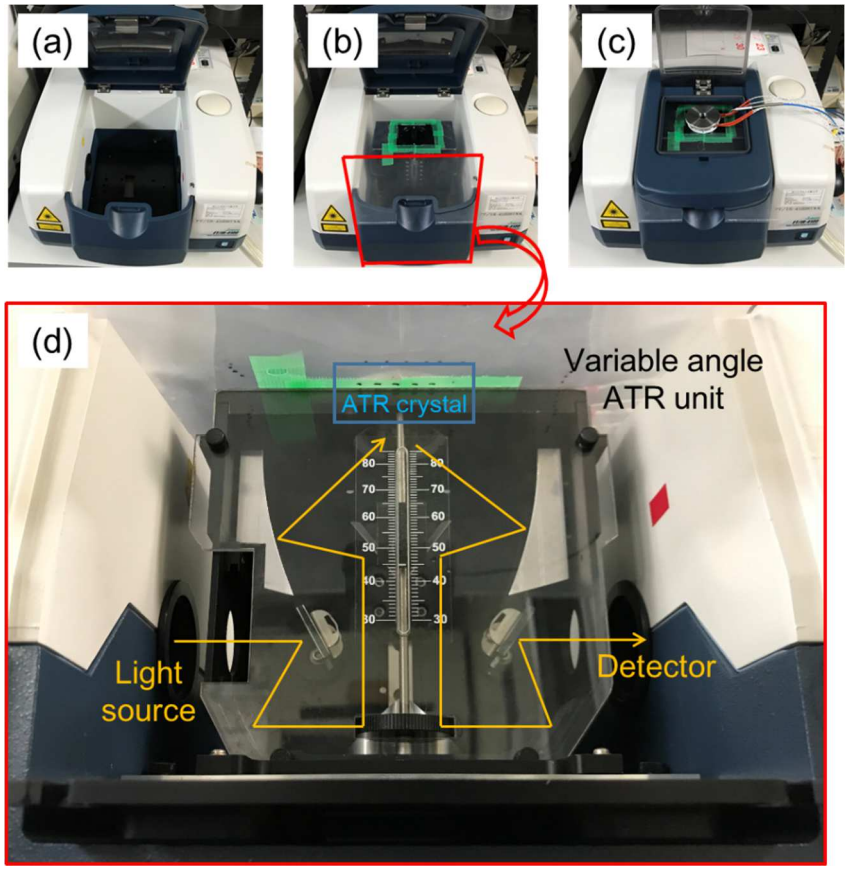

Fig. 5.2.2. (a) The sample compartment of the FT-IR spectrometer (Jasco FTIR4100). (b) A photograph of the sample compartment with the variable angle ATR unit (VeeMAX, PIKE). (c) A photograph after setting the new in situ heatable ATR-IR cell. (d) A photograph of the variable angle ATR unit with indication of light pathway.

In order to check the stability of the above ATR cell for in situ hydrothermal measurements, in situ ATR-IR spectroscopy for 0.1 mol l^{-1} glycine + ribose mixture solution with/without goethite layers at 80 °C for 48 hours was conducted. A sample solution (0.6 ml) was pipetted onto the ATR crystal and their IR spectral changes with time were measured every 300 seconds for 172800 seconds (48 hours) at 80 °C. The IR spectral measurements were accumulated for 64 scans with a wavenumber resolution of 4 cm^{-1} in the 400–7800 cm^{-1} spectral range. The goethite layers were made on the ATR crystal (ZnSe) in the same way as in Section 5.1. Background signal was measured just before turning on the heater for the interval measurements. Therefore, in situ ATR-IR spectra for the sample with the goethite layers did not incorporate absorption by goethite.

Fig. 5.2.3 shows representative ATR-IR spectra for 0.1 mol l^{-1} glycine + ribose mixture solution (+g) with and (-g) without goethite layers heated at 80 °C (0–48 hours) in the 700–4000 cm^{-1} spectral range, where they were shifted vertically for clarity. A spectrum for water vapor measured by this apparatus has been subtracted from each spectrum in the same way as in Section 5.2. They show strong

absorptions around 1640 and 3370 cm^{-1} due to vibrations of water molecules and a little increase with time in absorption by water vapor even after the spectral subtraction (Eizenberg and Kauzmann, 1969).

The newly-made cell is for a single reflection ATR crystal, while multiple reflection ATR crystal were used for the measurements at room temperature presented in Section 5.1. Therefore, absorption by water vapor on the light pathway might not be negligible in comparison with absorption by the sample in the domain of evanescent waves. Moreover, absorbance at smaller wavenumbers increased with time for each in situ measurement and absorbances at 795 and 900 cm^{-1} due to goethite decreased with time for the in situ measurement with the goethite layers. This spectral instability should be improved in the future study. This measurement system is still under development, especially in terms of preventing water vapor fluctuation for measurements with long time durations.

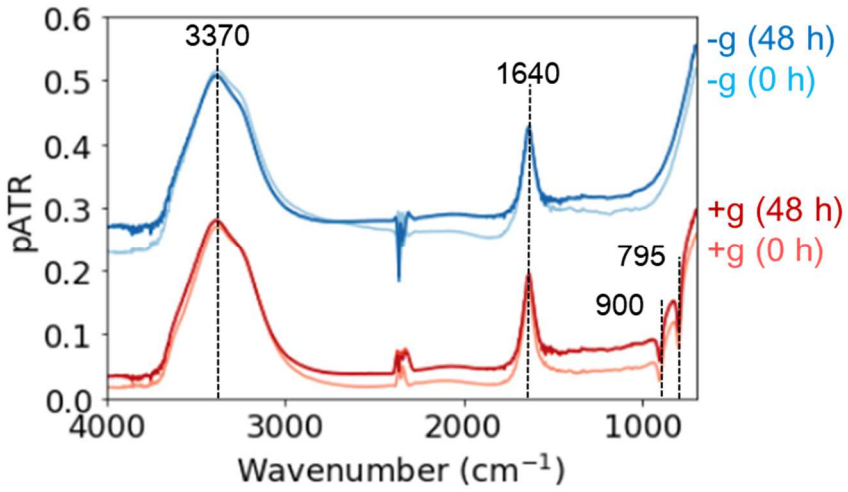

Fig. 5.2.3. Representative pATR-IR spectra for 0.1 mol l^{-1} glycine + ribose mixture solution (+g) with and (-g) without goethite layers heated at 80 °C (0–48 hours).

5.3. Conclusion

Direct monitoring of adsorption onto goethite of reactants and products of the simulated Maillard reaction by 0.1 mol l^{-1} glycine + ribose solutions was conducted on thin layers of goethite on an ATR crystal (ZnSe). IR spectral changes with time for the reactant (non-heated) and product (heated at 80 °C for 196 hours) solutions on the goethite layer were measured every 150 seconds for 10800 seconds at room temperature. Increases in peak heights at 1410, 1630 and 1710 cm^{-1} suggested fast adsorption of components with COO^{-}, COOH and COOR groups on positively charged goethite surface.

This adsorption process within a few hours at room temperature was faster than the formation enhancement of humic-like and brown products in several days (Chapter 4), suggesting that the adsorption process is not rate-limiting for the reaction enhancemnt. An in situ hydrothermal ATR-IR cell under development can be used for further detailed kinetic studies of surface processes on goethite layers at different temperatures (20–80 °C).

REFERENCES

Arfaioli, P., O. L. Pantini, M. Bosetto, G. G. Ristori. “Influence of clay minerals and exchangeable cations on the formation of humic-like substances (melanoidins) from D-glucose and L-tyrosine”. Clay Miner. 1999. 34. 487–497.

Carmona, P., M. Molina. “Raman and infrared spectra of D-ribose and D-ribose 5-phosphate”. J. Raman Spectrosc. 1990. 21. 395–400.

Chung, S. Y., S. H. Han, S. W. Lee, C. Rhee. “Effect of Maillard reaction products prepared from glucose–glycine model systems on starch digestibility”. Starch 2012. 64. 657–664.

Eisenberg, D.,W. Kauzmann. “Structure and properties of water”. Oxford University Press. 1969.

Hamamoto, M., M. Katsura, N. Nishiyama, R. Tonoue, S. Nakashima. “Transmission IR micro-spectroscopy of interfacial water between colloidal silica particles”. e-J. Surf. Sci. Nanotech. 2015. 13. 301–306.

Huang, Y. T., H.F. Liao, S. L. Wang, S. Y. Lin. “Glycation and secondary conformational changes of human serum albumin: study of the FTIR spectroscopic curve-fitting technique”. AIMS Biophys. 2016. 3. 247–260.

Hug, S. J. “In situ fourier transform infrared measurements of sulfate adsorption on hematite in aqueous solutions”. J. Colloid Interface Sci. 1997. 18. 415–422.

Hug, S. J., B. Sulzberger. “In situ Fourier transform infrared spectroscopic evidence for the formation of several different surface complexes of oxalate on TiO2 in the aqueous phase”. Langmuir 1994. 10. 3587–3597.

Ikan, R., Y. Rubinsztain, A. Nissenbaum, I. R. Kaplan. “Geochemical aspects of the Maillard reaction” in R. Ikan (Ed.). “The Maillard reaction: consequences for the chemical, life sciences”. John Wiley & Sons. 1996. 1–25.

[a]Kitadai, N., T. Yokoyama, S. Nakashima. “In situ ATR-IR investigation of L-lysine adsorption on montmorillonite”. J. Colloid Interface Sci. 2009. 338. 395–401.

[b]Kitadai N., T. Yokoyama, S. Nakashima. “ATR-IR spectroscopic study of L-lysine adsorption on amorphous silica”. J. Colloid Interface Sci. 2009. 329. 31–47.

Kitadai, N., T. Yokoyama amd S. Nakashima. “Temperature dependence of molecular structure of dissolved glycine as revealed by ATR-IR spectroscopy”. J. Mol. Struct. 2010. 981. 179–186.

Kumar, S., A. K. Rai, V. B. Singh and S. B. Rai. “Vibrational spectrum of glycine molecule”. Spectrochim. Acta Pt. A 2005. 61. 2741–2746.

Luengo, C., M. Brigante, J. Antelo, M. Avena. “Kinetics of phosphate adsorption on goethite: Comparing batch adsorption and ATR-IR measurements”. J. Colloid Interface Sci. 2006. 300. 511–518.

Masuda, K., T. Hamasaki, S. Nakashima, B. Habert, I. Martinez, S. Kashiwabara. “Structural change of water with solutes and temperature up to 100 °C in aqueous solutions as revealed by attenuated total reflectance infrared spectroscopy”. Appl. Spectrosc. 2003. 57. 274–281.

Max, J. J., M. Trudel, C. Chapados. “Infrared titration of aqueous glycine”. Appl. Spectrosc. 1998. 52. 226–233.

Olsson, R., R. Giesler, P. Persson. “Adsorption mechanisms of glucose in aqueous goethite suspensions”. J. Colloid Interface Sci. 2011. 353. 263–268.

Silverstein, R. M., G. C. Bassler, T. C. Morrill. “Spectrometric Identification of Organic Compounds”. Wiley. 1991.

Strauss, R., G. W. Brummer, N. J. Barrow. “Effects of crystallinity of goethite: II. Rates of sorption and desorption of phosphate”. Eur. J. Soil Sci. 1997. 48. 101–114.

Taguchi, K., Y. Sampei. “The formation, and clay mineral and $CaCO_3$ association reactions of melanoidins”. Org. Geochem. 1986. 10. 1081–1089.

Vlasova, N. N., L. P. Golovkova. “The adsorption of amino acids on the surface of highly dispersed silica”. Colloid J. 2004. 66. 657–662.

Zeltner, W. A., M. A. Anderson. “Surface charge development at the goethite/aqueous solution

interface: effects of CO_2 adsorption”. Langmuir. 1988. 4. 469–474.

CHAPTER 6

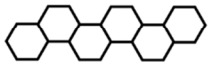

Summary and future perspectives

6.1. Summary

6.1.1. General introduction

"Humic substance" is a general term of polymerized high molecular weight organic matter, whose structure is not well defined, present in Earth's surface environments. The reactive functional groups of humic substances may influence environmental pollution by adsorbing and transporting pollutants, and promoting the chemical reactions (Stevenson, 1994). However, the processes and rates of formation of humic substances are complicated and poorly understood. On the other hand, the Maillard reaction is a continuous reaction between an amino group in amino acids and a carbonyl group in sugars producing polymerized brown-colored high molecular weight organic compounds, melanoidins (Maillard, 1912) leading to a formation of humic-like substances. The Maillard reaction is considered to be a dominant process in the aquatic environment such as at the bottom of a deep lake where there is few microorganisms (Stevenson, 1994).

In this thesis, for evaluating time scales of formation processes of humic-like substances simulated by the Maillard reaction, hydrothermal changes in glycine + ribose mixture solutions and their interactions with an iron hydroxide (goethite) were examined. In Chapter 2, in situ hydrothermal spectroscopic measurement systems for the simulated Maillard reactions were first developed. In situ IR and UV–Vis spectroscopic measurements for the Maillard reaction of 0.5 mol l^{-1} glycine + ribose mixture solution at 60–80 °C were conducted. In Chapter 3, for tracing UV spectral changes in detail, in situ UV–Vis spectroscopy for 0.1 mol l^{-1} glycine + ribose solutions at 60–80 °C was performed. Spectroscopic similarity between humic substances and the simulated Maillard reaction products was also discussed and validity of UV–Vis spectroscopy was suggested. In Chapter 4, changes with time in absorbance at 420 nm (indicator of humic substances) were analyzed at 60–80 °C in the presence and absence of an iron hydroxide (goethite). Enhancement of reaction rates in the presence of goethite was recognized. Effects of initial concentrations (0.5 or 0.1 mol l^{-1}) were also noticed. In order to examine surface processes on goethite during the simulated Maillard reaction, adsorption on goethite of reactants and products of the Maillard reaction at room temperature was studied by attenuated total reflection infrared (ATR-IR) spectroscopy (Chapter 5). In this chapter, these results are summarized again and overall discussion and future perspectives are presented.

6.1.2. Development of in situ hydrothermal spectroscopic measurement systems for the simulated Maillard reaction

For stable in situ IR and UV–Vis spectroscopic measurements for the Maillard reaction by 0.5 mol l^{-1} glycine + ribose mixture solution as a reaction simulating formation processes of humic-like substances, the original heatable liquid cell (Fig. 6.1.1) was newly designed and constructed.

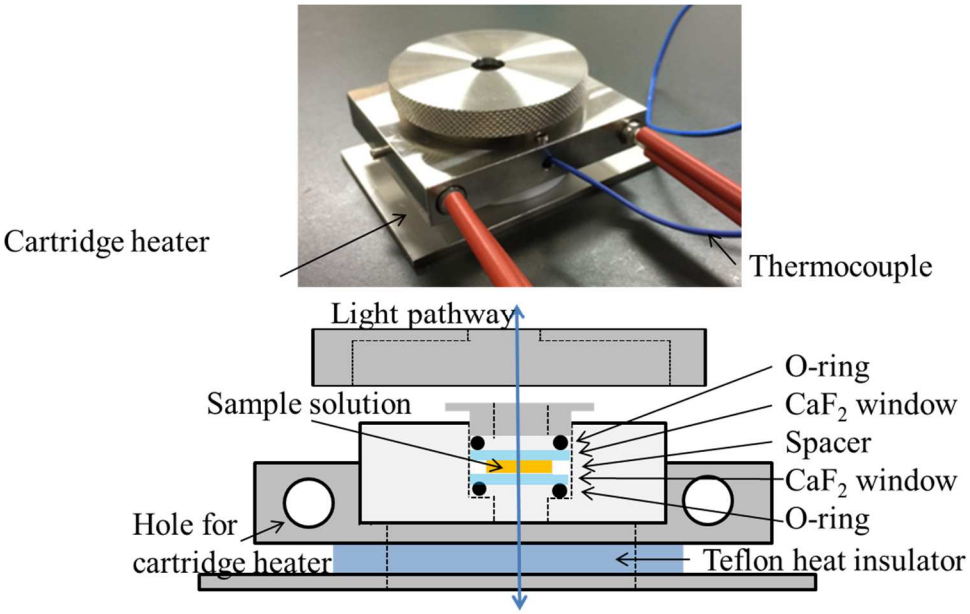

Fig. 6.1.1. An overview and a cross section of the new heatable liquid cell.

First, for tracing degradation of the reactants by the Maillard reaction, in situ IR spectroscopic measurements using the above heatable liquid cell were conducted. Representative in situ IR spectra for 0.5 mol l^{-1} glycine + ribose mixture solutions heated at 80 °C (0–48 hours) in the 400–7800 cm^{-1} spectral range are shown in Fig.6.1.2. They show peaks around 1600, 3400, 5200 and 7000 cm^{-1} corresponding to vibrations of water molecules (Eizenberg and Kauzmann, 1969). PTFE spacers of 0.05 mm thick enabled unsaturation of absorbance in the 900–1800 cm^{-1} spectral range. The peaks around 5200 and 7000 cm^{-1} due to water were not saturated neither. Constancy of these bands suggested the stability of the hydrothermal system without solution escape.

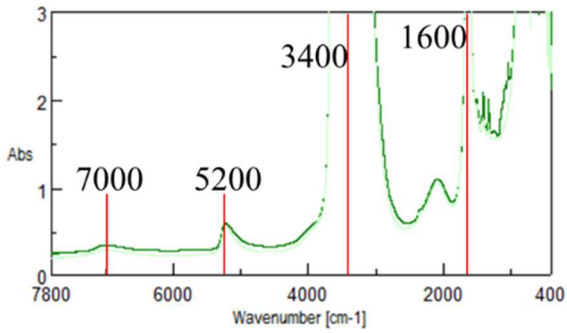

Fig. 6.1.2. Representative IR spectra of 0.5 mol l^{-1} glycine + ribose mixture solutions heated at 80 °C (0–48 hours) in the 400–7800 cm^{-1} spectral range.

The decreasing 1100 and 1330 cm^{-1} band area (baseline: 1020–1170 and 1290–1360 cm^{-1}, respectively) were analyzed as indicators of amounts of ribose and glycine, respectively (Carmona and Molina, 1990; Kumar et al., 2004). The decreases with time in the band area were fitted by the exponential equation assuming the first order reaction (Fig. 6.1.3). Apparent first order rate constants for decreases in 1100 (k_{1100}) and 1330 (k_{1330}) cm^{-1} band area were determined at 60–80 °C. They are listed in Table 6.1.1 and shown in Fig. 6.1.4a.

The Arrhenius plots of k_{1100} and k_{1330} and T (333–350 K) (Fig. 6.1.4a) gave linear trends and the fitted lines give the E_a (activation energy) and A (frequency factor) by the Arrhenius equation:

$$\ln k = \ln A - \frac{E_a}{RT}$$

By extrapolating these linear trends to a representative Earth surface temperature of 15 °C, half-lives ($t_{1/2}$) for ribose and glycine decreases were estimated to be about 2.3 and 2.1 years, respectively.

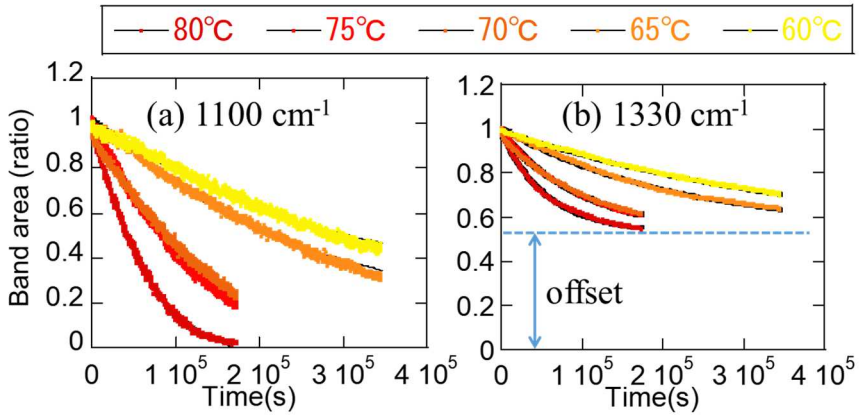

Fig. 6.1.3. Changes with time in normalized (a) 1100 cm^{-1} (ribose) and (b) 1330 cm^{-1} (glycine) band areas during in situ IR spectroscopy of 0.5 mol l^{-1} glycine + ribose mixture solutions heated at 60, 65, 70, 75 and 80 °C with exponential fitting curves (the first order reaction).

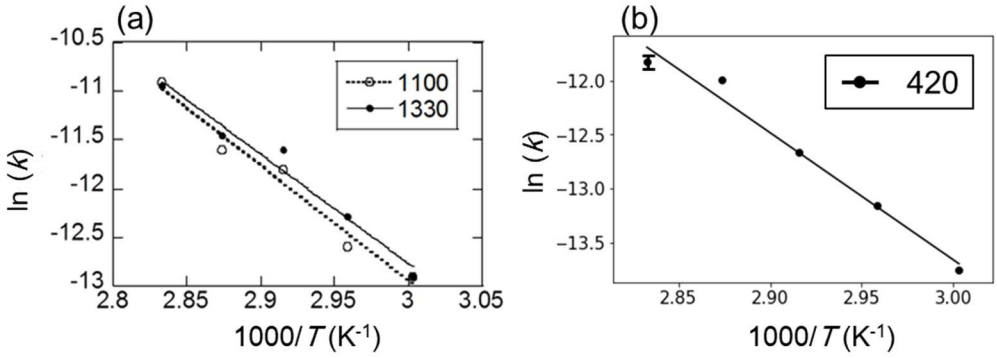

Fig. 6.1.4. The Arrhenius plots of (a) k_{1100} and $k_{1330,}$ and (b) k_{420}, and their fitting lines.

Table 6.1.1. The activation energy E_a, and the frequency factor A values obtained from the fittings of data in Fig. 6.1.4 by the Arrhenius equations and k_{1100}, k_{1330}, k_{420} values and half-lives of the first order reaction stage at 15 °C estimated by extrapolation of the fitted Arrhenius equations.

	E_a (kJ mol^{-1})	A (s^{-1})	k at 15 °C (s^{-1})	Half-life at 15 °C (y)
Ribose decrease (1100 cm^{-1})	98	4.8×10^{9}	9.4×10^{-9}	2.3
Glycine decrease (1330 cm^{-1})	93	1.2×10^{9}	1.4×10^{-8}	2.1
Browning (420 nm)	98	2.7×10^{9}	4.5×10^{-9}	4.9

Second, for tracing formation of brown products by the Maillard reaction, in situ UV–Vis spectroscopic measurements of 0.5 mol l^{-1} glycine + ribose mixture solutions heated at 60–80 °C (0–144 hours) using the same heatable liquid cell were conducted. Constancy of the sample thickness was checked by IR spectroscopy before and after each in situ UV–Vis spectroscopic measurement and 5200 cm^{-1} band area (average value of before and after) was used for normalizing the experimental spectra in terms of the solution thickness. In situ UV–Vis spectra (Fig. 6.1.5) showed that absorbance at shorter wavelength increased more for longer heating durations. Spectral saturation occurred in UV region (200–400 nm) (not shown) because of strong absorption by UV active products.

Absorbance at 420 nm with one-point base at 800 nm (Vis_{420}) was employed as an indicator of browning during the Maillard reaction (Stamp and Labuza, 1983). Their changes with time during the in situ measurements at each heating temperature were fitted by the exponential equation assuming the first order reaction (Fig. 6.1.6) and k_{420} and $t_{1/2}$ values were obtained.

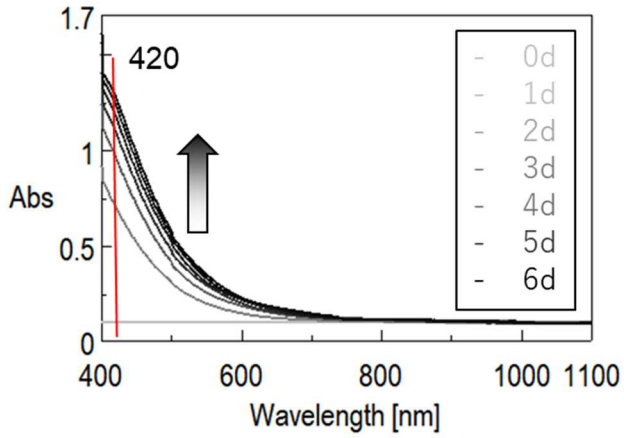

Fig. 6.1.5. Representative in situ visible spectra for the product solutions of 0.5 mol l^{-1} glycine + ribose mixture solutions heated at 80 °C for 0, 1, 2, 3, 4, 5 and 6 days. Red line shows absorbance at 420 nm (Vis_{420}).

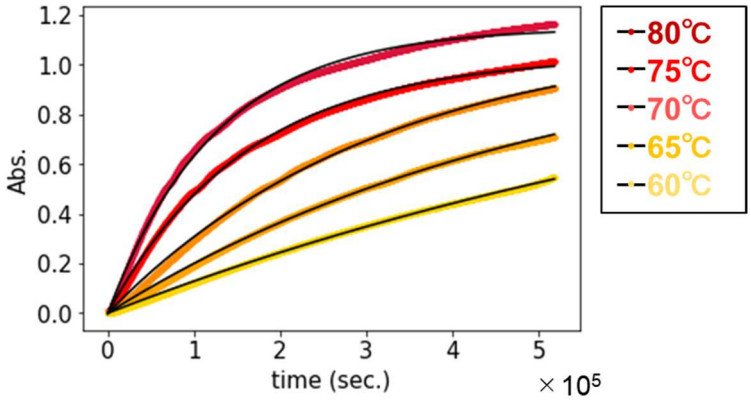

Fig. 6.1.6. Changes in Vis_{420} with time during the in situ measurements of 0.5mol l^{-1} glycine + ribose mixture solutions heated at 60, 65, 70, 75, and 80 °C with the fitting curves (the first order reaction). Changes at 80 °C are for the representative series and changes for the other two experiments were not shown.

The Arrhenius plots of k_{420} and T (333–350 K) (Fig. 6.1.4b) gave a linear trend and the fitted line gives the E_a (activation energy) and A (frequency factor) by the Arrhenius equation (Table 6.1.1). Previous kinetic analyses of the batch Maillard reactions reported wide ranges of activation energies (16–238 kJ mol^{-1}) possibly due to different experimental conditions and kinetic analyses (van Boekel, 2001). The present data by in situ IR and visible measurements with the activation energy of 90–100 kJ mol^{-1} can give constraints on the better understanding of the Maillard reaction (Table 6.1.1).

The k_{420} values at 60–80 °C was extrapolated to lower temperatures by the Arrhenius equation (Table 6.1.1). The half life ($t_{1/2}$) for increase in browning product (420 nm) is about 4.9 years, slightly longer than about 2 years for decreases in reactants (ribose and glycine).

6.1.3. Spectroscopic similarity between humic substances and the simulated Maillard reaction products

The spectral changes for 0.5 mol l^{-1} glycine + ribose mixture solution in UV range were not traced because of spectral saturation even using a 0.05 mm thickness spacer (Fig. 6.1.5). Therefore, for tracing UV spectral changes, similar measurements at lower initial concentrations were needed. In Chapter 3, in situ UV–Vis spectroscopic measurements for the Maillard reaction of 0.1 mol l^{-1} glycine + ribose mixture solution at 60–80 °C were conducted.

First, in order to check validity of using UV–Vis spectra for monitoring progress of the Maillard reaction, batch heating experiments of 0.1 mol l^{-1} glycine + ribose solutions at 80 °C were conducted directly in solution states. The product solutions were analyzed by (1) UV–Vis spectroscopy, (2) 3D-EEM fluorescence spectroscopy, (3) SELC, (4) IR spectroscopy, (5) HSQC-NMR spectroscopy and (6) MALDI-TOF-MS. Generalized 2D-COS were also used to examine correlations among some of the above spectroscopic data.

A) Representative UV–Vis spectra for 0.1 mol l^{-1} glycine + ribose mixture solutions heated at 80 °C for 0, 24, 48, 72, 96, 120, 144 and 168 hours (diluted 100 times) (Fig. 6.1.7a) showed that a band around 280 nm increased with time and that absorbance at shorter wavelength increased more for longer heating durations. A spectrum for the solution heated for 168 hours and that after dialysis (> 3500 Da) (Fig. 6.1.7b) showed that absorption in the UV region generally decreased after dialysis, in particular around 280 nm. On the other hand, SEC chromatograms by 280 nm suggested the formation with time of small molecular weight components with 280 nm absorption. These were considered to include furfural, one of reported intermediates of the Maillard reaction having an absorption peak around 280 nm (Martinez et al., 2000). By 2D correlation spectroscopic analyses, a band around 280 nm above the baseline of 245–315 nm were suggested to be taken as a measure of the formation of furfural-like intermediates.

B) Absorption in the UV region generally decreased after dialysis, while broad and featureless absorption remained in the visible region (Fig. 6.1.7b). This indicated the presence of larger products as well as 3D-EEM spectra (Fig. 6.1.8) and chromatograms by fluorescence intensity at Ex. 345 nm/Em. 430 nm. The fluorescence maxima resembled to those of natural humic solutions reported in a previous research (Nagao et al., 2003) (Fig. 6.1.8). By 2D correlation spectroscopic analyses, it was suggested that 254 nm absorbance with a one-point base at 600 nm (UV_{254}) can be employed as a measure of the humic-like products.

C) IR and HSQC-NMR spectra for 0.1 mol l^{-1} glycine + ribose mixture solutions heated at 80 °C for 168 hours showed peaks of glycine and ribose together with some new peaks of the products including aliphatic and aromatic components.

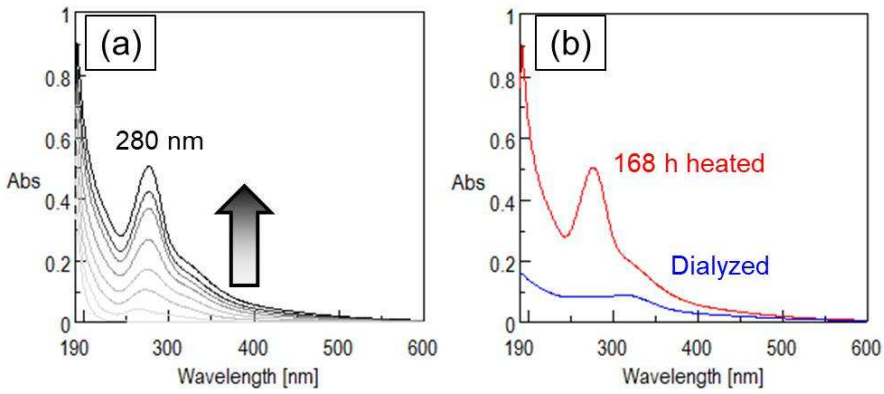

Fig. 6.1.7 (a) Representative UV–Vis spectra for the product solutions of 0.1 mol l^{-1} glycine + ribose mixture solutions heated at 80 °C for 0, 24, 48, 72, 96, 120, 144 and 168 hours (diluted 100 times) and (b) spectra for the 168 hours heated solution and for the dialyzed solution (> 3500 Da) (diluted 100 times).

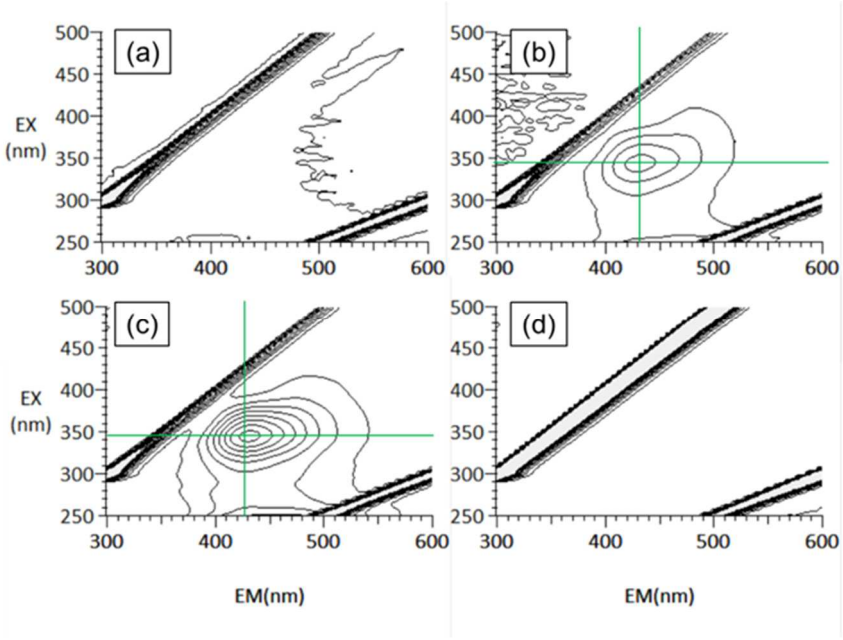

Fig. 6.1.8. Representative 3D-EEM spectra for the 0.1 mol l^{-1} glycine + ribose mixture solutions heated at 80 °C for (a) 0, (b) 96 and (c) 168 hours, and (d) the dialyzed solution. All the solutions were diluted 100 times. Contour intervals are 2.5 intensity units. Fluorescence intensity maximum positions at Ex. 345 nm/Em. 430 nm are indicated.

Second, in order to evaluate precise kinetic data for the progress of the Maillard reaction by using 280 nm and 254 nm absorbances, in situ UV–Vis spectroscopy with the original heatable liquid cell was conducted on 0.1 mol l^{-1} glycine + ribose mixture solutions heated at 60, 65, 70, 75 and 80 °C for 0–144 hours. Changes with time in band area around 280 nm (UV_{280}) and absorbance at 254 nm (UV_{254}) were divided into an early induction stage and a later apparent first order reaction stage. The changes in the later apparent first order stage were fitted by the following equations:

$$UV_{280} = C_1\left(1 - \exp\left(-k_{280}(t-\tau)\right)\right)$$
$$UV_{254} = C_1\left(1 - \exp\left(-k_{254}(t-\tau)\right)\right)$$

where k_{280} and k_{254} were apparent first order reaction rate constants and τ was considered to be a starting time of the later apparent first order stage. The fitting curves are shown in Fig.6.1.9 on the UV_{280} and UV_{254} changes. The fittings gave k_{280}, k_{254} and τ for UV_{280} and UV_{254}. In addition, τ was used as a kinetic parameter determining time scales of the reaction reflecting periods of the induction stage, and pseudo reaction rate constants in the induction stage ($k^{ind}{}_{280}$ and $k^{ind}{}_{254}$) were defined by $1/\tau$.

Kinetic analyses of the obtained reaction rate constants by the Arrhenius equation gave the activation energies and frequency factors. Fig. 6.1.10 shows the Arrhenius plots of k_{280}, $k^{ind}{}_{280}$, k_{254} and $k^{ind}{}_{254}$ values and their fitting lines. The obtained reaction rate constants at 60–80 °C were extrapolated to 15 °C by the Arrhenius equation. The obtained E_a, A and time scale values at 15 °C were listed in Table 6.1.2, where time scale values at 15 °C for the later stage were half-lives for k_{280} and k_{254} at 15 °C, and those for the induction stage were determined by reciprocals of $k^{ind}{}_{280}$ and $k^{ind}{}_{254}$ at 15 °C.

The time scale values at 15 °C for the induction stage (2.6 and 0.1 years) are much shorter than those for the later stage (20 and 174 years), and time scales of the whole reaction may be controlled by the later stage.

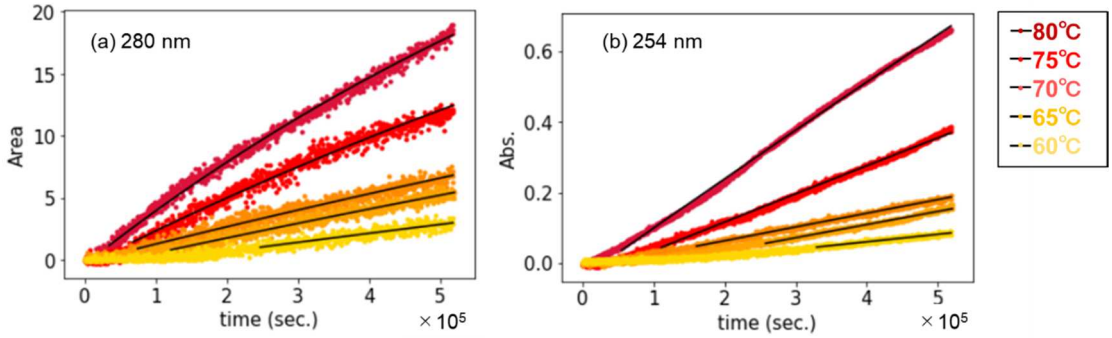

Fig. 6.1.9. Changes in (a) UV_{280} and (b) UV_{254} with time during the in situ measurements of 0.1mol l^{-1} glycine + ribose mixture solutions heated at 60, 65, 70, 75, and 80 °C with the fitting curves (the first order reaction).

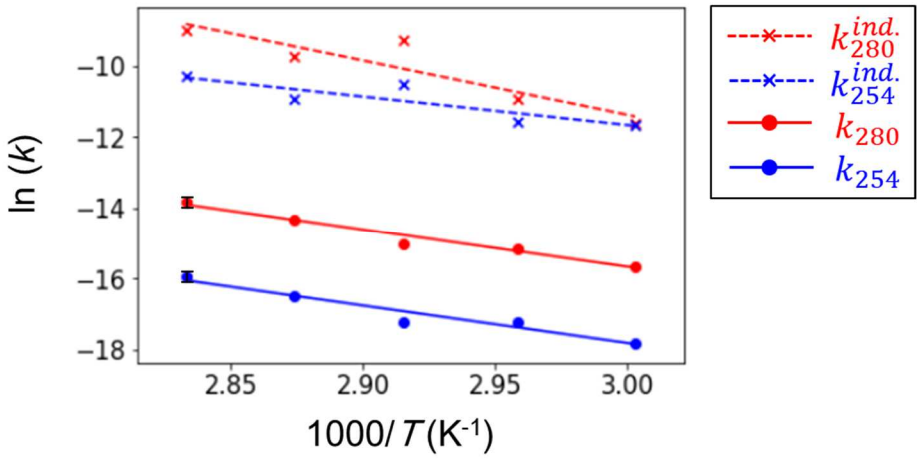

Fig. 6.1.10. The Arrhenius plots of k_{280}, k^{ind}_{280}, k_{254} and k^{ind}_{254} values and their fitting lines.

Table 6.1.2. The obtained E_a, A and the time scale values at 15 °C for the reactions in the induction and the first reaction stages of (a) 280 nm band area and (b) 254 nm absorbance in the heating experiments of 0.1 mol l^{-1} glycine + ribose mixture solutions at 60, 65, 70, 75 and 80 °C.

		E_a (kJ mol^{-1})	A (s^{-1})	Time scale values at 15 °C (years)
(a) 280 nm	Later 1st order stage	87	8.1×10^{6}	20
	Early induction stage	127	8.9×10^{14}	2.57
(b) 254 nm	Later 1st order stage	88	1.0×10^{6}	174
	Early induction stage	66	2.2×10^{5}	0.11

6.1.4. Effects of goethite on the simulated Maillard reaction

The original heatable liquid cell enabled in situ spectroscopic measurements for the simulated Maillard reaction by glycine + ribose mixture solution forming humic-like substances in infrared (Chapter2), visible (Chapter 2) and ultraviolet (Chapter 3) range. They were conducted in solution state simulating reactions in the aqueous environment. On the other hand, solid-liquid interfaces are crucial for dynamic behavior of Earth systems, because most of reactions and transport of materials occur at mineral-water interfaces (Nakashima et al., 2004). In Chapter 4, in order to examine effects of goethite on spectral changes with time during the Maillard reaction between glycine and ribose forming humic-like substances, batch heating experiments of 0.1 mol l^{-1} glycine + ribose mixture solution with/without goethite were conducted at 60, 70 and 80 °C. Goethite is one of representative inorganic soil constituents and is playing important roles in the environment as an adsorbent and a catalyst (Liu et al., 2014). In this study, goethite was prepared by aging precipitates formed in $FeCl_3$ and NaOH mixture solution. The products were analyzed by visible, Raman and IR spectroscopy and X-ray diffractometry and they were suggested to be mainly composed of goethite.

UV–Vis spectroscopy was conducted on the batch samples of 0.1 mol l^{-1} glycine + ribose mixture solution with/without goethite heated at 60, 70 and 80 °C. Spectral saturation occurred in UV region (200–400 nm) because of strong absorption by UV active products. Therefore, absorption in visible range is mainly analyzed. Changes in absorbance at 420 nm with one-point base at 800 nm (Vis_{420}) with time at each heating temperature were fitted by the same exponential equation assuming the first order reaction as in Chapter 3 (Fig. 6.1.11). The fitting by the Arrhenius equation for the apparent first order reaction rate constant k_{420} and T (333–350 K) in the Arrhenius diagram (Fig. 6.1.12) gave the E_a and A values. The values of k_{420} for in situ experiments for 0.5 mol l^{-1} at 60–80 °C and the fitting line by the Arrhenius equation are also shown in Fig. 6.1.12. Table 6.1.3 lists the E_a and A values obtained from the fitting by the Arrhenius equation, together with k_{420} values and half-lives of the first order reaction stage at 15 °C estimated by extrapolation of the Arrhenius equation.

The obtained apparent first order reaction constants k_{420} were larger in the presence of goethite, thus the half-life of the first order reaction stage at 15 °C was smaller in the presence of goethite (105 < 1990 years). This indicates reaction enhancement by goethite. The reaction rates k_{420} at 0.1 mol l^{-1} were about 3 orders of magnitudes smaller than those for 0.5 mol l^{-1} glycine + ribose mixture solution heated at 60–80 °C without goethite, suggesting that higher initial concentration of the reactants can make the reaction faster (Fig. 6.1.12). These effects of goethite and initial concentrations should be considered in evaluating time scales of formation of humic-like substances in the real environment.

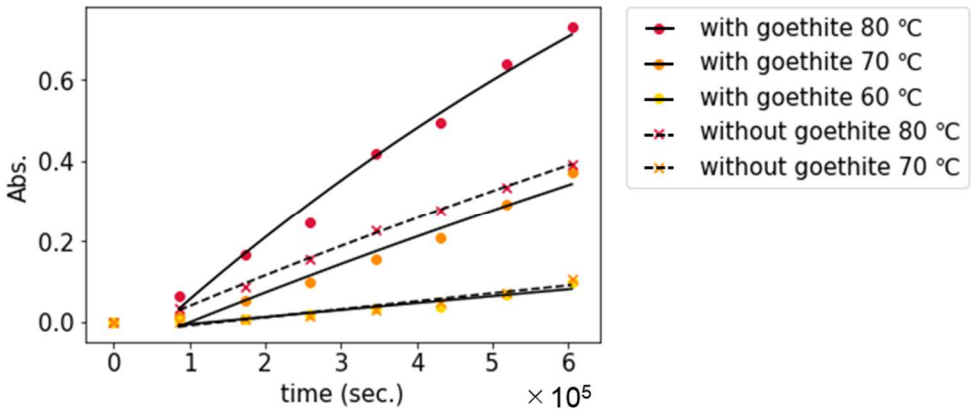

Fig. 6.1.11. Changes in Vis_{420} with time for the batch samples of 0.1 mol l^{-1} glycine + ribose mixture solutions with goethite heated at 60, 70 and 80 °C (red, orange and yellow filled circles) and those without goethite heated at 70 and 80 °C (red and orange crosses). The fitting curves (the first order reaction) are overlaid.

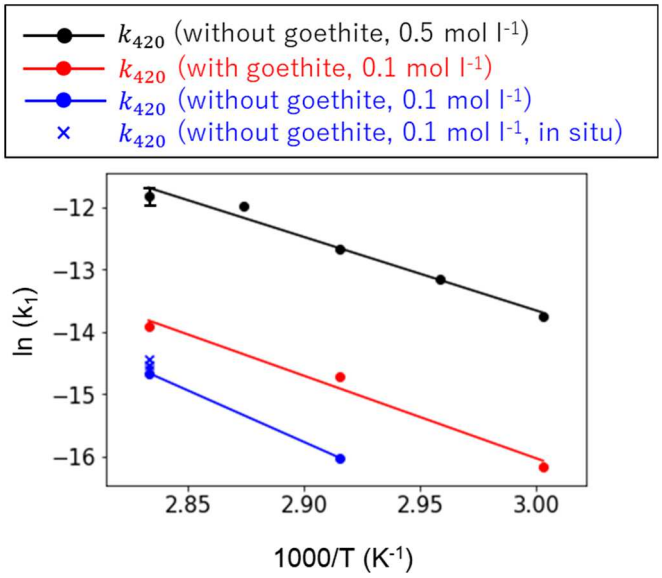

Fig. 6.1.12. The Arrhenius plots of k_{420} values in the in situ heating experiments for 0.5 mol l^{-1} glycine + ribose mixture solutions without goethite (black filled circles) and the batch experiments for 0.1 mol l^{-1} glycine + ribose mixture solutions with/without goethite (red/blue filled circles) with their fitting lines. Blue cross shows the Arrhenius plot of k_{420} values in the in situ heating experiments for 0.1 mol l^{-1} glycine + ribose mixture solution without goethite (Chapter 3).

Table 6.1.3.The E_a, A values obtained from the fitting by the Arrhenius equation and k_{420} values and half-lives of the first order reaction stage at 15 °C estimated by extrapolation of the Arrhenius equation.

	E_a (kJ mol^{-1})	A (s^{-1})	k_{420} at 15 °C (s^{-1})	Half-life at 15 °C (y)
0.5 mol l^{-1} (in situ without goethite)	98	2.7×10^{9}	4.5×10^{-9}	4.9
0.1 mol l^{-1} (batch with goethite)	110	2.0×10^{10}	2.1×10^{-10}	105
0.1 mol l^{-1} (batch without goethite)	137	9.1×10^{13}	1.1×10^{-11}	1990

6.1.5. Adsorption of the simulated Maillard reaction reactants and products on goethite studied by in situ attenuated total reflection infrared (ATR-IR) spectroscopy

In Chapter 4, enhancement of the Maillard reaction by goethite was suggested. In order to examine surface processes on minerals during the simulated Maillard reaction, adsorption on goethite of reactants and products of the Maillard reaction at room temperature was studied by attenuated total reflection infrared (ATR-IR) spectroscopy. The thin layers of goethite were made on the ATR crystal (ZnSe) (Fig. 6.1.13) and IR spectral changes after dropping 0.1 mol l^{-1} glycine + ribose solutions (reactant solution) and those heated at 80 °C for 196 hours (product solution) on the goethite layers were traced. Laser scanning confocal microscopy (LSCM) for the deposited goethite layer on the ATR crystal suggested that the goethite layer was mostly thinner than the penetration depth of evanescent waves in the order of several hundred nm. Therefore, ATR-IR spectra can include both solutes dissolved in water nearby the goethite surface and those adsorbed on goethite surfaces besides goethite layer itself.

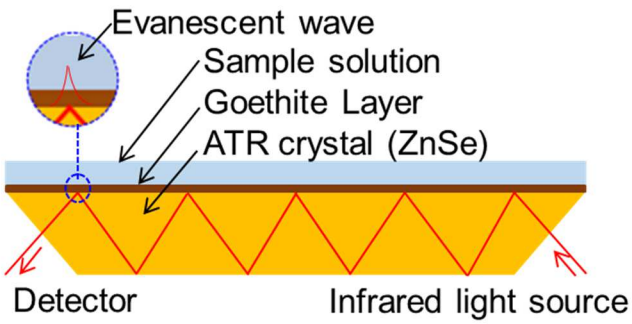

Fig. 6.1.13. A schematic figure of the attenuated total reflection (ATR) crystal (ZnSe) with thin layers of goethite used in ATR-IR measurements.

IR spectral changes with time for the reactant (non-heated) and product (heated at 80 °C for 196 hours) solutions on the goethite layer were measured every 150 seconds for 10800 seconds (3 hours) at room temperature. Fig. 6.1.14. shows representative difference IR spectra (t = 0, 1, 2 and 3 hours) from t = 0 spectrum for (R) the reactant solution without goethite, (R+g) the reactant solution on goethite, (P) the product solution without goethite and (P+g) the product solution on goethite. Increases in peak heights at 1410, 1630 and 1710 cm^{-1} suggested fast adsorption of components with COO^{-}, COOH and COOR groups on positively charged goethite surface (Zeltner and Anderson, 1988; Silverstein et al., 1991; Max et al., 1998; Kitadai et al., 2010). Adsorbed amounts onto goethite were generally larger for the product solution than for the reactant solution. This adsorption process within a few hours at room temperature was faster than the formation enhancement of humic-like and brown products in several days at 60–80 °C (Chapter 4) suggesting that later processes on the goethite surface

after the fast adsorption are rate-limiting for the reaction enhancement. An in situ hydrothermal ATR-IR cell (Fig. 6.1.15) under development can be used for further detailed kinetic studies including surface processes on goethite layers at different temperatures (20–80 °C).

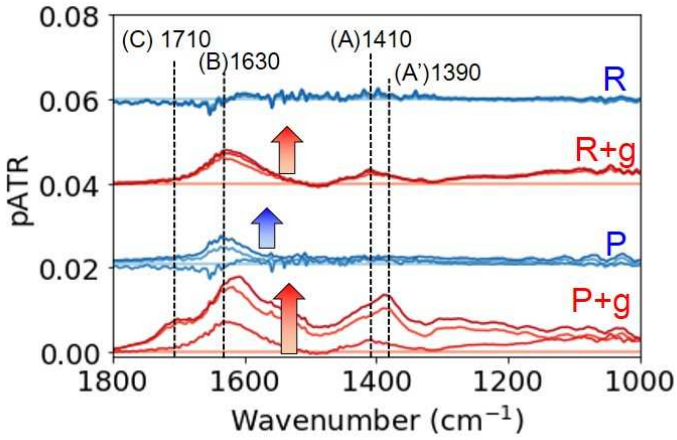

Fig. 6.1.14. Representative difference IR spectra (t = 0, 1, 2 and 3 hours) from t = 0 spectrum for (R) the reactant solution without goethite, (R+g) the reactant solution on goethite, (P) the product solution without goethite and (P+g) the product solution on goethite.

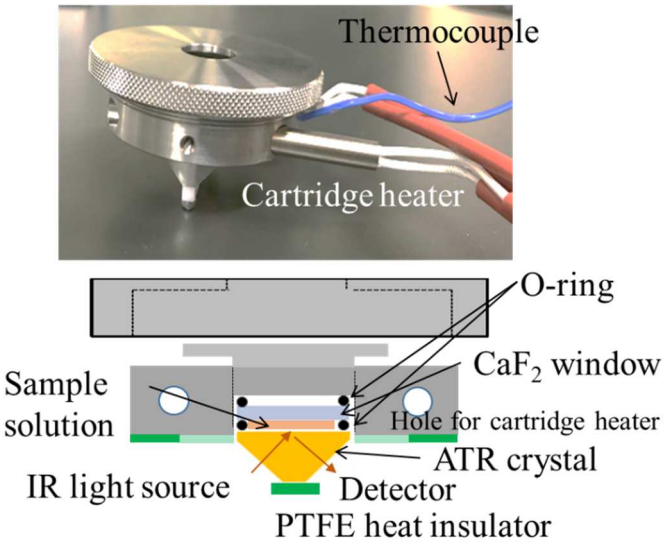

Fig. 6.1.15. An overview and a cross section of the new heatable cell for ATR-IR spectroscopy.

6.1.6 Overview of time scales for formation of humic-like substances by the Maillard reaction

In situ hydrothermal measurement systems for IR and UV–Vis spectroscopy were applied on the aqueous reaction simulating the Maillard reaction by glycine and ribose forming humic-like substances (Chapters 2 and 3) giving the kinetic parameters of the reaction. The batch experiments (Chapter 4) and in situ ATR-IR measurements (Chapter 5) suggested interactions between the reactants and products of the Maillard reaction and goethite. The time scales for the simulated Maillard reaction at a representative Earth surface temperature of 15 °C ranged from a few years to a few thousand years. The reaction rate constants increased by larger initial concentrations and presence of minerals like goethite. In the following, overview of time scales for formation of humic-like substances by the Maillard reaction is discussed.

From the above kinetic analyses, the simulated Maillard reaction can be simplified by dividing them to initial and later stages. The initial stage includes degradation stage of glycine and ribose represented by loss of their structure (C-O and NH_2 groups) as described in Chapter 2. Their estimated reaction rates at 0.5 mol l^{-1} reactant solution were larger than those for the visible changes represented by increase in 420 nm absorbance (Fig. 6.1.4, Table 6.1.1). Moreover, the spectral changes at 420 nm started just after beginning of the heating measurement (Fig. 6.1.6). Therefore, the initial process of the reactants' degradation can be negligible in estimating time scales of the visible changes.

For the experiments on 0.1 mol l^{-1} reactant solution, the spectral changes at 254, 280 and 420 nm (UV_{254}, UV_{280} and Vis_{420}) in UV–Vis range can be divided to the initial induction stage and the later progress stage as described in Chapters 3 and 4. The kinetic analyses suggested shorter time scales for the induction stage than those for the later progress stage. Therefore, the later progress stage described by the first order reaction can be a rate-determining step for these UV–Vis changes.

On the other hand, Chapter 4 suggested enhancement by goethite of the first order spectral changes at 420 nm during the simulated Maillard reaction. Since Chapter 5 suggested more adsorption of the products on goethite than that of the reactants, this enhancement can be more effective on the later processes by the adsorption of intermediate products on goethite surfaces.

Considering these, the apparent first order UV–Vis changes in the simulated Maillard reaction by glycine and ribose forming humic-like substances can be summarized as the following. Table 6.1.4 lists the apparent first order reaction rates k^1 and half-lives at 15 °C of the first order reaction stage in changes in UV_{254}, UV_{280} and Vis_{420} estimated by extrapolation of the Arrhenius equation. The order of time scales ($Vis_{420} > UV_{254} > UV_{280}$) at a lower initial concentration (0.1 mol l^{-1} reactant solution) suggests that the furfural-like intermediates absorbing 280 nm were firstly produced and the later humic-like products absorbing UV range including 254 nm followed. Finally, more highly conjugated π electron compounds absorbing in the visible range including 420 nm were produced. Since dark-

brown color is one of the typical features of humic substances (Stevenson, 1994), Vis_{420} can be employed as a surrogate indicator of the simulated formation processes of humic-like substances.

The time scale of the reaction can therefore be represented by the half-lives of Vis_{420} changes, and is possibly around 5 years at a minimum and 2000 years at a maximum (Table 6.1.4). These time scales depend on the initial reactant concentration and presence/absence of goethite. It should be noted that effects of goethite appear to be smaller than the concentration effects. However, few data are available on concentrations of amino acids and sugars in the natural environment. Moreover, contents of goethite-like iron hydroxides in soils and sediments are not measured frequently and considered to be generally smaller than 1 wt% (Nakashima and Moriizumi, 2018). Reasonable evaluation of time scales with appropriate natural concentrations are difficult.

Table 6.1.4. The apparent first order reaction rates k^1 and half-lives at 15 °C of the first order reaction stage estimated by extrapolation of the Arrhenius equation.

	k^1 at 15 °C (s^{-1})	Half-life at 15 °C (y)
Vis_{420} at 0.5 mol l^{-1} (in situ without goethite)	4.5×10^{-9}	4.9
UV_{280} at 0.1 mol l^{-1} (in situ without goethite)	1.1×10^{-9}	20
Vis_{420} at 0.1 mol l^{-1} (batch with goethite)	2.1×10^{-10}	105
UV_{254} at 0.1 mol l^{-1} (in situ without goethite)	1.3×10^{-10}	174
Vis_{420} at 0.1 mol l^{-1} (batch without goethite)	1.1×10^{-11}	1990

Therefore, I tried first to compare the evaluated time scales for formation of humic-like substances with some natural examples without concrete data sets on initial reactant concentrations and goethite contents. The formation of humic-like substances in the bottom sediments of Ago bay, Mie Prefecture, Japan has been studied in 2004–2006 by Otsuka and Nakashima (unpublished data). They extracted pore waters from bottom sediments at three depth fractions (0–3, 3–6, 6–9 cm) on 2 different locations (Takonobori and Tategami). Total organic carbon (TOC: mg/g dry samples) and fluorescence intensities at Ex. 310 nm/Em. 430 nm of the samples were measured. It should be noted that Ex. 310 nm/Em. 430 nm was a fluorescence maximum wavelength for the sediment samples and similar to that used as a measure of humic-like substances in Section 6.1.3 (Chapter 3: Fig. 6.1.8). The fluorescence intensities were normarized by TOC (mgOrgC) (*F/TOC*) and plotted against the depth (Fig. 6.1.16a and b). By using sedimentation rates at these locations (Momoshima et al., 2008), the fluorescence intensities normarized by TOC (*F/TOC*) can be plotted against time (Fig. 6.1.16c, d).

F/TOC increased from 2.8 to 5.5 $mgOrgC^{-1}$ for Tategami (Fig. 6.1.16d) in about 30 years. An exponential fitting for Tategami assuming the first order reaction by the following equation

$$F/TOC = C_1(1 - \exp(-k^1 t)) + C_2$$

gave an apparent rate constant k^1 of 1.3×10^{-9} s^{-1}, C_1 of 6.0 and C_2 of 1.2. The k^1 had a similar order of

magnitudes to the k^1 for changes in Vis_{420} and UV_{280} (4.5×10^{-9} and 1.1×10^{-9} s^{-1}) extrapolated to 15 °C from the experimental data (in situ without goethite) (Table 6.1.4). Although Takonobori samples did not give appropriate exponential fitting because of small changes in *F/TOC* among the samples, they showed *F/TOC* increase from 3.4 to 4.4 $mgOrgC^{-1}$ (Fig. 6.1.16c) in about 30 years.

The time scales estimated by extrapolations from experimental results were about 5 to 20 years, close to 30 years of changes in *F/TOC* observed at Ago bay sediments. Therefore, the simulated Maillard reaction by glycine and ribose can give constraints on the better understanding of the time scales of formation processes of humic-like substances.

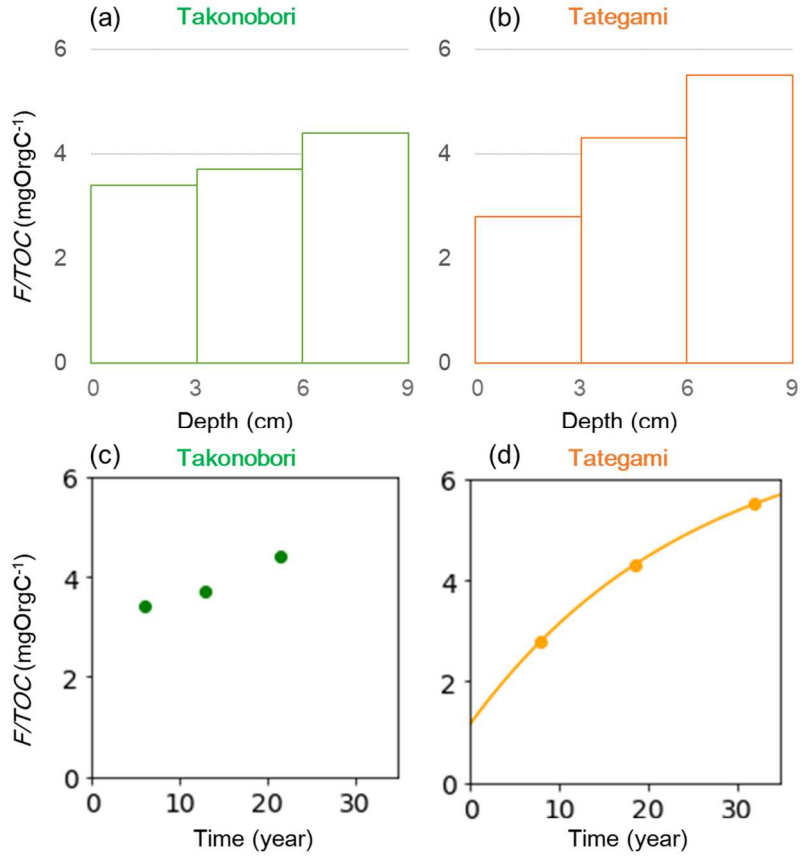

Fig. 6.1.17. The fluorescence intensities normalized by TOC (*F/TOC*) plotted against depth for (a) Takonobori and (b) Tategami samples. Those plotted against time evaluated from sedimentation rates for pore waters from 3 depth fractions of the bottom sediments at (c) Takonobori and (d) Tategami, with a fitting curve for Tategami samples.

6.2. Problems and future perspectives

This thesis aimed at evaluating time scales for formation processes of humic-like substances simulated by the Maillard reaction. Hydrothermal experiments and IR and UV–Vis spectroscopy on the Maillard reaction by glycine and ribose suggested the time scales around 5 years at a minimum and 2000 years at a maximum at a representative Earth surface temperature of 15 °C. This is in agreement with a few decades of time scale for an increase in fluorescence intensities in the bottom sediments of Ago bay, possibly due to the formation of humic-like substances. The present method can be applied to the Maillard reaction under other experimental conditions with various initial concentrations of reactants in future studies. These further researches will give constraints on the better understanding of the time scales of formation processes of humic-like substances.

On the other hand, the batch experiments and in situ ATR-IR measurements in the presence of goethite suggested interactions between the reactants and products of the Maillard reaction and goethite. However, few data points in the batch experiments prevented precise kinetic analyses. Moreover, hydrothermal changes in the reactants and products of the Maillard reaction adsorbed on goethite could not be detected by the ATR-IR method. Therefore, development of a new in situ hydrothermal measurement systems is needed (e.g. hydrothermal in situ IR and visible micro-spectroscopy, hydrothermal in situ ATR-IR spectroscopy).

Further analyses of natural samples should also be performed for time scale evaluation for formation processes of humic-like substances. The study on Ago bay sediments (Section 6.1.6) is one of good practical examples. However, natural samples are complex mixtures of organics and inorganics masking direct measurements for changes in humic substances in the natural environment. Moreover, destructive procedures such as alkaline extraction or drying for humic substances' analyses may limit precise examination of natural organic matter in its original form without modification (Lehmann and Kleber, 2015). I have been developing 3D-EEM spectroscopy for soils and sediments in solid phases as one of the direct characterization methods for humic-like materials in complex mixtures of organic and inorganic compounds.

By these further improvements of measurement methods of humic-like substances, time scales and fates of humic-like substances in the formation, decomposition, transportation and interaction with inorganic materials such as minerals can be quantitatively described in the future.

REFERENCE

van Boekel, M. A. J. S. “Kinetic aspects of the Maillard reaction: a critical review”. Nahrung 2001. 45(3). 150–159.

Carmona, P. and M. Molina. “Raman and infrared spectra of D-ribose and D-ribose 5-phosphate”. J. Raman Spectrosc. 1990. 21. 395–400.

Eisenberg, D. and W. Kauzmann. “Structure and properties of water”. Oxford University Press. 1969.

Kitadai, N., T. Yokoyama amd S. Nakashima. “Temperature dependence of molecular structure of dissolved glycine as revealed by ATR-IR spectroscopy”. J. Mol. Struct. 2010. 981. 179–186.

Kumar, S., A. K. Rai, V. B. Singh and S. B. Rai. “Vibrational spectrum of glycine molecule”. Spectrochim. Acta Pt. A 2005. 61. 2741–2746.

Lehmann, J., M. Kleber. “The Contentious Nature of Soil Organic Matter”. Nature 2015. 528. 60–68.

Liu, H., T. Chen, R. L. Frost. “An overview of the role of goethite surfaces in the environment”. Chemosphere 2014. 103. 1–11.

Maillard, L. C. “Action of Amino Acids on Sugars. Formation of Melanoidins in a Methodical Way”. C. R. Hebd. Séances Acad. Sci. 1912. 154. 66–68.

Nagao, S., T. Matsunaga, Y. Suzuki, T. Ueno, H. Amano. “Characteristics of Humic Substances in the Kuji River Waters as Determined by High-performance Size Exclusion Chromatography with Fluorescence Detection”. Wat. Res. 2003. 37(17). 4159–4170.

Nakashima, S., M. Moriizumi. “On site analyses of soils - Measurements of colors and visible - near infrared spectra -”. Bunseki 2018. 9. 369–370. (In Japanese)

Nakashima, S., C. J. Spiers, L. Mercury, P. Fenter, M. H. Hochella, Jr. ”Physicochemistry of thin film water in geological and biological systems –current issues and new developments–”. in S. Nakashima, C. J. Spiers, L. Mercury, P. Fenter and M. H. Hochella, Jr. (Eds.) “Physicochemistry of Water in Geological and Biological Systems: Structures and Properties of Thin Aqueous Films”. Universal Academy Press, Inc. 2004. 1–15.

Martinez, A., M. E. Rodriguez, S. W. York, J. F. Preston, L. O. Ingram. “Use of UV Absorbance to Monitor Furans in Dilute Acid Hydrolysates of Biomass”. Biotechnol. Prog. 2000. 16(4). 637–641.

Max, J. J., M. Trudel, C. Chapados. “Infrared titration of aqueous glycine”. Appl. Spectrosc. 1998. 52. 226–233.

Momoshima, N., Y. Ueda, S. Sugihara, Y. Yamagata, H. Kokubu. “Investigation of sedimentation rate in Ago Bay, Japan by lead-210 dating”. Chikyukagaku (Geochemistry) 2008. 42. 99–111.

Silverstein, R. M., G. C. Bassler, T. C. Morrill. “Spectrometric Identification of Organic Compounds”. Wiley. 1991.

Stamp, J. A. and T. P. Labuza. “Kinetics of the Maillard reaction between aspartame and glucose in solution at high temperatures”. J. Food Sci. 1983. 48(2). 543–544.

Stevenson, F. J. Stevenson. “Humus Chemistry: Genesis, Composition, Reactions“. Wiley, 1994.

Silverstein, R. M., G. C. Bassler, T. C. Morrill. “Spectrometric Identification of Organic Compounds”. Wiley. 1991.

List of publications and presentations

Publications

1. Yuki Nakaya, Satoru Nakashima. “In situ IR transmission spectroscopic observation and kinetic analyses of initial stage of the Maillard reaction as a simulated formation process of humic substances”. Chemistry Letters, 2016. 45(10). 1204–1206.

2. Yuki Nakaya, Satoru Nakashima, Mihoko Moriizumi. “Non-destructive spectroscopic tracing of simulated formation processes of humic-like substances based on the Maillard reaction”. Applied Spectroscopy, 2018. 72(8). 1189–1198.

3. Yuki Nakaya, Katsuya Okada, Yudai Ikuno, Satoru Nakashima. “Spectroscopic study of effects of goethite surfaces on the simulated maillard reaction forming humic-like substances”. E-Journal of Surface Science and Nanotechnology, 2018. 16. 411–418.

Presentations in international conferences

1. Yuki Nakaya, Satoru Nakashima. “A heatable liquid cell for in situ spectroscopic observation of geochemical reactions”. International Symposium on Present and Future of Material Sciences, Osaka, Japan. 2015. Poster presentation.

2. Yuki Nakaya, Satoru Nakashima. “In situ spectroscopic observation and kinetic analyses of aqueous organic geochemical reactions”. International Workshop of Organic Geochemistry in Osaka, Osaka, Japan. 2016. Poster presentation.

3. Yuki Nakaya, Satoru Nakashima, Takahiro Otsuka, Mihoko Moriizumi. “Time scale evaluation for the formation of humic substances based on the Maillard reaction”. 18th International Conference of International Humic Substances Society, Kanazawa, Japan. 2016. Poster presentation.

4. Yuki Nakaya, Satoru Nakashima. “The simulated Maillard reaction forming humic substances at the surface of goethite as studied by attenuated total refrection infrared (ATR-IR) spectroscopy”. The 8th International Symposium on Surface Science, Ibaraki, Japan. 2017. Poster presentation.

5. Yuki Nakaya, Satoru Nakashima, Mihoko Moriizumi, Masahiro Oguchi, Shinsuke Kashiwagi, Nobuyuki Naka. “Three dimensional excitation emission matrix (3D-EEM) fluorescence spectroscopy for soil powder samples without extraction”. 19th International Conference of International Humic Substances Society, Albena Resort, Bulgaria. 2018. Oral presentation.

6. Yuki Nakaya, Satoru Nakashima, Mihoko Moriizumi, Masahiro Oguchi, Shinsuke Kashiwagi, Nobuyuki Naka. “Effects of fluorescence quenching of soil powder samples in fluorescence spectroscopy”. International Workshop on Organic Matter Spectroscopy 2018, Carqueiranne, France. 2018 Oral presentation.